JAERI-M
93-201

JAERI CONTRIBUTION FOR THE IAEA COORDINATED RESEARCH PROGRAM PHASE III (CRP-3) ON "OPTIMIZING OF REACTOR PRESSURE VESSEL SURVEILLANCE PROGRAMMES AND THEIR ANALYSIS"

October 1993

Kunio ONIZAWA, Masahide SUZUKI
and Shuzo UEDA*

日本原子力研究所
Japan Atomic Energy Research Institute

JAERI-Mレポートは，日本原子力研究所が不定期に公刊している研究報告書です。
入手の問合わせは，日本原子力研究所技術情報部情報資料課（〒319-11茨城県那珂郡東海村）あて，お申しこしください。なお，このほかに財団法人原子力弘済会資料センター（〒319-11 茨城県那珂郡東海村日本原子力研究所内）で複写による実費頒布をおこなっております。

JAERI-M reports are issued irregularly.
Inquiries about availability of the reports should be addressed to Information Division, Department of Technical Information, Japan Atomic Energy Research Institute, Tokai-mura, Naka-gun, Ibaraki-ken 319-11, Japan.

編集兼発行　日本原子力研究所
印　　刷　㈱原子力資料サービス

JAERI-M 93-201

JAERI Contribution for the IAEA Coordinated Research Program Phase III (CRP-3) on "Optimizing of Reactor Pressure Vessel Surveillance Programmes and Their Analysis"

Kunio ONIZAWA, Masahide SUZUKI and Shuzo UEDA*

Department of Reactor Safety Research
Tokai Research Establishment
Japan Atomic Energy Research Institute
Tokai-mura, Naka-gun, Ibaraki-ken

(Received September 10, 1993)

As a part of IAEA coordinated research program on irradiation embrittlement of RPV steels, JAERI performed irradiation study using seven materials with varying copper and nickel contents. Irradiation of test specimens was conducted in JMTR of JAERI/Oarai and post irradiation tests including fracture toughness were done at hot laboratory at JAERI/Tokai. The following conclusions were drawn:

(1) With increasing Ni contents from 0.1 to 1.18 wt%, radiation hardening and therefore embrittlement became larger.
(2) The increase of yield stress can be correlated with hardness increase and Charpy transition temperature shift.
(3) In the upper shelf region, irradiation response on fracture toughness was well correlated with radiation hardening, while no good correlation was found between Charpy energy decrease and radiation hardening.

Keywords: Reactor Pressure Vessel, Neutron, Irradiation Embrittlement, Chemical Composition, Transition Temperature, Fracture Toughness, Correlation, Integrity, Surveillance

---

This work was carried out in the framework of IAEA coordinated research program entitled "Optimizing of reactor pressure vessel surveillance programmes and their analysis."
* Nuclear Power Engineering Corporation

原子炉圧力容器監視試験法の最適化に関するIAEA協力研究 Phase Ⅲ 計画における原研の試験結果

日本原子力研究所東海研究所原子炉安全工学部
鬼沢　邦雄・鈴木　雅秀・植田　脩三*

（1993年9月10日受理）

原子炉圧力容器鋼の照射脆化に関するIAEA協力研究 Phase Ⅲ 計画の一環として，原研ではニッケル及び銅含有量を変えた7種類の圧力容器鋼材を用いて中性子照射試験を実施した。中性子照射試験はJMTRで行い，破壊靭性試験を含む照射後試験は東海ホットラボにて実施した。得られた結論は次の通りである。

(1) 鋼材中のニッケル含有量の増加（0.1－1.18 wt%）に比例して，照射硬化・脆化は増加する。

(2) 中性子照射による降伏応力の増加は，硬さの増加及びシャルピー遷移温度シフトと良い相関がある。

(3) 上部棚温度域では，破壊靭性の照射による低下と照射硬化には良い相関があるが，シャルピー吸収エネルギと照射硬化には良い相関は認められなかった。

本研究は，IAEAとの協力研究「原子炉圧力容器鋼材の中性子照射脆化に関する最適試験法の確立」として実施したものである。

東海研究所：〒319－11　茨城県那珂郡東海村白方字白根2－4
＊　原子力発電技術機構

Contents

目　　次

1. INTRODUCTION

1.1 Objectives of IAEA CRP Phase III

The phase III of IAEA coordinated research program (CRP-3) entitled "Optimizing of Reactor Pressure Vessel Surveillance Programmes and Their Analysis," was initiated in 1983. The main objective of this phase of the program is to consolidate the now increasing body of knowledge on irradiation embrittlement and the techniques used to determine its significance. To achieve this objective the overall program will seek to make major contributions in the followings[1]:

(a) Optimizing of the means for measuring fracture resistance,
(b) Establishing correlations between different mechanical test methods used for measuring irradiation response,
(c) Understanding of the underlying mechanisms responsible for embrittlement, and
(d) Establishing method for ameliorating embrittlement.

Fifteen countries took part in this program. The participant countries are Argentine, Austria, Belgium, Czechoslovakia, Finland, France, Germany, Hungary, India, Japan, Russia, Switzerland, United Kingdom and United States. Eighteen kinds of materials were provided to the IAEA from Japan[2] for this program, and several steels which were used in the phase II of CRP were also used in some countries. This report summarizes the results of JAERI program in the framework of the CRP-3.

1.2 Outline of JAERI Program

Seven kinds of RPV steels were tested in the JAERI program.

Charpy impact, tensile, Vickers hardness and fracture toughness tests were performed before and after irradiation in Japan Materials Testing Reactor (JMTR) at JAERI Oarai research establishment. Post irradiation tests were done at Research Hot Laboratory of JAERI Tokai Research Establishment. Overall test matrix of JAERI is shown in Table 1.

The research objectives of the JAERI program in the framework of the CRP-3 are;

(1) to identify the effect of chemical composition (particularly Ni) on irradiation response,

(2) to establish the method for measuring fracture resistance, and

(3) to examine the correlation between irradiation responses of different mechanical properties.

2. EXPERIMENTAL PROCEDURE

2.1 Materials

Chemical compositions of the steels used (JPD, JPF, JPH, JPI, JPJ, JFL and JRQ) are shown in Table 2[2]. These materials were selected to cover a wide range of chemical compositions, in copper, nickel and phosphorus contents, which elements are very important from the point of irradiation embrittlement. Figure 1 shows the compositional range of these seven materials, comparing with the estimated range of Japanese PWR pressure vessel steels. Three laboratory melts (JPD, JPF and JPH) were selected for studying the effect of Nickel. Heat treatments of these steels are summarized in Table 3. The cooling rate after normalizing for the thin laboratory melts was almost identical to the rate in quenching at the quarter thickness position of heavy section

Charpy impact, tensile, Vickers hardness and fracture toughness tests were performed before and after irradiation in Japan Materials Testing Reactor (JMTR) at JAERI Oarai research establishment. Post irradiation tests were done at Research Hot Laboratory of JAERI Tokai Research Establishment. Overall test matrix of JAERI is shown in Table 1.

The research objectives of the JAERI program in the framework of the CRP-3 are;

(1) to identify the effect of chemical composition (particularly Ni) on irradiation response,

(2) to establish the method for measuring fracture resistance, and

(3) to examine the correlation between irradiation responses of different mechanical properties.

2. EXPERIMENTAL PROCEDURE

2.1 Materials

Chemical compositions of the steels used (JPD, JPF, JPH, JPI, JPJ, JFL and JRQ) are shown in Table 2[2]. These materials were selected to cover a wide range of chemical compositions, in copper, nickel and phosphorus contents, which elements are very important from the point of irradiation embrittlement. Figure 1 shows the compositional range of these seven materials, comparing with the estimated range of Japanese PWR pressure vessel steels. Three laboratory melts (JPD, JPF and JPH) were selected for studying the effect of Nickel. Heat treatments of these steels are summarized in Table 3. The cooling rate after normalizing for the thin laboratory melts was almost identical to the rate in quenching at the quarter thickness position of heavy section

steels. For heavy section steels (JPI, JPJ, JFL and JRQ), specimens were prepared from the quarter thickness position of materials.

2.2 Irradiation

Test specimens of above materials were irradiated in JMTR. The core configuration of JMTR is shown in Figure 2. Eight irradiation capsules of No.1 to No.8 were irradiated at F-12 hole in the second Beryllium reflector region of JMTR core. The specimens encapsuled in each capsule are shown in Appendix A.

The fast neutron fluence of which neutron energy was greater than 1 MeV was measured by activation method using pure iron wires for each capsule. For the determination of neutron fluence, $^{54}Fe(n,p)^{54}Mn$ reaction was used. The effective cross section of this reaction is 64.5 millibarn which is determined using nuclear data library, ENDF/B-IV, and the neutron spectrum obtained by ANISN[3]. Neutron energy spectrum of a capsule is shown in Figure 3. Four iron dosimeters encapsuled by aluminum, called fluence monitor, were installed at adequate positions in each capsule. After being taken out from the capsule, the fluence monitors were measured by gamma-ray spectrum measurement system. Neutron fluence, FL, is defined by the equation given below.

$$FL = A \times \frac{G}{NoMF} \times \frac{1}{S} \times \frac{t_i}{(1-e^{-Ct_i})e^{-Ct_w}} \qquad (1)$$

where FL: neutron fluence, A: measured activity,
G: atomic mass unit, No: Avogadro's number,
M: dosimeter weight, F: isotopic abundance,
S: effective cross section, t_i: irradiation time,
t_w: cooling time, C: decay constant.

The axial distribution of neutron fluence in the capsule was estimated by the values obtained from four fluence monitors in capsule and the database of the fluence values determined by past experiments at the same irradiation hole. Figure 4 shows a typical distribution of fast neutron fluence with energy greater than 1 MeV as a function of the axial position of the capsule. The distributions of fast neutron fluence for all capsules are summarized in Appendix A. The ratio of neutron fluence with energy greater than 0.1 MeV to that for 1 MeV is approximately 2.6. Displacement per atom (dpa) for iron by the irradiation to 2×10^{19} n/cm^2 (E>1MeV) in this irradiation hole is about 0.031.

Aimed neutron fluence for capsules of No.1 to No.7 was 2×10^{19} n/cm^2 (E>1MeV), and 4×10^{19} n/cm^2 (E>1MeV) for No.8. Fast neutron flux was approximately 1×10^{13} n/cm^2s (E>1MeV) for all capsules. The irradiation temperature was controlled mostly in the range from 280 °C to 300 °C for all capsules. The measured temperature ranges in the capsules during irradiation are summarized in Appendix B.

2.3 Mechanical Tests

Charpy impact tests were performed using a test machine with the capacity of 300 J. Testing apparatus and specimens were prepared in accordance with JIS B7722 and JIS Z2202 respectively. The radius of the hammer striking edge is 2 mm. The impact velocity of hammer was approximately 5 m/s. Configuration and dimensions of the specimen are shown in Figure 5(a). The notch orientations of the specimens were T-L direction for plate and L-C direction for forging.

Charpy transition curves were obtained by fitting all data to the following equation[4],

$$CVN = A + B \times \tanh((T-T_o)/C) \quad (2)$$

where CVN: Absorbed Energy, Lateral Expansion or Fracture Appearance,

T: Test Temperature,

A,B,C,T_o: Fitting Constants.

Tensile tests were conducted at several temperatures ranging from -100 °C to 290 °C using an electromechanical servo type test machine with the capacity of 100 kN. Tensile specimen had dimensions of 4 mm in diameter and 22 mm in gauge length (Figure 5(b)). The crosshead speed during tensile tests was 0.2 mm/min. The specimen direction was perpendicular to rolling direction or forging axis of materials. Vickers hardness tests were done using a half of broken Charpy specimen with an applied load of 98 N.

Two types of specimen were used to measure the fracture toughness. One was a precracked Charpy type specimen (Figure 5(c)), and another was a compact type specimen (12.5mm thick disk-shaped compact, 0.5T-DCT: Figure 5(d), and 25mm thick standard compact, 1T-CT: Figure 5(e)). Crack plane orientations of all specimens were T-L direction for plate and L-C direction for forging. The specimens were prepared in accordance with ASTM E399[5]. Fracture toughness testing was performed mostly according to ASTM E813 method[6]. Precracking of specimens was performed before irradiation using fatigue load of 10 Hz sinusoidal wave in air. Maximum stress intensity factor during precracking was less than 30 $MPa\sqrt{m}^{0.5}$. The ratio of initial crack length to specimen width was about 0.55. After precracking, side groove of 10% of thickness was machined in each side for compact type specimen.

In the transition temperature range, using a precracked Charpy type specimen, a fracture toughness was determined by the onset of cleavage fracture that corresponded to the occurrence of

a sudden load drop. The fracture toughness (K_{JC}) was converted from the J-integral value at the onset of cleavage fracture. The crosshead speed for bending was 0.1 mm/min.

For compact type specimen tested at upper shelf temperature, unloading compliance method based on ASTM E813-89 was applied to obtain J_{IC} and J-integral resistance (J-R) curve from single specimen. Multiple specimen technique was also used to determine J_{IC} in some cases. The crosshead speed was 0.5 mm/min.

3. RESULTS AND DISCUSSION

All results of mechanical tests, i.e. tensile, Charpy impact, fracture toughness and Vickers hardness tests, are summarized in Appendices C to F.

3.1 Effects of Chemical Composition on Irradiation Embrittlement

Laboratory melts were selected for the evaluation of Ni effect on irradiation embrittlement. Figure 6 shows the increase of yield stress at room temperature as a function of Ni content. Clearly radiation hardening became larger with increasing Ni content, although neutron fluence value of high Ni steel was lower than that of low Ni steel. As known well, copper affects the irradiation hardening and embrittlement greatly. Figure 7 shows the increase of yield stress at room temperature caused by irradiation as a function of Cu contents. It is clear that irradiation hardening became larger with increasing Cu content.

For Charpy properties, comparing the results of JPD (0.1% Ni) and JPF (0.62% Ni), JPF exhibited higher shift of Charpy 41J transition temperature (Figure 8). Unfortunately, the transition temperature of JPH (1.18% Ni) could not be obtained owing to

a sudden load drop. The fracture toughness (K_{JC}) was converted from the J-integral value at the onset of cleavage fracture. The crosshead speed for bending was 0.1 mm/min.

For compact type specimen tested at upper shelf temperature, unloading compliance method based on ASTM E813-89 was applied to obtain J_{IC} and J-integral resistance (J-R) curve from single specimen. Multiple specimen technique was also used to determine J_{IC} in some cases. The crosshead speed was 0.5 mm/min.

3. RESULTS AND DISCUSSION

All results of mechanical tests, i.e. tensile, Charpy impact, fracture toughness and Vickers hardness tests, are summarized in Appendices C to F.

3.1 Effects of Chemical Composition on Irradiation Embrittlement

Laboratory melts were selected for the evaluation of Ni effect on irradiation embrittlement. Figure 6 shows the increase of yield stress at room temperature as a function of Ni content. Clearly radiation hardening became larger with increasing Ni content, although neutron fluence value of high Ni steel was lower than that of low Ni steel. As known well, copper affects the irradiation hardening and embrittlement greatly. Figure 7 shows the increase of yield stress at room temperature caused by irradiation as a function of Cu contents. It is clear that irradiation hardening became larger with increasing Cu content.

For Charpy properties, comparing the results of JPD (0.1% Ni) and JPF (0.62% Ni), JPF exhibited higher shift of Charpy 41J transition temperature (Figure 8). Unfortunately, the transition temperature of JPH (1.18% Ni) could not be obtained owing to

experimental trouble. However, it can be concluded that Ni increase in the range investigated promotes irradiation embrittlement.

Cu and Ni affect the degree of irradiation embrittlement greatly. However, as seen in Figure 9, the degree of embrittlement seems to be also affected by the steel production history, because steels produced in thinner thickness differed greatly with thicker ones, though the reason for this discrepancy is not clear enough at the moment.

Decrease of upper shelf energy (ΔUSE) can be predicted by U.S. NRC Regulatory Guide (RG) 1.99 Rev.2[7]. Figure 10 shows the relation between the predicted USE values and measured ones in percentage decrease. Although the USE value after irradiation for JPI was not determined, the decrease of USE was estimated to be less than 10% based on the load-displacement records of which a specimen indicated 90% shear fracture. This figure indicates that RG 1.99 Rev.2 overestimates for JPI, JFL and JPD, which are with either low Cu or low Ni contents. On the other hand, RG 1.99 Rev.2 underestimates for JPJ by 10%, which is also with low Cu. The prediction curve by RG 1.99 Rev.2 includes only Cu contents above 0.10 wt% for base metal, but this result suggests that the decrease of USE may also be affected by other variables.

3.2 Fracture Toughness Change due to Neutron Irradiation

3.2.1 Fracture Toughness in Transition Region

Temperature dependence of static cleavage fracture toughness values was obtained before and after irradiation using precracked Charpy specimens of JPI, JPJ and JRQ. Figure 11 shows the data of static fracture toughness K_{JC} values obtained from the

materials. The precise shifts of transition temperature, however, could not be determined, because the numbers of data points were not sufficient for statistical analysis (only four to five data in the transition region).

3.2.2 Fracture Toughness in Upper Shelf Region

Crack initiation toughness and crack growth resistance data of heavy section steels were obtained using a compact type specimen with 20% side groove. Figure 12 shows J-R curves of JRQ at 200 °C for both unirradiated and irradiated conditions. The J-R curve was lowered by neutron irradiation. For unirradiated condition, it is seen that the slope of J-R curve, dJ/da, depended on the specimen size of 0.5T(12.5mm thick) and 1T(25mm thick), and dJ/da of 0.5T was smaller than that of 1T.

Size effect of quasi crack initiation toughness, J_Q, according to ASTM E813 method is shown in Figure 13. Although valid J_{IC} was obtained at only limited condition of low toughness, J_Q data of both 0.5T-DCT and 1T-CT including J_{IC} were almost equal to each other with some scatter in the high toughness region. Therefore, it is meaningful to use J_Q values for the discussion for the irradiation effect on ductile crack initiation toughness.

Figure 14 shows the J_Q and J_{IC} values at 200 °C and 290 °C as a function of fast neutron fluence. Valid J_{IC} values were obtained only from JRQ steel after irradiation, because other steels, particularly JFL, had very high toughness before irradiation. This figure indicates that neutron irradiation affects fracture toughness significantly for JFL and JRQ, but less for JPI, although there are few data for each material with large scatters after irradiation. After neutron irradiation to a fluence of 2×10^{19} n/cm^2 (E>1MeV), fracture toughness was lowered by roughly 30% and 25% for JFL and JRQ, and 10% and 15% for JPI and

JPJ, respectively.

It is also indicated from Figure 14 that these steels keep the upper shelf fracture toughness over 180 kJ/m^2 till 4-5 x 10^{19} n/cm^2.

On the other hand, size effect on crack growth resistance, dJ/da, is apparent for unirradiated condition as shown in Figure 15. In this figure, dJ/da values were defined by the slope of J-R curve at which crack extension was 1 mm, dJ/dal, because J-R curves were fitted to power law equation according to ASTM E813. All data of dJ/dal of 0.5T-DCT are smaller than that of 1T-CT except one data point that is nearly equivalent.

To eliminate the size effect in J-R curve, modified J-integral, J_M, has been proposed by Ernst[8]. Figure 16 shows J_M-R curves for unirradiated JRQ at 200 °C. The comparison of J_M values between 1T-CT and 0.5T-DCT still indicates the slight difference due to specimen size. However, since smaller specimen provides lower toughness, this size effect in J_M-R curve can be considered as a conservatism. It is necessary to improve the evaluation and application method of small specimen fracture toughness data from structural analysis viewpoint.

3.3 Correlation between Mechanical Properties for Evaluation of Embrittlement

3.3.1 Yield Stress, Hardness and Charpy Shift

Figure 17 shows the correlation between the increases of yield stress and hardness caused by irradiation. Both properties were measured at room temperature. The regression line is expressed by the following relation.

$$\Delta\sigma_y = 3.32 \times \Delta Hv \qquad (r=0.84) \qquad (3)$$

where $\Delta\sigma_y$ = Yield stress increase (MPa),

ΔHv = Vickers hardness increase (VHN),

r = Correlation factor.

This correlation means that the strength change caused by irradiation can be measured by means of hardness testing for materials with a wide range in composition of RPV steels.

Figure 18 shows the correlation between the shifts in Charpy 41J transition temperature and yield stress increase.

$$\Delta T_{41J} = \alpha \times \Delta\sigma_y \qquad (4)$$

α: coefficient, 0.4 ~ 0.75

where ΔT_{41J} = Charpy 41J shift (°C).

Here, again the steel production history appears to have an influence on irradiation response. That is, materials produced in thinner thickness had a smaller coefficient of about 0.4, while materials produced in larger thickness had about 0.75.

3.3.2 Fracture toughness and Charpy properties

The important correlation is the shifts of brittle-ductile transition temperature in Charpy impact energy and fracture toughness. In some codes for integrity evaluation of reactor pressure vessel, such as ASME Boiler and Pressure Vessel Code Sec. XI[9], the transition of fracture toughness is assumed to be equivalent to that of Charpy impact energy. In this respect, however, as mentioned earlier, precise comparison could not be made, although tendency of the shift was in accordance with the Charpy shift. Further more irradiation data are necessary for statistical analysis.

In upper shelf region, Charpy upper shelf energy is used to evaluate the safety of reactor pressure vessel in some codes. For example, U.S. 10 CFR part 50[10] provides that reactor vessel steel must maintain upper shelf energy no less than 68 J throughout the life of the vessel. However, to assess the integrity of the vessel based on fracture mechanics concept, actual fracture toughness data are needed not only in the transition range but also in upper shelf temperature range.

Figure 19 shows the percentage decrease of fracture toughness, ΔJ_Q, versus $\Delta\sigma_y$. Except for a high toughness forging material JFL that scattered largely in fracture toughness after irradiation, three plate materials have a good correlation as indicated by a dotted line in the figure. Although the datum of JFL was deviated largely, the reason for this is not clear at the moment. For upper shelf energy, although severely embrittled materials show lower USE values, the correlation between radiation hardening and USE decrease was weak exhibiting large scatter as shown in Figure 20. Comparing with the Figures 19 and 20, better ΔJ_Q-$\Delta\sigma_y$ correlation is seen, indicating the advantage that fracture toughness is predictable directly from $\Delta\sigma_y$ for the integrity assessment of RPV in upper shelf region. It is, however, to be noted that the statistical analysis including the consideration of size effect is necessary to evaluate the irradiation effect on fracture toughness.

4. CONCLUSION

Irradiation experiments were performed using seven materials with varying Cu and Ni contents. Irradiation was conducted in JMTR of JAERI/Oarai and post irradiation tests including fracture toughness tests were done at hot laboratory in JAERI/Tokai. The

In upper shelf region, Charpy upper shelf energy is used to evaluate the safety of reactor pressure vessel in some codes. For example, U.S. 10 CFR part 50[10] provides that reactor vessel steel must maintain upper shelf energy no less than 68 J throughout the life of the vessel. However, to assess the integrity of the vessel based on fracture mechanics concept, actual fracture toughness data are needed not only in the transition range but also in upper shelf temperature range.

Figure 19 shows the percentage decrease of fracture toughness, ΔJ_Q, versus $\Delta\sigma_y$. Except for a high toughness forging material JFL that scattered largely in fracture toughness after irradiation, three plate materials have a good correlation as indicated by a dotted line in the figure. Although the datum of JFL was deviated largely, the reason for this is not clear at the moment. For upper shelf energy, although severely embrittled materials show lower USE values, the correlation between radiation hardening and USE decrease was weak exhibiting large scatter as shown in Figure 20. Comparing with the Figures 19 and 20, better ΔJ_Q-$\Delta\sigma_y$ correlation is seen, indicating the advantage that fracture toughness is predictable directly from $\Delta\sigma_y$ for the integrity assessment of RPV in upper shelf region. It is, however, to be noted that the statistical analysis including the consideration of size effect is necessary to evaluate the irradiation effect on fracture toughness.

4. CONCLUSION

Irradiation experiments were performed using seven materials with varying Cu and Ni contents. Irradiation was conducted in JMTR of JAERI/Oarai and post irradiation tests including fracture toughness tests were done at hot laboratory in JAERI/Tokai. The

conclusions obtained were:

(1) With increasing Ni contents from 0.1 to 1.18 wt%, radiation hardening and therefore embrittlement became larger.

(2) Size effect on fracture toughness in upper shelf region was not evident for crack initiation toughness but apparent for ductile crack growth resistance.

(3) The increase of yield stress can be correlated with hardness increase and Charpy transition temperature shift.

(4) In upper shelf region, the irradiation response on fracture toughness was well correlated with radiation hardening, while no good correlation was found between USE decrease and radiation hardening.
However, it is necessary to optimize the fracture toughness test method which enables statistical analyses.

ACKNOWLEDGMENTS

The authors wish to thank Mr. A. Kohsaka, the Director of Department of Reactor Safety Research, Dr. K. Shibata, the Head of Reactor Component Reliability Research Laboratory, JAERI and other members of the Laboratory for their helpful discussion and suggestions, and also like to thank especially Messrs. T. Watanabe and R. Kato of JAERI for their technical support.

Thanks are also due to many staffs in JMTR Project and Research Hot Laboratory for performing material irradiation and conducting the post irradiation tests, respectively.

In addition, the authors appreciate members of CRP Sub-

conclusions obtained were:

(1) With increasing Ni contents from 0.1 to 1.18 wt%, radiation hardening and therefore embrittlement became larger.

(2) Size effect on fracture toughness in upper shelf region was not evident for crack initiation toughness but apparent for ductile crack growth resistance.

(3) The increase of yield stress can be correlated with hardness increase and Charpy transition temperature shift.

(4) In upper shelf region, the irradiation response on fracture toughness was well correlated with radiation hardening, while no good correlation was found between USE decrease and radiation hardening.
However, it is necessary to optimize the fracture toughness test method which enables statistical analyses.

ACKNOWLEDGMENTS

The authors wish to thank Mr. A. Kohsaka, the Director of Department of Reactor Safety Research, Dr. K. Shibata, the Head of Reactor Component Reliability Research Laboratory, JAERI and other members of the Laboratory for their helpful discussion and suggestions, and also like to thank especially Messrs. T. Watanabe and R. Kato of JAERI for their technical support.

Thanks are also due to many staffs in JMTR Project and Research Hot Laboratory for performing material irradiation and conducting the post irradiation tests, respectively.

In addition, the authors appreciate members of CRP Sub-

Committee (Chairman: Prof. Emeritus of the university of Tokyo, Y. Ando) of the Atomic Energy Research Committee, Japan Welding Engineering Society for their great support.

This program was initiated in 1985 by the late Dr. S. Miyazono, who was the Head of Mechanical Strength and Structure Laboratory at that time.

REFERENCES

[1] L.E.Steele et al., "Results of the International Atomic Energy Agency (IAEA) Coordinated Research Programs on Irradiation Effects on Advanced Pressure Vessel Steels," Effect of Radiation on Material, ASTM STP 870, 1985, pp.863-899.

[2] CRP Sub-Committee, "Manufacturing History and Mechanical Properties of Japanese Materials Provided for The International Atomic Agency," Japan Welding Engineering Society, Oct. 1986

[3] S.Shimakawa et al., "Present Status of Neutron Dosimetry in the JMTR," presented at the Second Asian Symposium on Research Reactor, 1989.

[4] Oldfield, W., "Curve Fitting Impact Test Data: A Statistical Procedure," ASTM Standardization News, Vol.3, No.11, Nov. 1975, pp.24-29.

[5] ASTM E399-83, "Standard Test Method for Plane-Strain Fracture Toughness," ASTM Standards, Vol.03.01.

[6] ASTM E813-81 and -89, "Standard Test Method for J_{IC}, a Measure of Fracture Toughness," ASTM Standards, Vol.03.01.

[7] Revision 2 of U.S. NRC Regulatory Guide 1.99, "Radiation Damage to Reactor Vessel Materials," U.S. Nuclear Regulatory Commission, 1988.

Committee (Chairman: Prof. Emeritus of the university of Tokyo, Y. Ando) of the Atomic Energy Research Committee, Japan Welding Engineering Society for their great support.

This program was initiated in 1985 by the late Dr. S. Miyazono, who was the Head of Mechanical Strength and Structure Laboratory at that time.

REFERENCES

[1] L.E.Steele et al., "Results of the International Atomic Energy Agency (IAEA) Coordinated Research Programs on Irradiation Effects on Advanced Pressure Vessel Steels," Effect of Radiation on Material, ASTM STP 870, 1985, pp.863-899.

[2] CRP Sub-Committee, "Manufacturing History and Mechanical Properties of Japanese Materials Provided for The International Atomic Agency," Japan Welding Engineering Society, Oct. 1986

[3] S.Shimakawa et al., "Present Status of Neutron Dosimetry in the JMTR," presented at the Second Asian Symposium on Research Reactor, 1989.

[4] Oldfield, W., "Curve Fitting Impact Test Data: A Statistical Procedure," ASTM Standardization News, Vol.3, No.11, Nov. 1975, pp.24-29.

[5] ASTM E399-83, "Standard Test Method for Plane-Strain Fracture Toughness," ASTM Standards, Vol.03.01.

[6] ASTM E813-81 and -89, "Standard Test Method for J_{IC}, a Measure of Fracture Toughness," ASTM Standards, Vol.03.01.

[7] Revision 2 of U.S. NRC Regulatory Guide 1.99, "Radiation Damage to Reactor Vessel Materials," U.S. Nuclear Regulatory Commission, 1988.

[8] Ernst, H.A., "Material Resistance and Instability Beyond J-Controlled Crack Growth," Elastic-Plastic Fracture: Second Symposium, ASTM STP 803, 1983, pp.I191-I213.

[9] Section XI of ASME Boiler and Pressure Vessel Code, Appendix A, "Analysis of Flaws," American Society of Mechanical Engineers, New York, 1986.

[10] Title 10, Code of Federal Regulations, Part 50, U.S. Government Printing Office, Washington DC, 1987.

Table 1 Overall test matrix of JAERI program

Test \ Material		JPD	JPF	JPH	JPI	JPJ	JFL	JRQ
Charpy Impact		○/○	○/○	○/○*	○/○※	○/○	○/○	○/○
Tensile	Small	○/○	○/○	○/○	○/○	○/○	○/○	○/○
	Standard				○/	○/	○/	○/
Vickers hardness		○/○	○/○	○/○	○/○	○/○	○/○	○/○
Static Fracture Toughness	Precrack Charpy				○/○	○/○		○/○
	0.5TDCT				○/○	○/○	○/○	○/○
	1T-CT				○/	○/	○/	○/

*: Transition Temperature was not determined.

※: Upper Shelf Energy was not determined.

*1/*2

＊1 : Unirradiated

＊2 : Irradiated

Table 2 Chemical composition of materials used in JAERI

(wt%)

Element / Material	C	Si	Mn	P	S	Cu	Ni	Cr	Mo	V	Al	Specification	Thickness (mm)
JPD	0.19	0.27	1.45	0.006	0.001	0.16	0.10	0.15	0.55	0.01	0.019	(A533B1 - Ni)	30
JPF	0.18	0.27	1.49	0.020	0.001	0.16	0.62	0.15	0.55	0.01	0.010	(A533B1)	30
JPH	0.18	0.27	1.45	0.006	0.001	0.17	1.18	0.15	0.54	0.01	0.021	(A533B1 + Ni)	30
JPI	0.18	0.21	1.50	0.006	0.001	0.01	0.69	0.17	0.57	0.001	0.012	A533B-1	163
JPJ	0.18	0.21	1.41	0.005	0.001	0.05	0.64	0.10	0.50	<0.003	—	A533B-1	250
JFL	0.17	0.25	1.44	0.004	0.002	0.01	0.75	0.20	0.51	0.004	0.016	A508-3	290
JRQ	0.18	0.24	1.42	0.017	0.004	0.14	0.84	0.12	0.51	0.002	0.014	A533B-1	225

Characteristics of Materials

○JPD, JPF and JPH: High Copper and Variation of Nickel, Laboratory Melts

○JPI, JPJ and JFL: Low Sensitivity, Heavy Section Steels

○JRQ: High Sensitivity, Heavy Section Steel for Reference

Table 3 Heat treatment condition of materials used in JAERI

Material	Heat Treatment Conditions
JPD JPF JPH	N: 880 °C×1h+AC, T1: 670 °C×80m+AC
JPI	Q: 880 °C×4h+WC, T1: 670 °C×7.5h+AC, T2: 620 °C×40h+FC
JPJ	Q: 880 °C×7h15m+WC, T1: 655 °C×8h40m AC, T2: 617.5 °C×41h25m+FC
JFL	Q: 880 °C×9h+WC, T1: 640 °C×9h+AC, T2: 610-630 °C×16.5h+FC
JRQ	N: 900 °C×4.5h+AC, Q: 880 °C×13h+WC, T1: 665 °C×12h+AC, T2: 620 °C×40h+FC

Heat Treatments
- N: Normalizing
- Q: Quenching
- T1: Tempering
- T2: Simulated Post Weld Heat Treatment

Cooling Conditions
- AC: Air Cooling
- WC: Water Cooling
- FC: Furnace Cooling

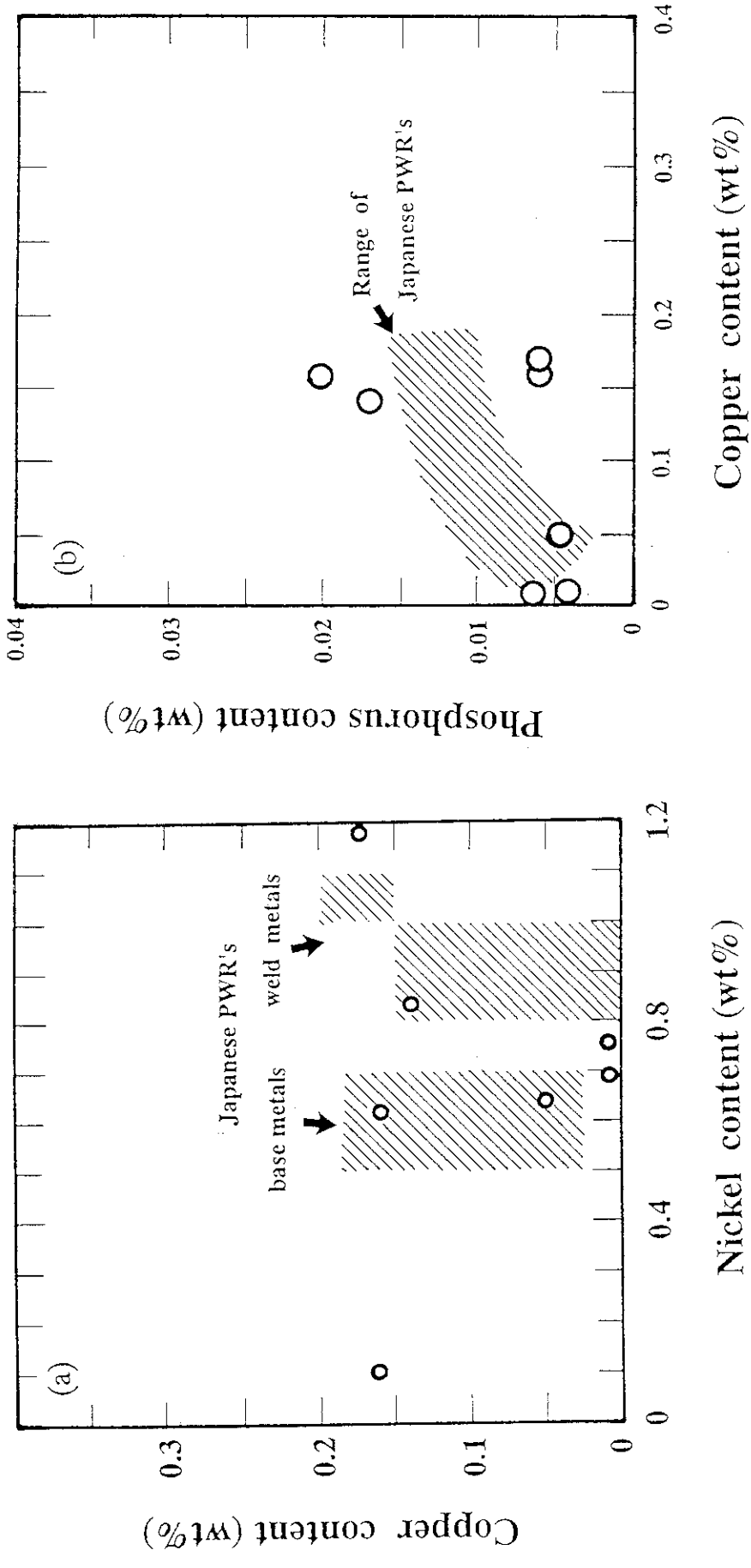

Fig. 1 Copper versus nickel (a) and phosphorus versus copper (b) contents of materials used in the present irradiation experiments. Estimated ranges of the Japanese PWR steels are also drawn as slanting lines.

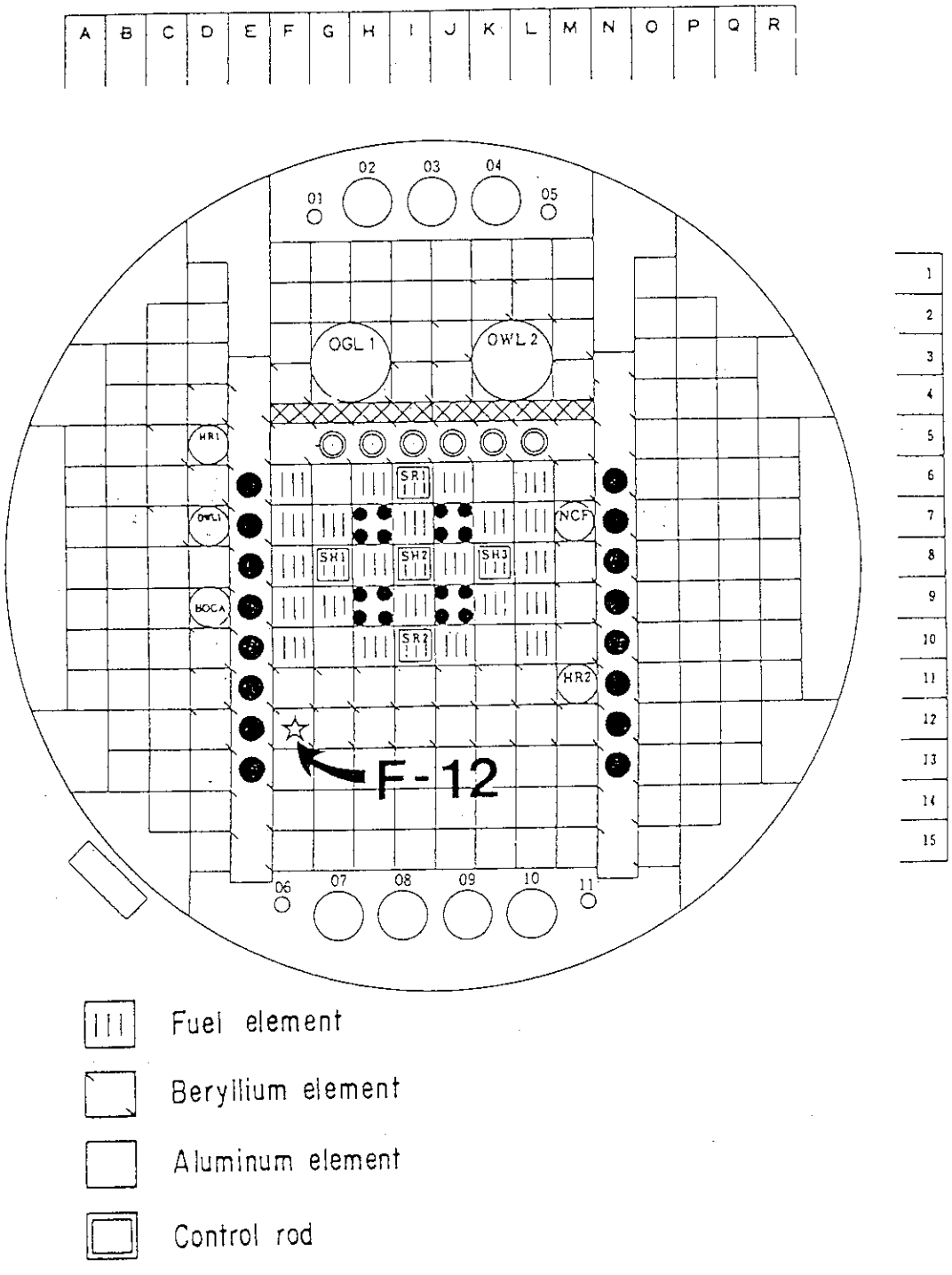

Fig. 2 Core configuration of JMTR.

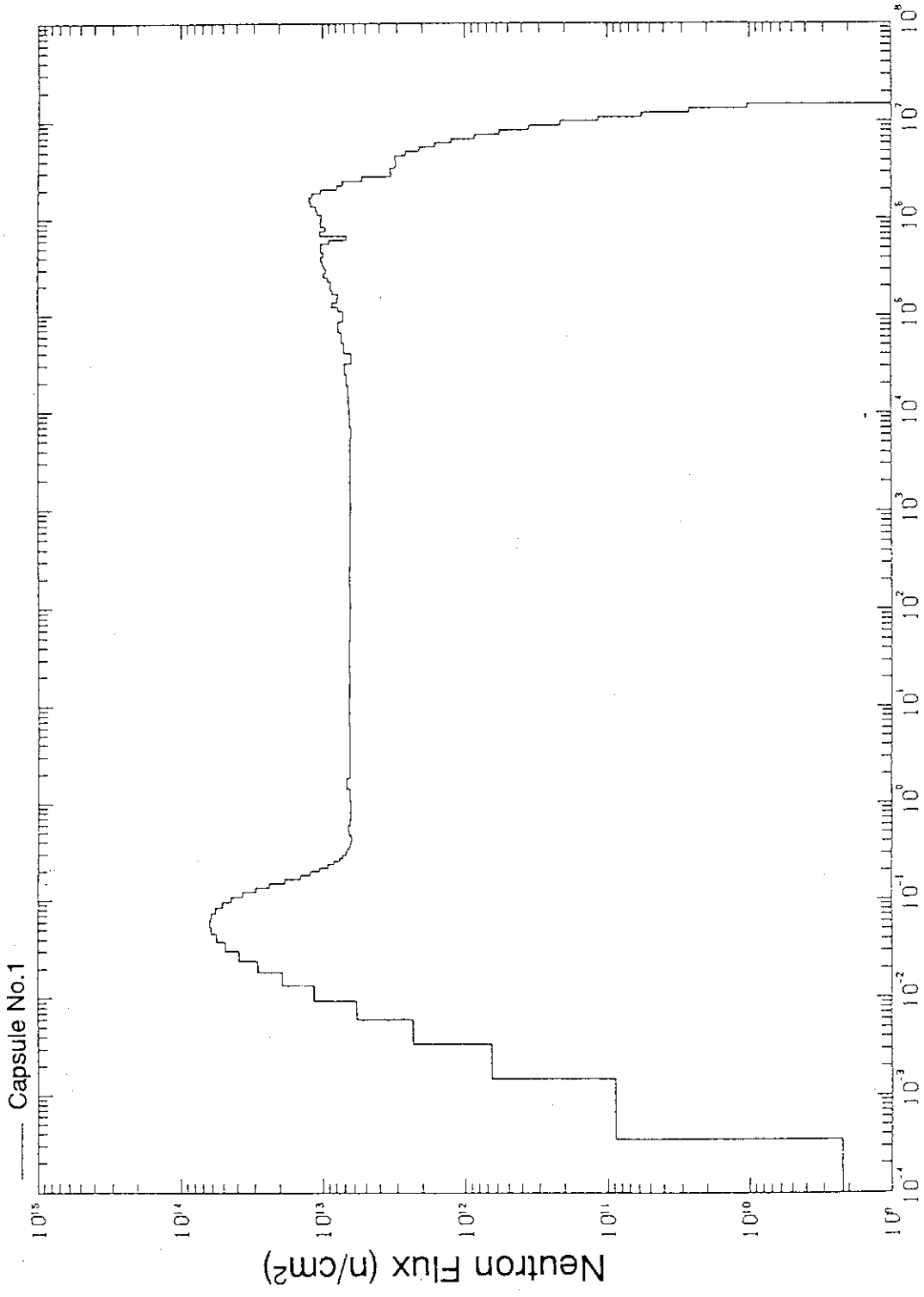

Fig. 3 Typical neutron energy spectrum of a irradiation capsule.

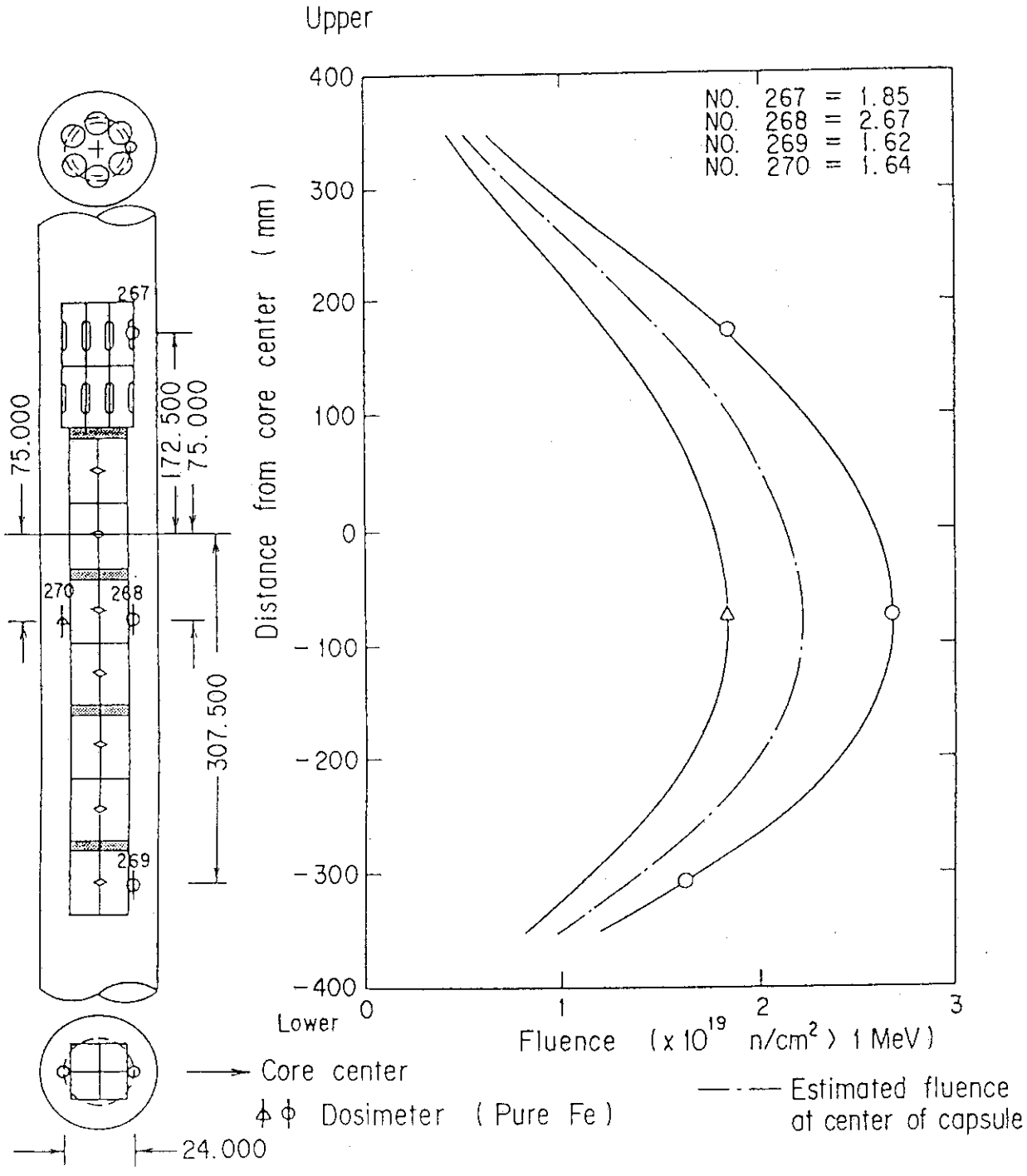

Fig. 4 An example of irradiation capsule arrangement and fast neutron fluence distribution in the axial direction.

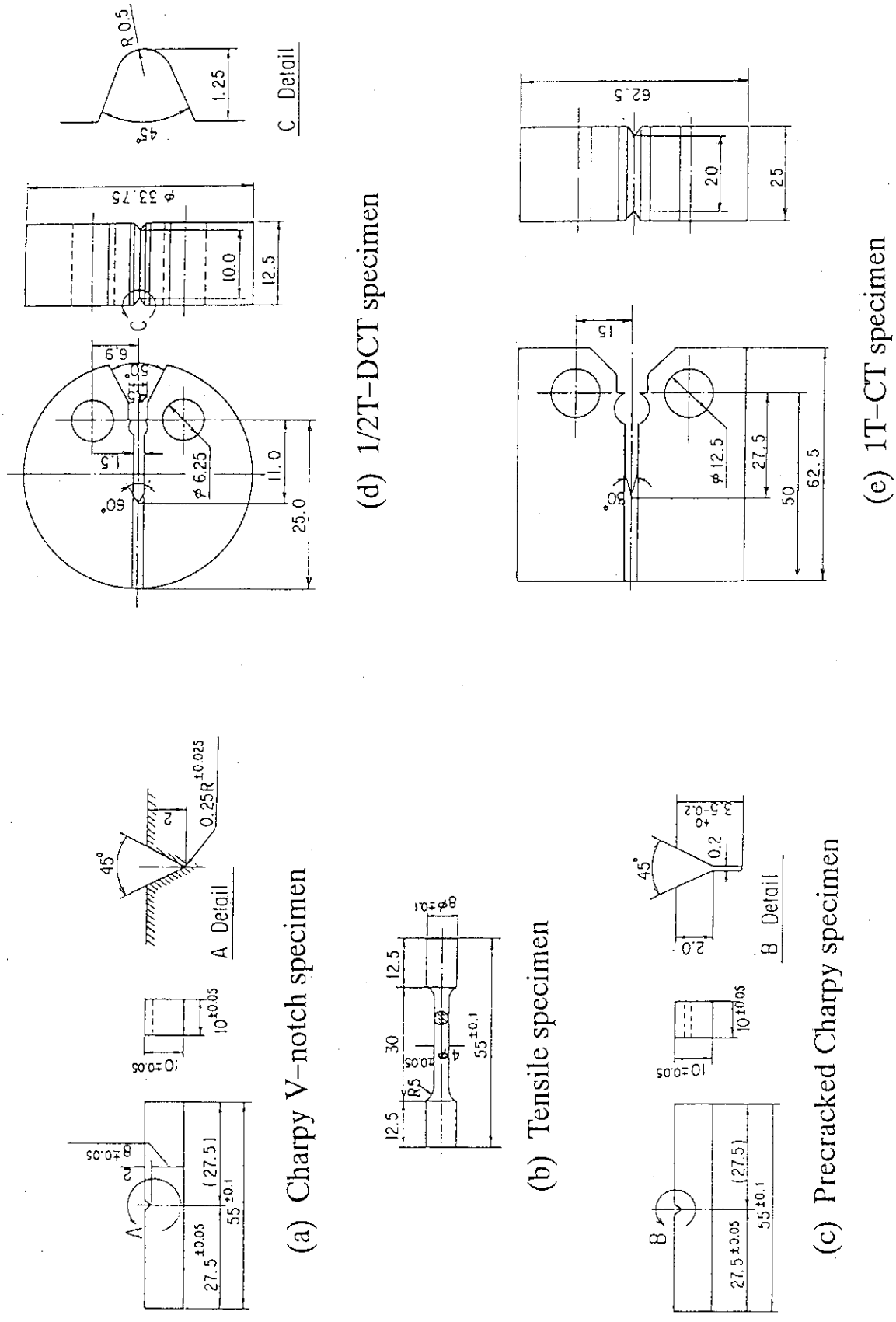

(a) Charpy V－notch specimen

(b) Tensile specimen

(c) Precracked Charpy specimen

(d) 1/2T－DCT specimen

(e) 1T－CT specimen

Fig. 5 Configurations and dimensions of test specimens.

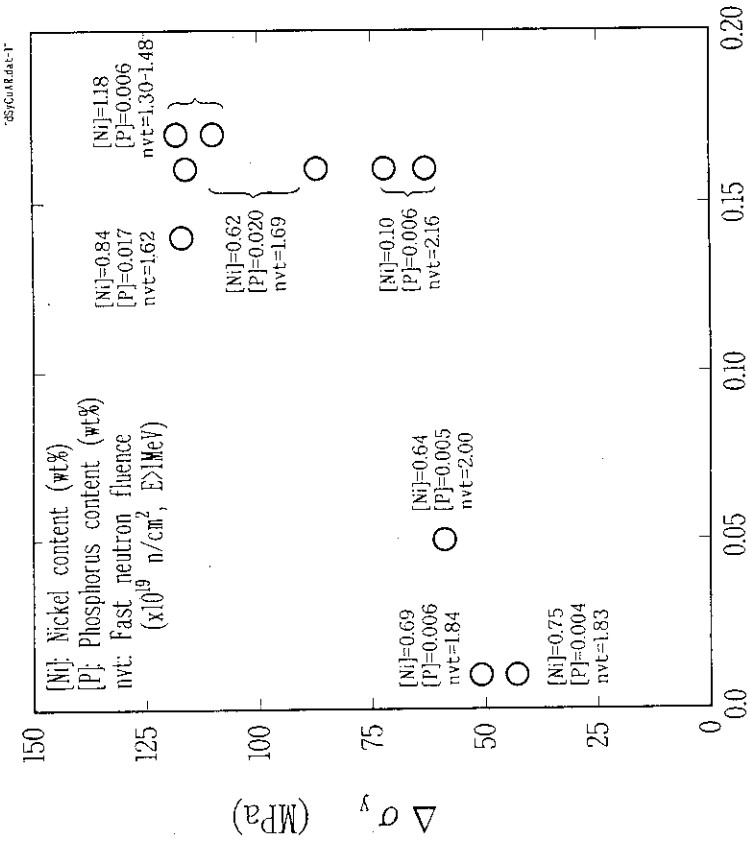

Fig. 7 Effect of Cu content in steel on increase of yield strength.

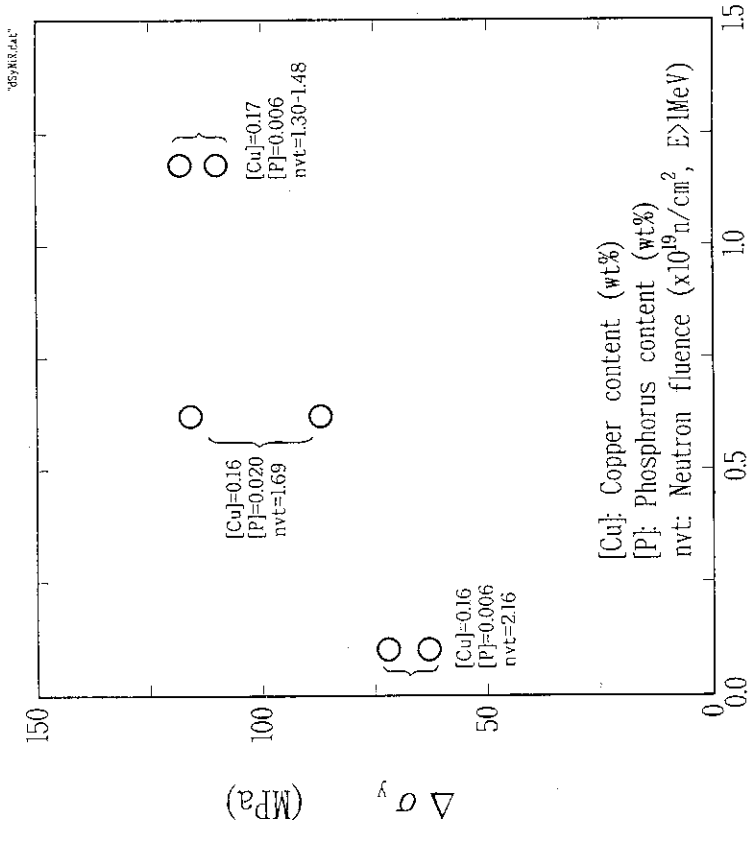

Fig. 6 Effect of Ni content in steel on increase of yield strength.

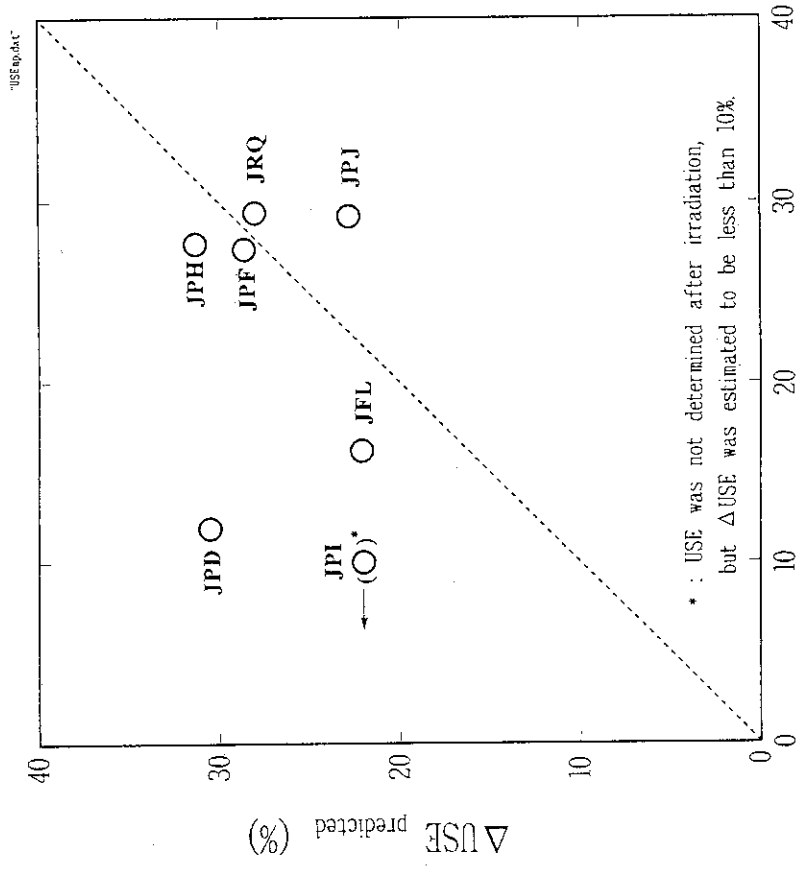

Fig. 9 Comparison of measured decrease of Charpy upper shelf energy and predicted one by USNRC Regulatory Guide 1.99.

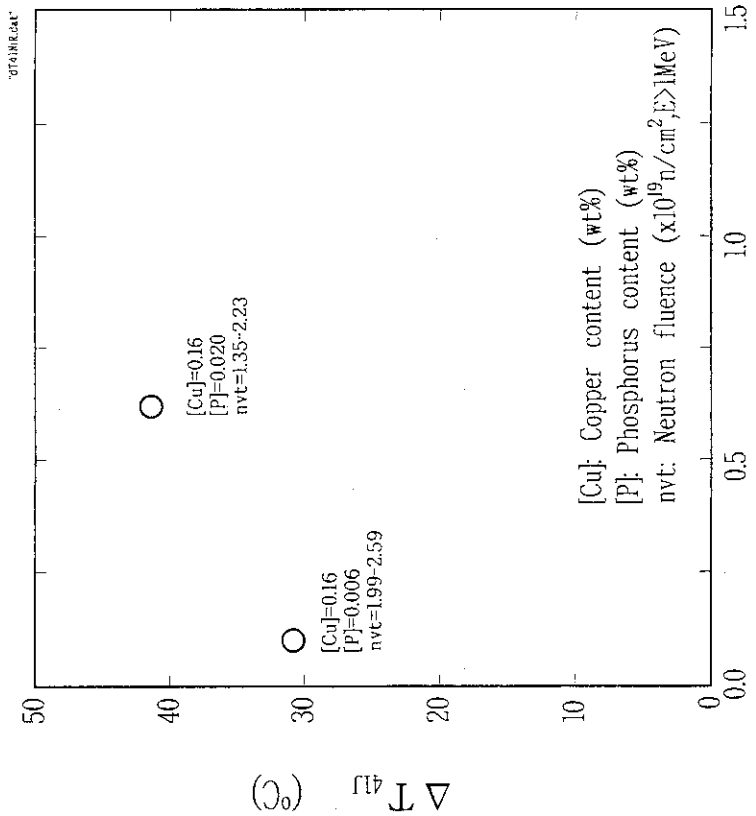

Fig. 8 Effect of Ni content in steel on Charpy 41J shift.

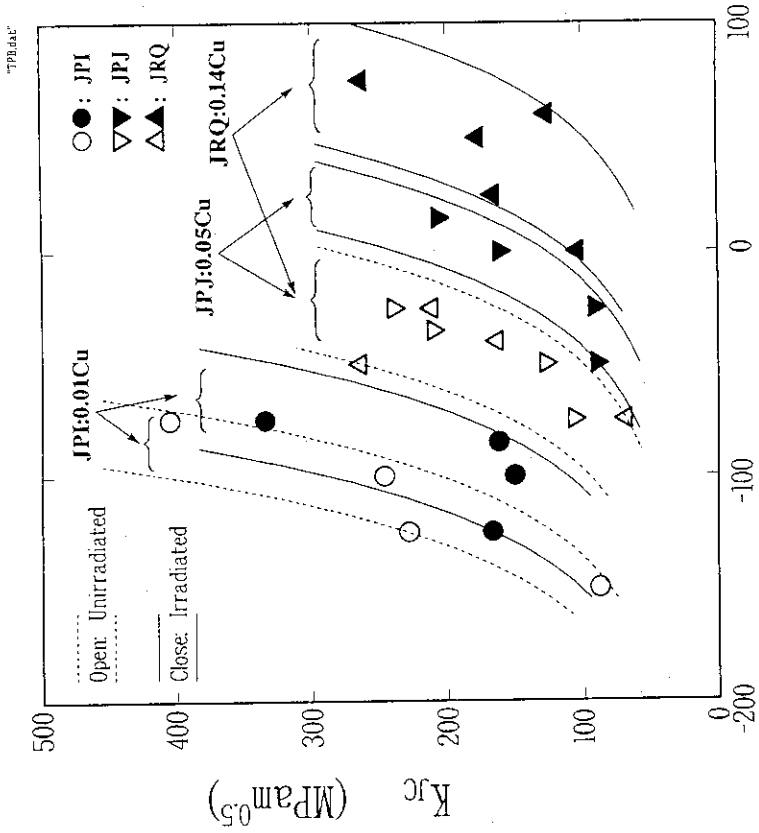

Fig. 11 Fracture toughness values obtained from precracked Charpy type specimens before and after irradiation.

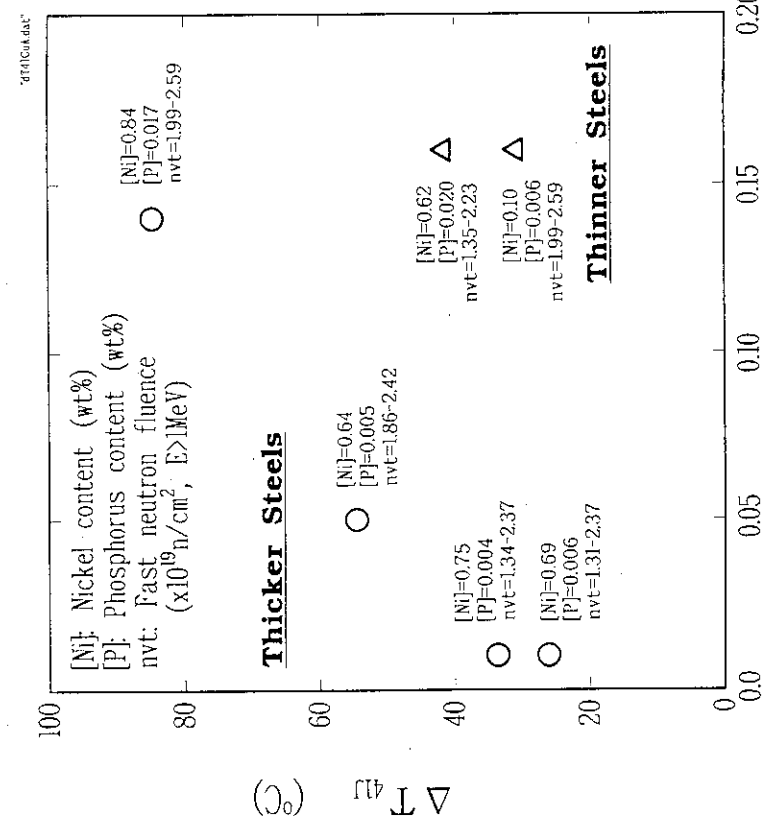

Fig. 10 Effect of Cu content in steel on Charpy 41J shift.

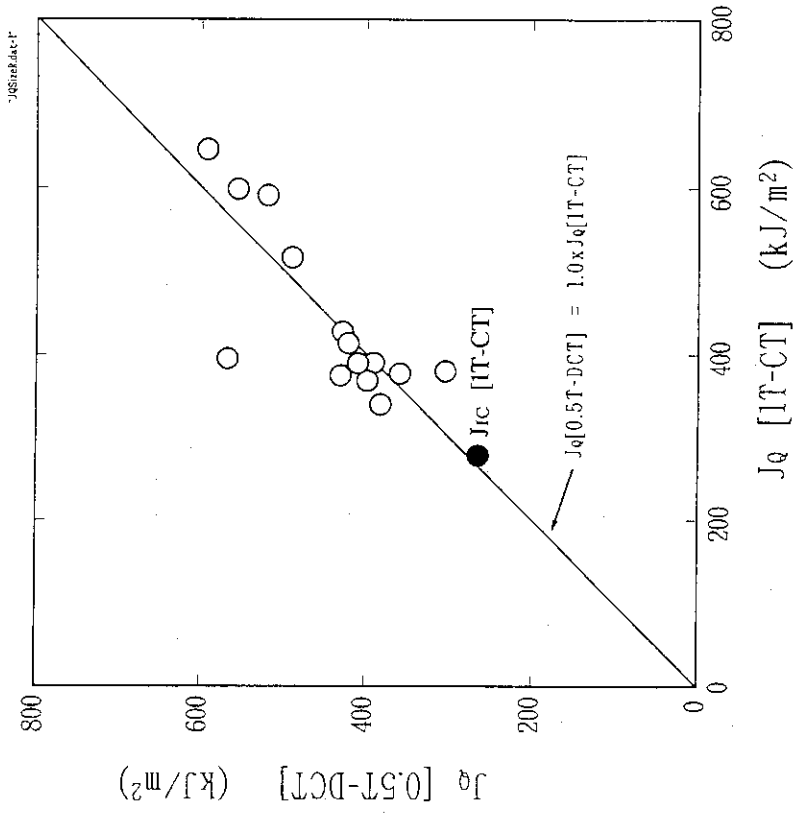

Fig. 13 Size effect on fracture toughness, J_Q, obtained from compact type specimens.

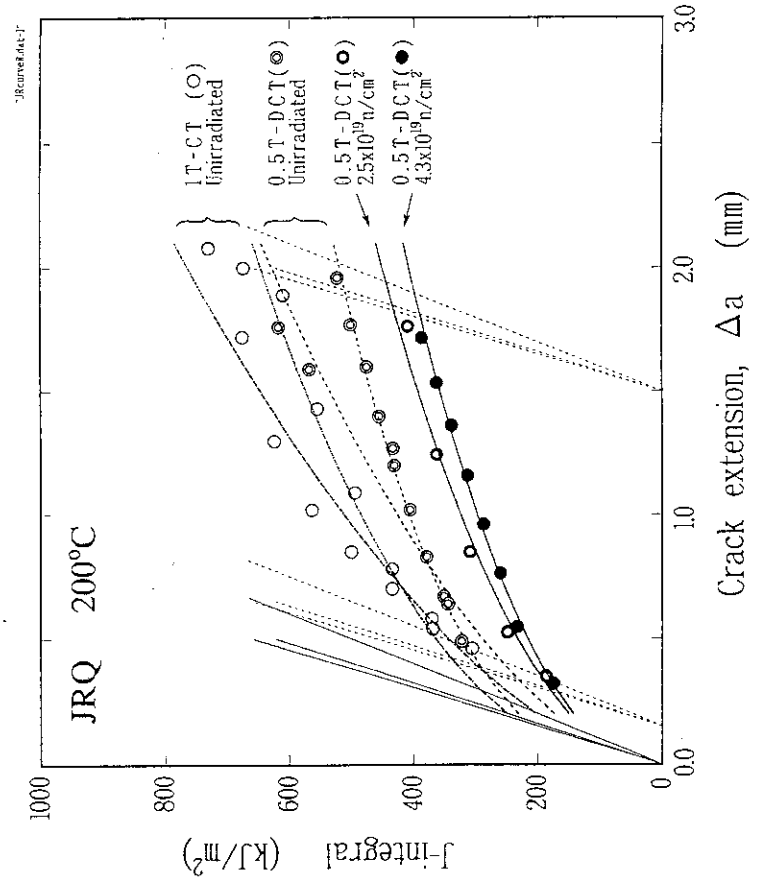

Fig. 12 J－R Curves of JRQ at 200 ℃

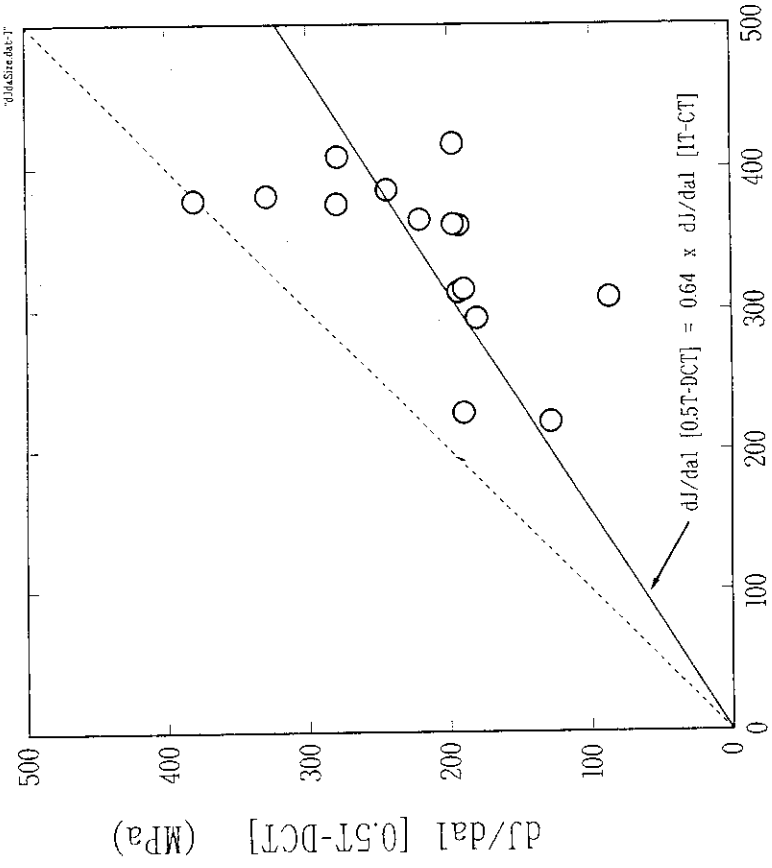

Fig. 15 Size effect on crack growth resistance, dJ/da, obtained by compact type specimens.

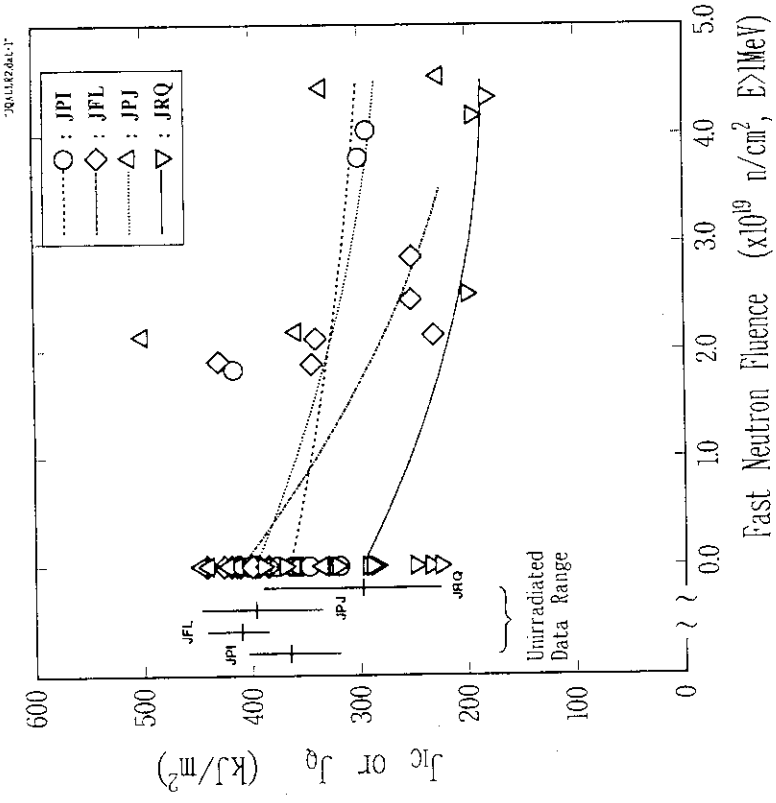

Fig. 14 Decrease of upper shelf fracture toughness as a function of fast neutron fluence.

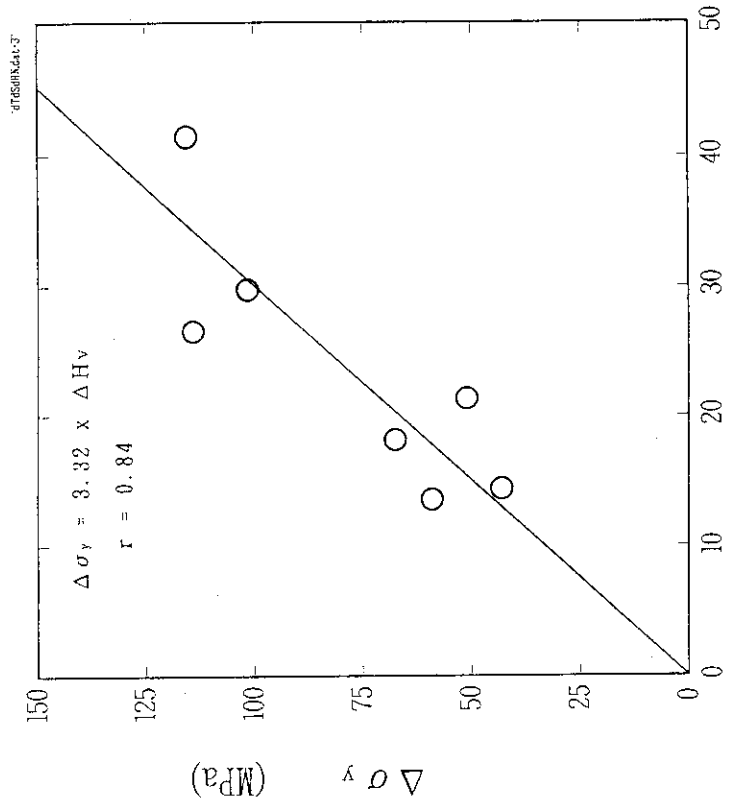

Fig. 17 Correlation between the increases of yield strength and Vickers hardness by irradiation

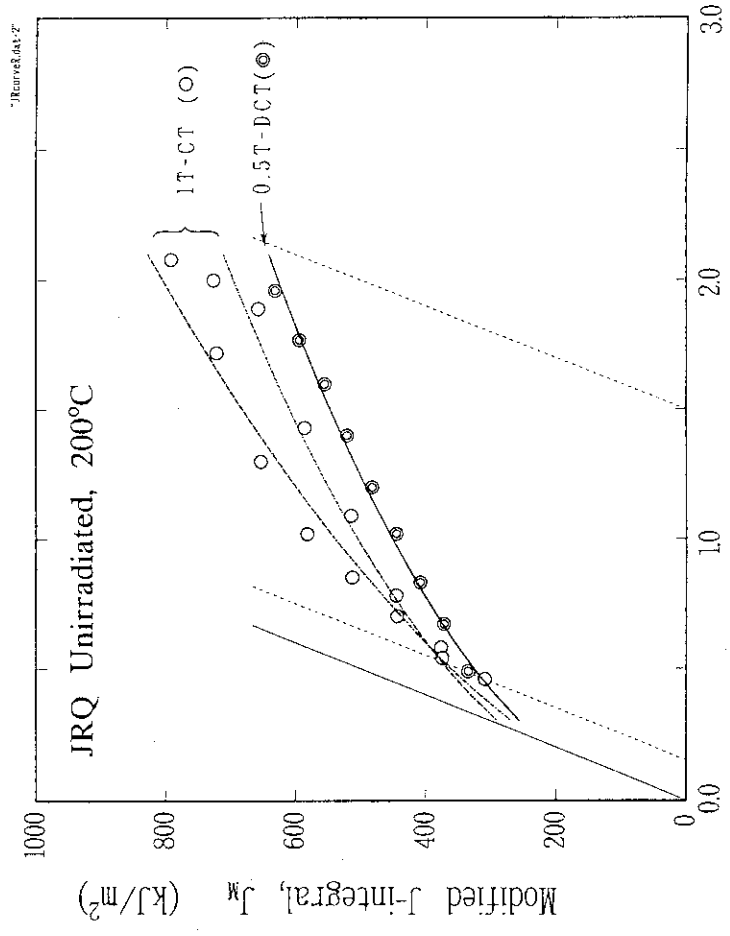

Fig. 16 J_M－R curves of unirradiated JRQ at 200 ℃

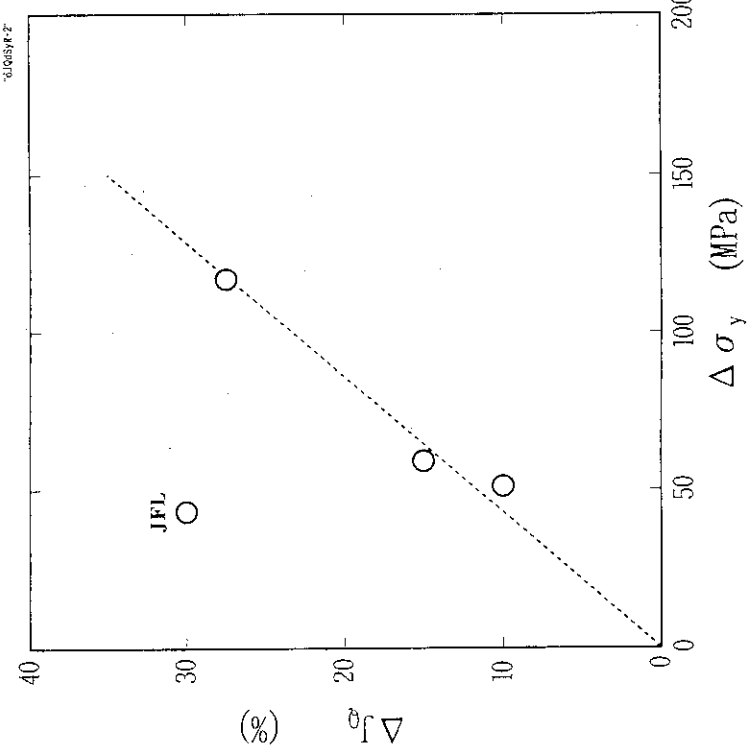

Fig. 19 Correlation between the percentage decrease of fracture toughness and increase of yield strength by irradiation

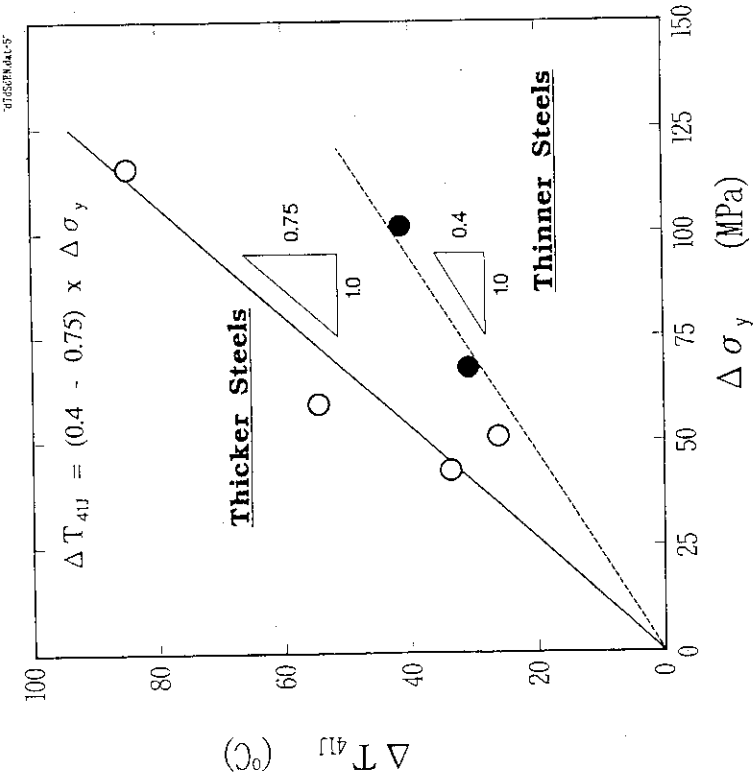

Fig. 18 Correlation between Charpy 41J shift and increase of yield strength by irradiation

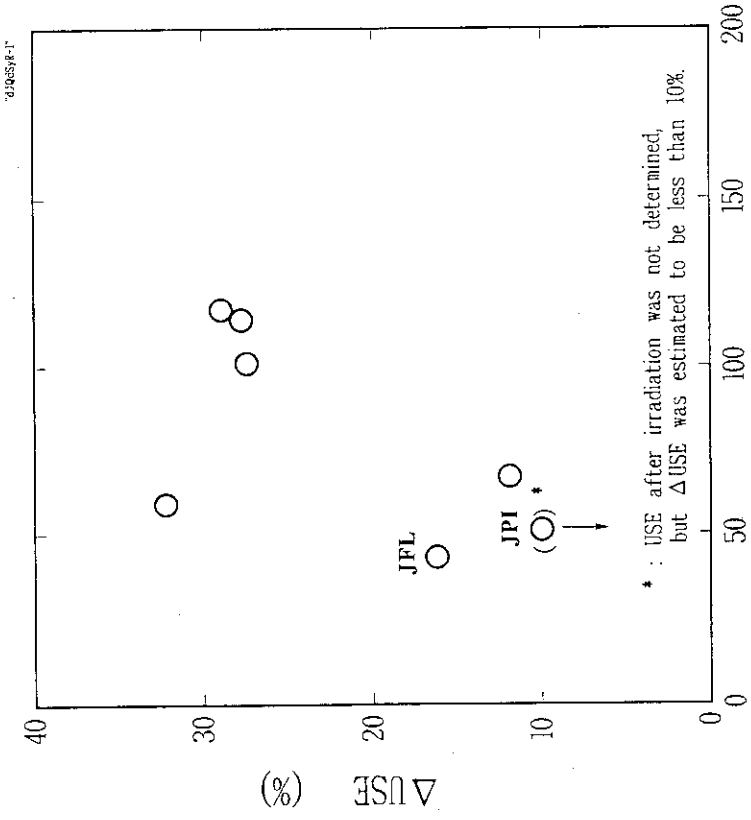

Fig. 20 Correlation between the percentage decrease of USE and increase of yield strength by irradiation

APPENDIX A

Fast and Thermal Neutron Fluence Distributions in Irradiation Capsules

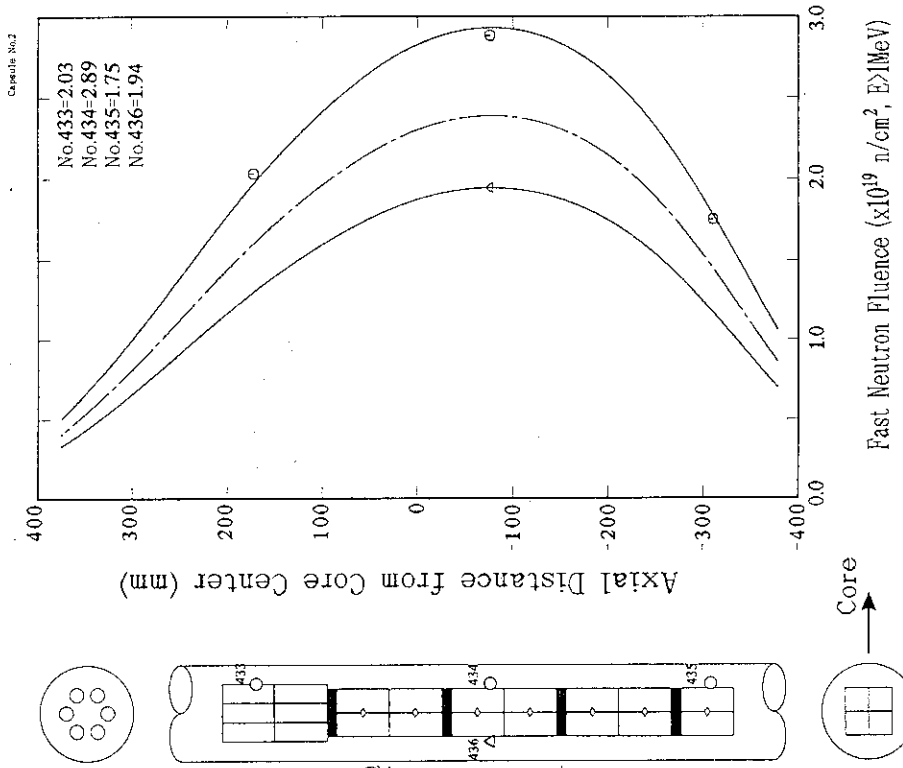

Figure A－2　Fast Neutron Fluence Distribution in the Axial Position of Irradiation Capsule No.2.

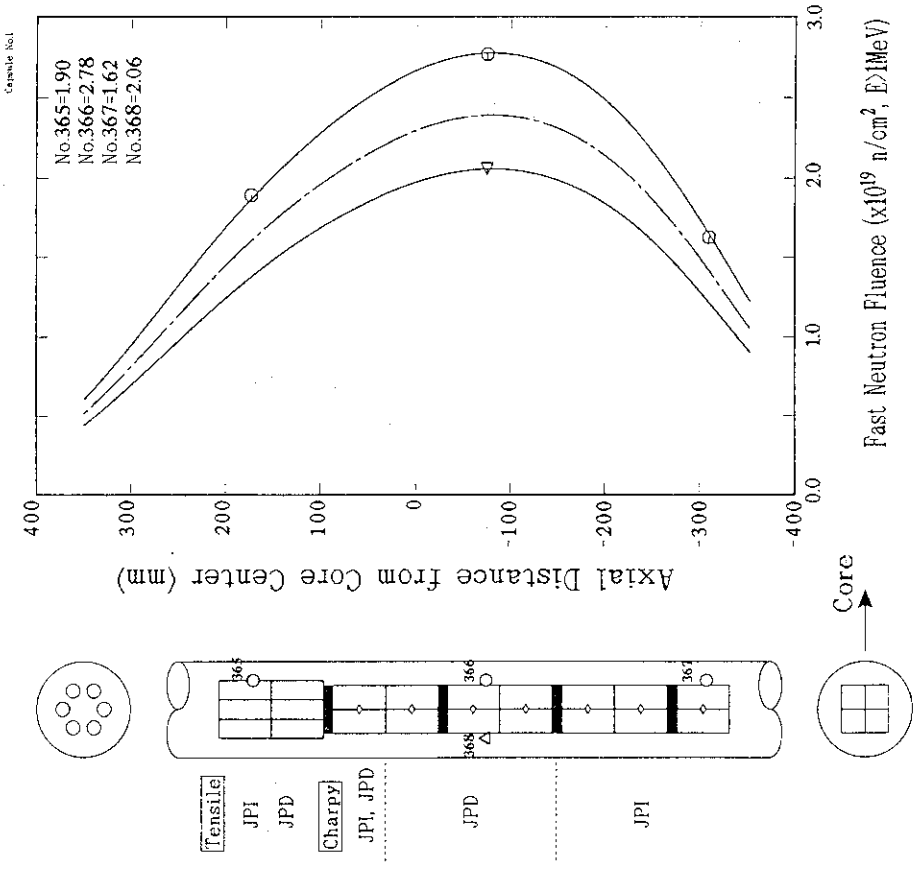

Figure A－1　Fast Neutron Fluence Distribution in the Axial Position of Irradiation Capsule No.1.

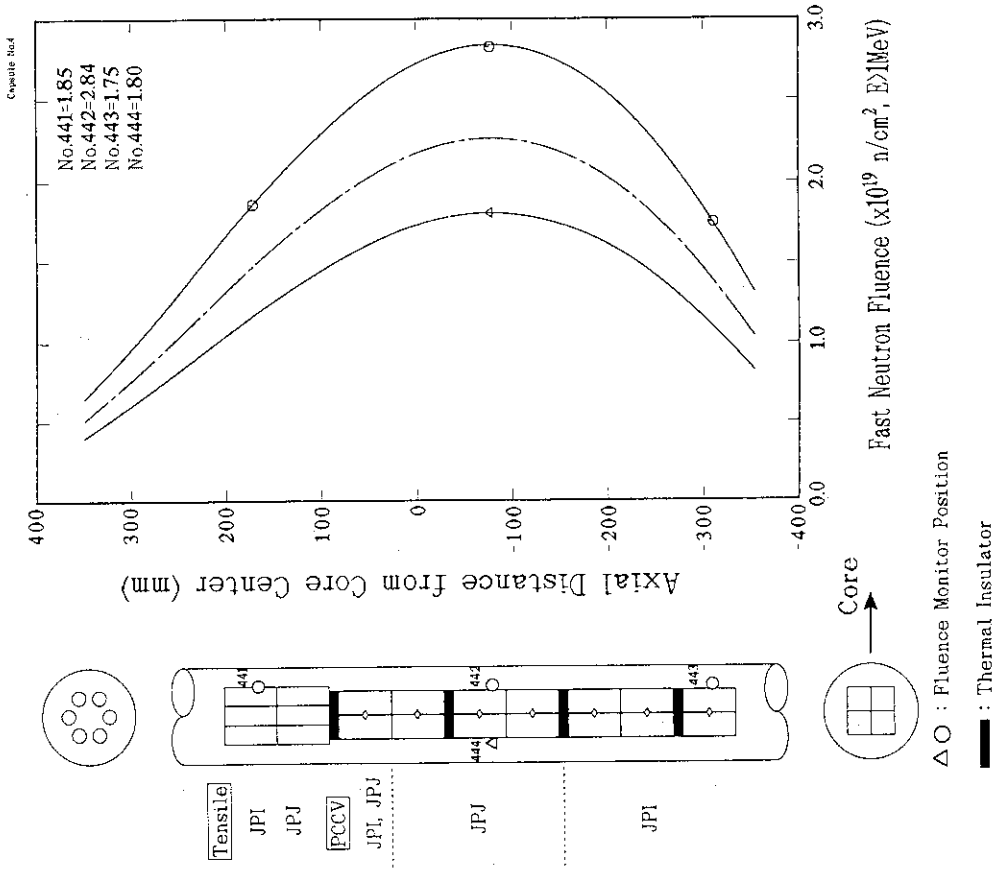

Figure A－4　Fast Neutron Fluence Distribution in the Axial Position of Irradiation Capsule No.4.

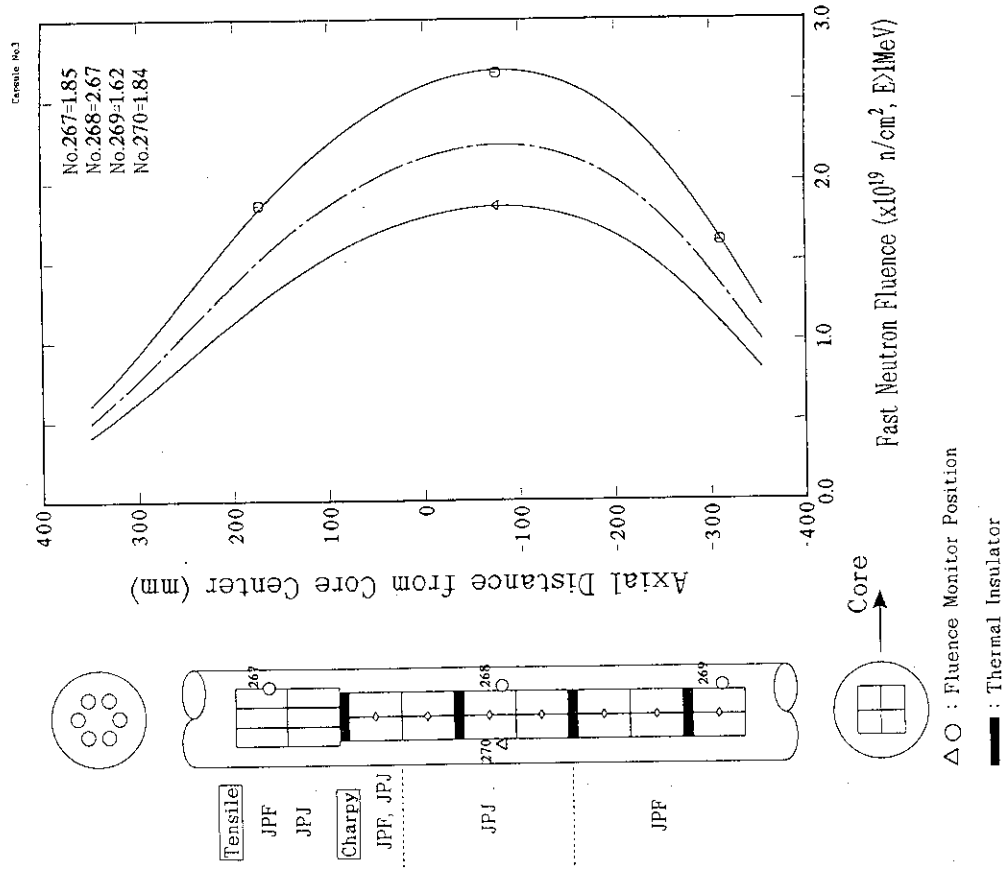

Figure A－3　Fast Neutron Fluence Distribution in the Axial Position of Irradiation Capsule No.3.

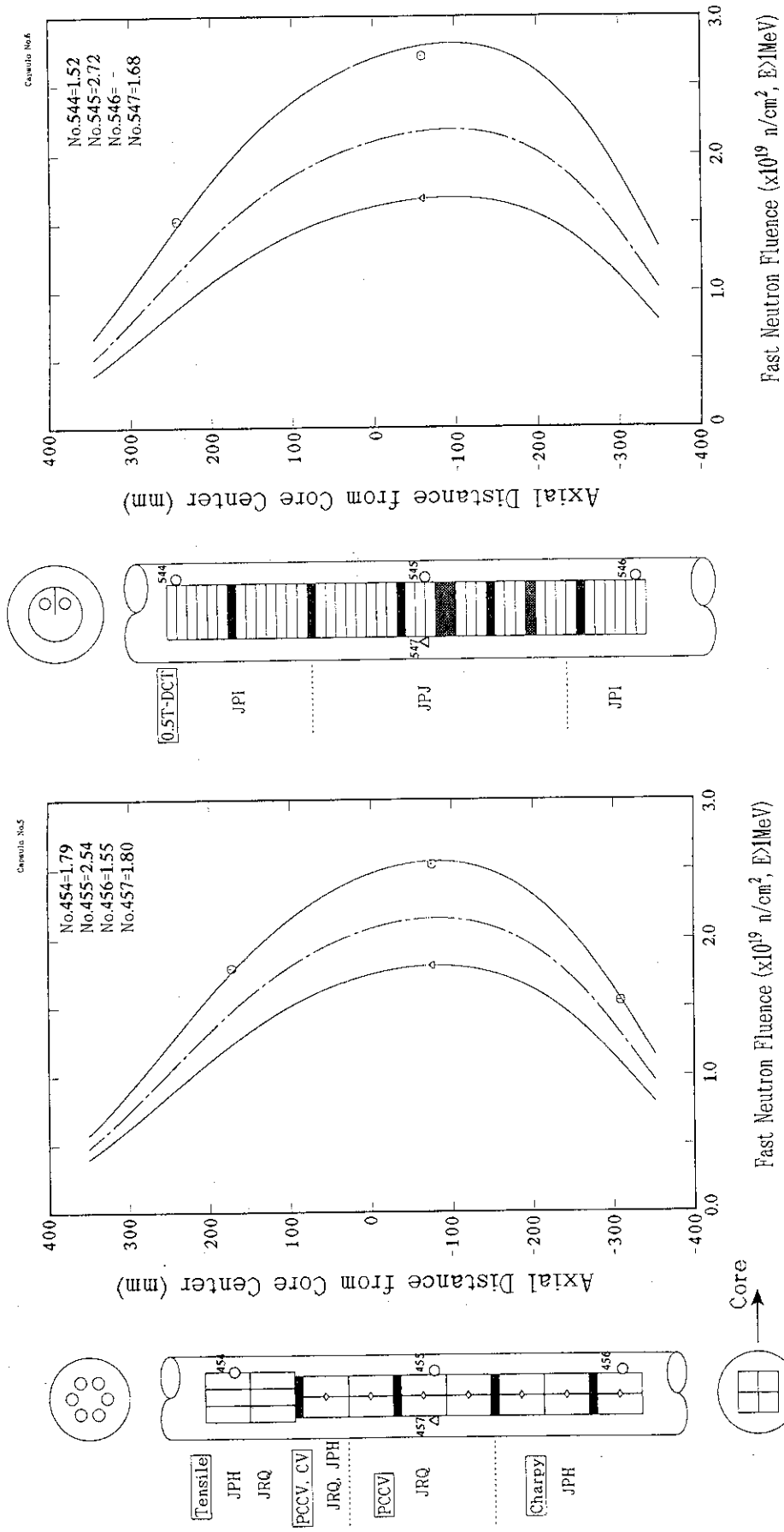

Figure A－5 Fast Neutron Fluence Distribution in the Axial Position of Irradiation Capsule No.5.

Figure A－6 Fast Neutron Fluence Distribution in the Axial Position of Irradiation Capsule No.6.

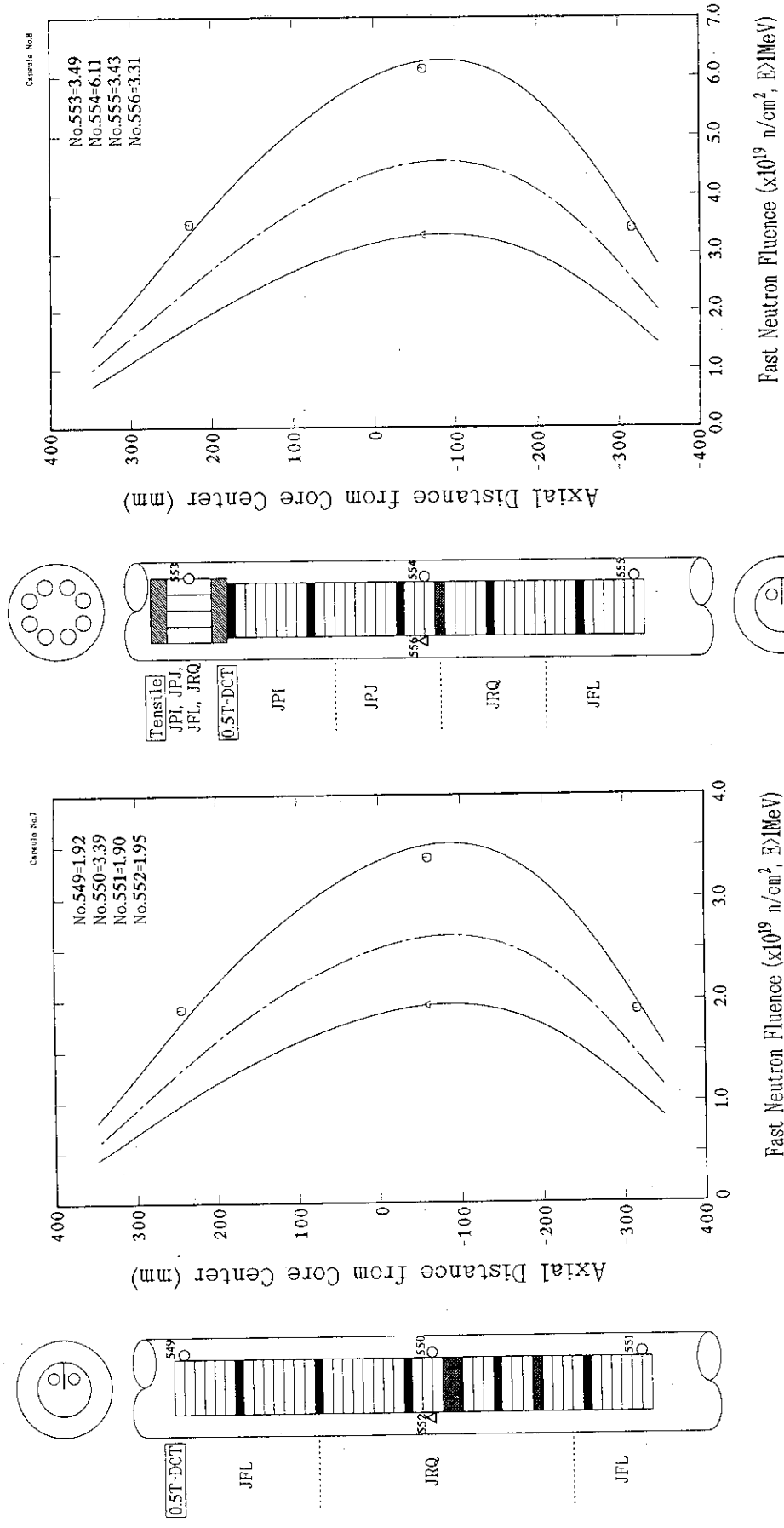

Figure A－7 Fast Neutron Fluence Distribution in the Axial Position of Irradiation Capsule No.7.

Figure A－8 Fast Neutron Fluence Distribution in the Axial Position of Irradiation Capsule No.8.

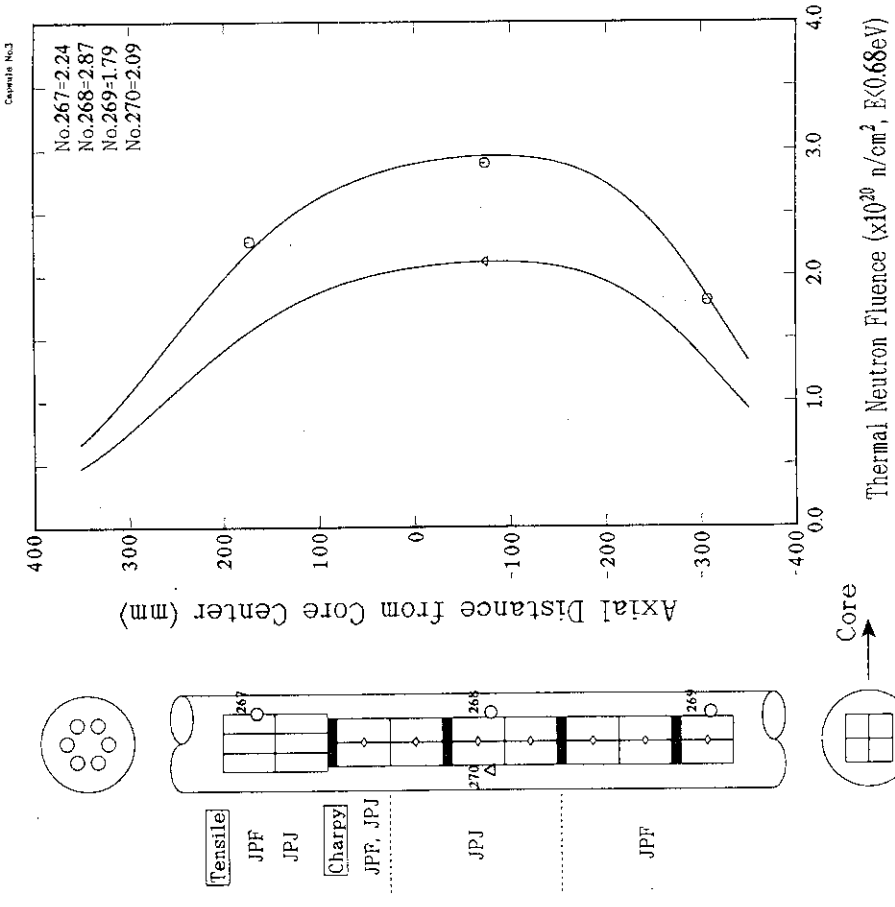

Figure A－9 Thermal Neutron Fluence Distribution in the Axial Position of Irradiation Capsule No.3.

APPENDIX B

Measured Temperature during Irradiation

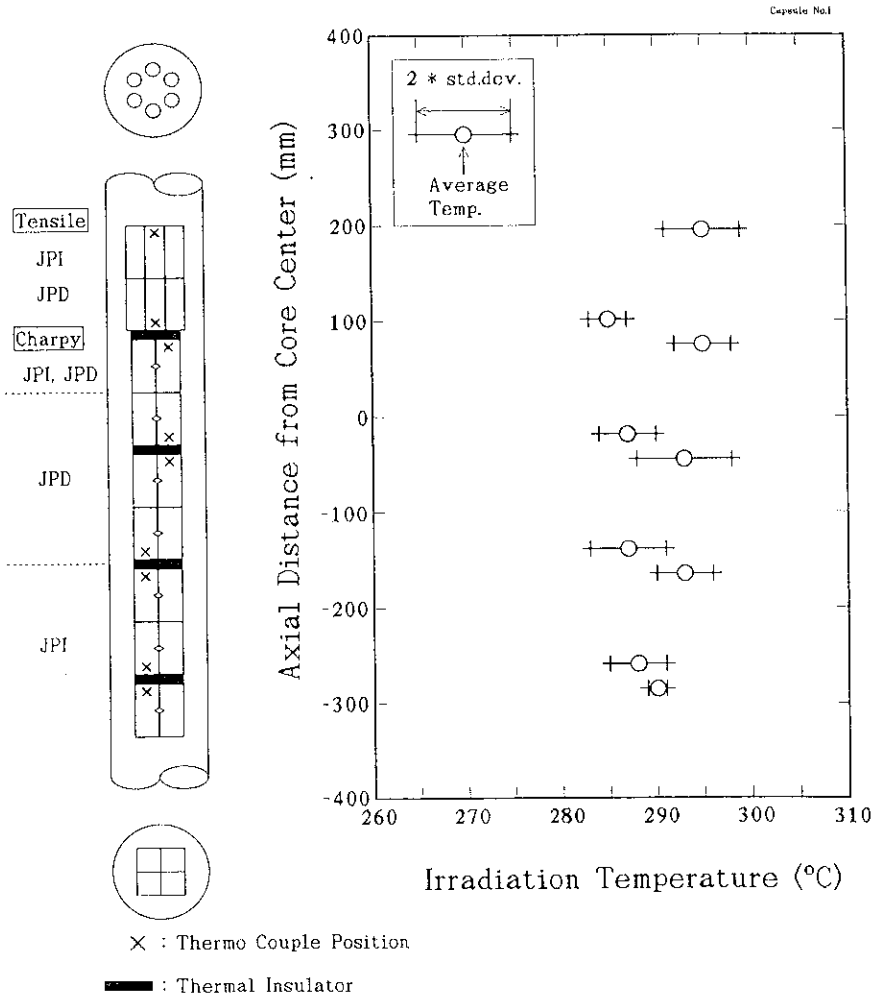

Figure B-1 Irradiation Temperature Range in the Irradiation Capsule No.1.

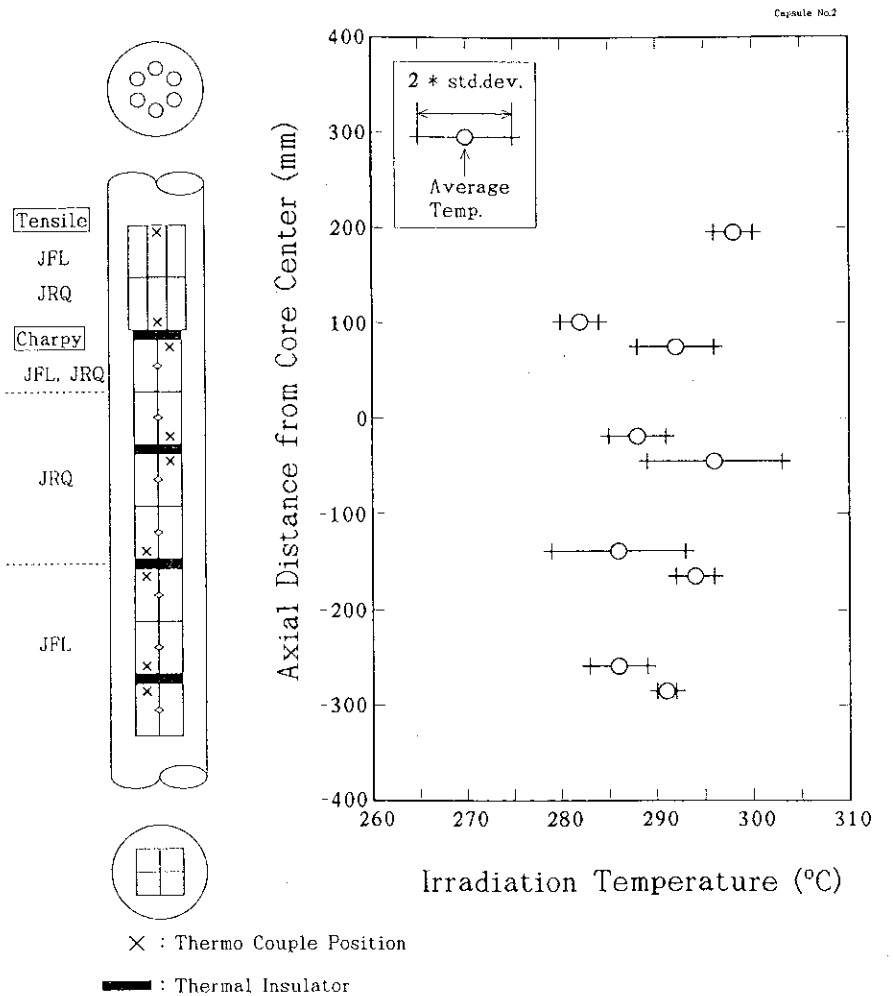

Figure B-2 Irradiation Temperature Range in the Irradiation Capsule No.2.

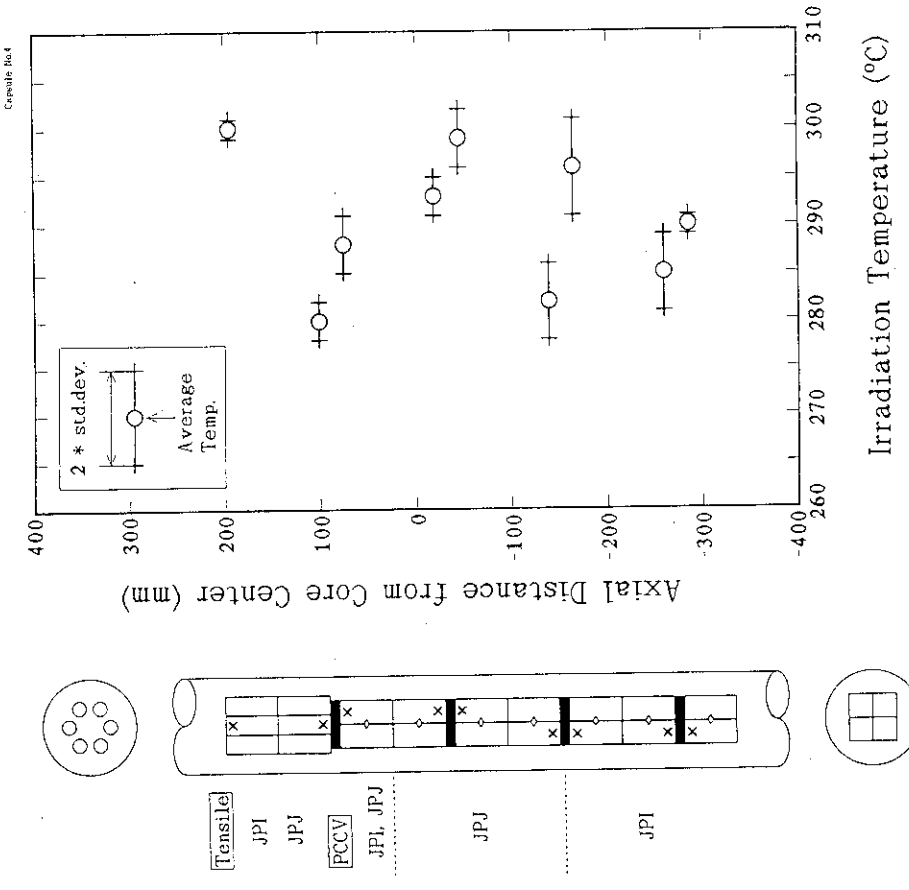

Figure B－4　Irradiation Temperature Range in the Irradiation Capsule No.4.

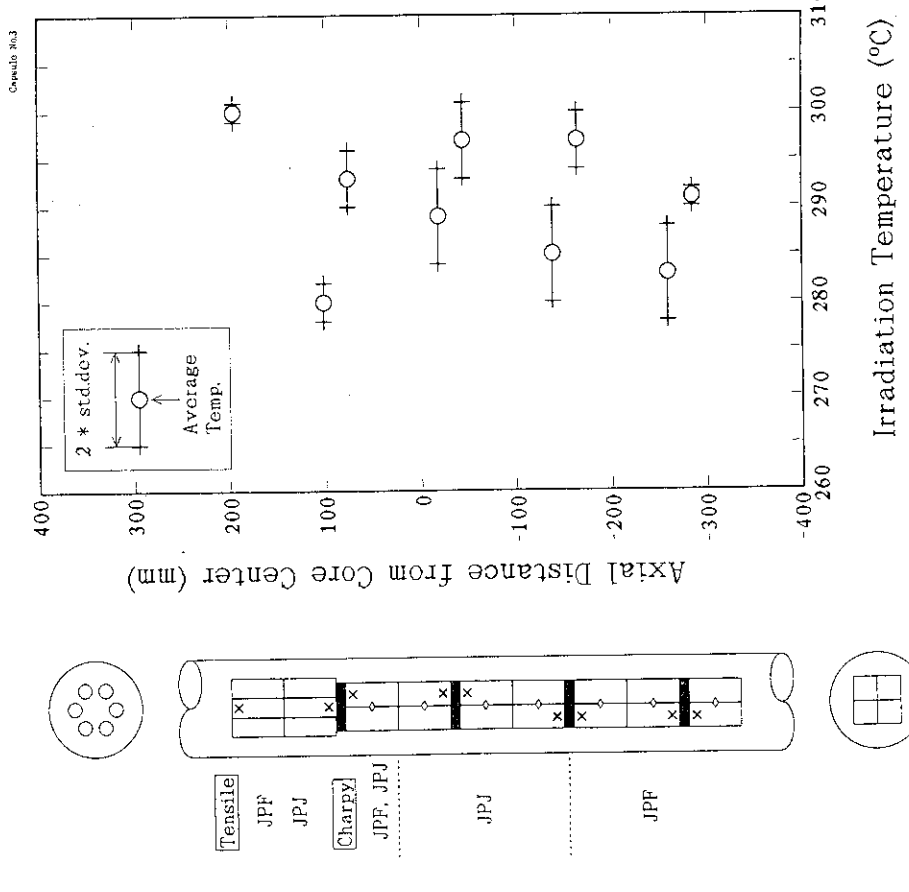

Figure B－3　Irradiation Temperature Range in the Irradiation Capsule No.3.

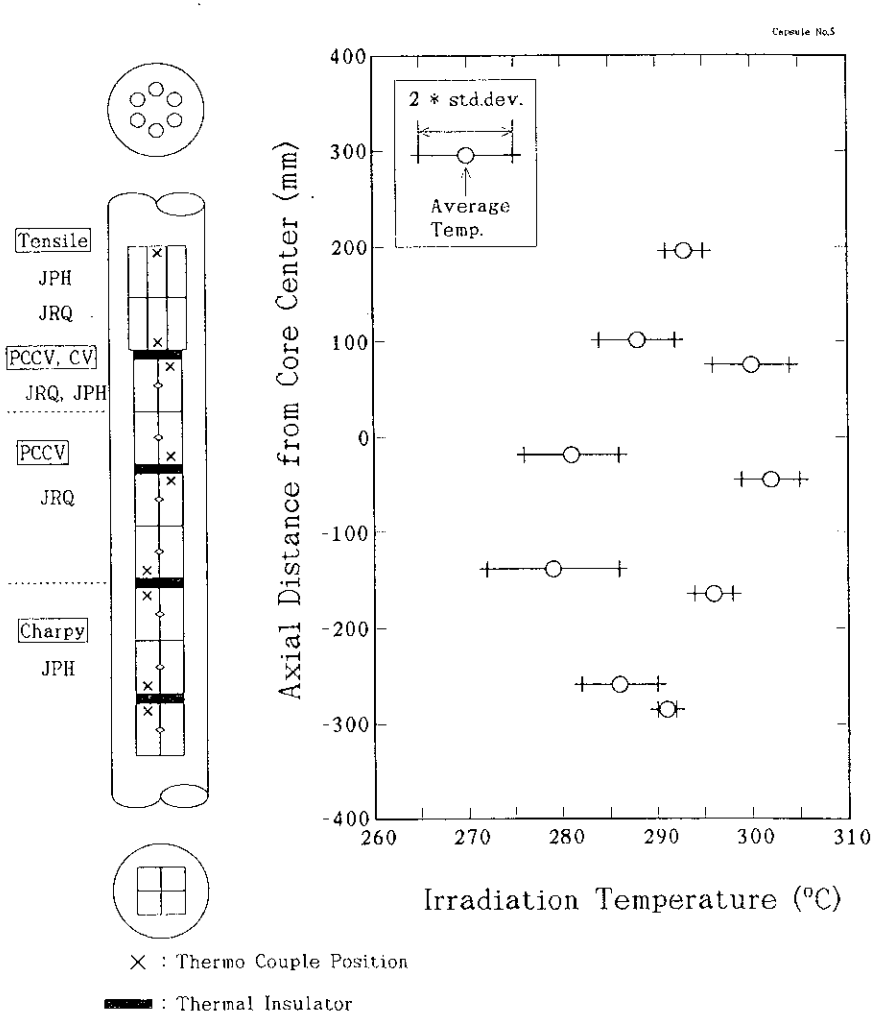

Figure B–5 Irradiation Temperature Range in the Irradiation Capsule No.5.

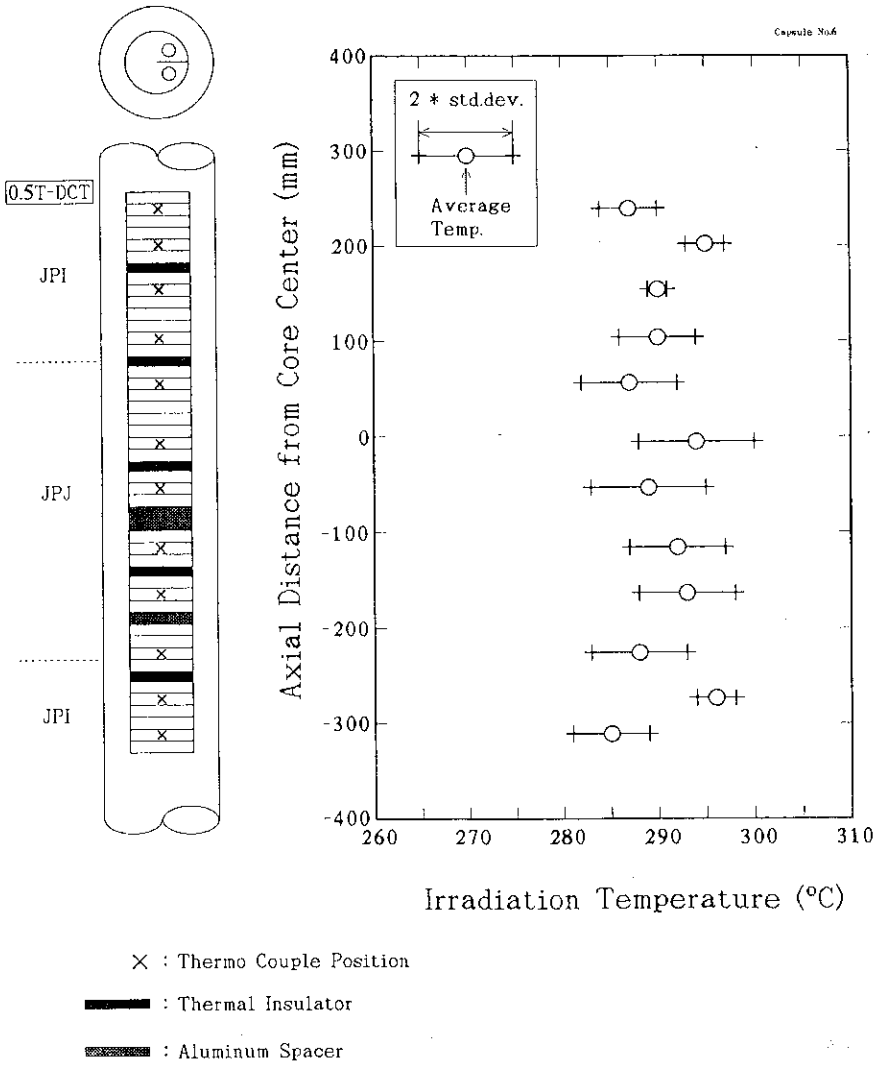

Figure B–6 Irradiation Temperature Range in the Irradiation Capsule No.6.

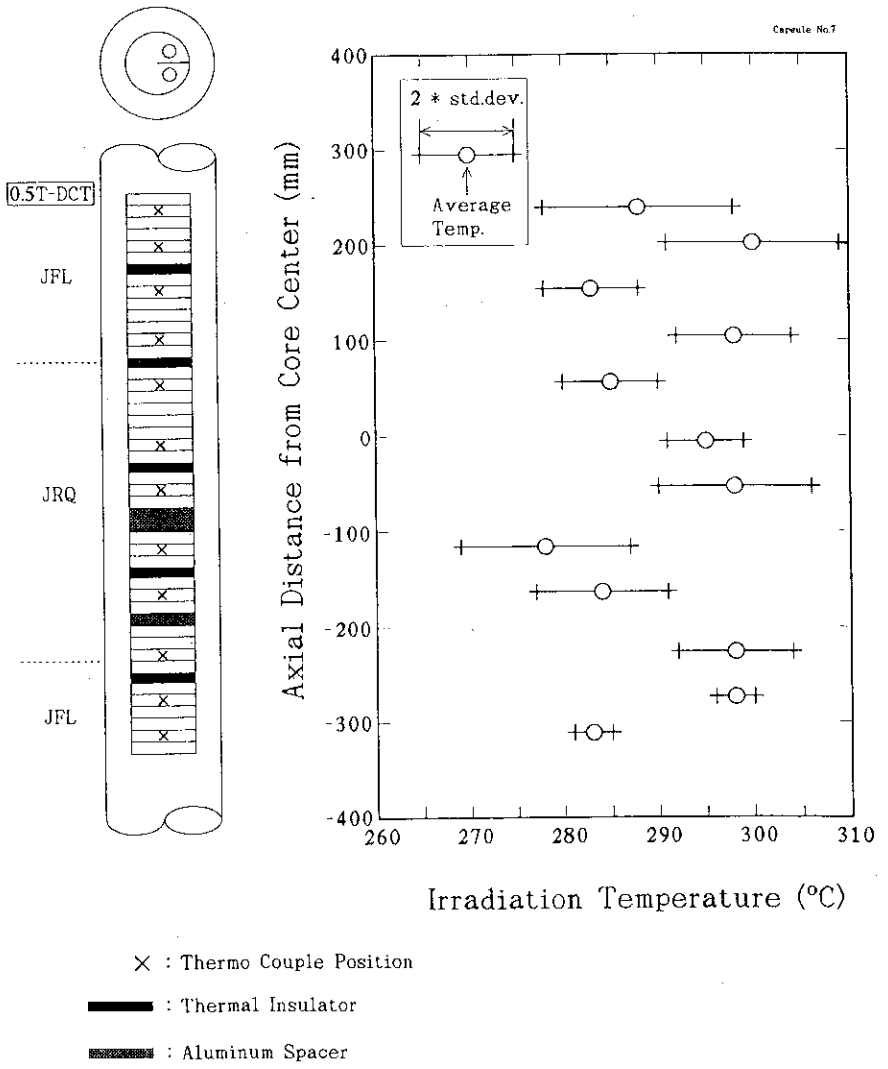

Figure B–7 Irradiation Temperature Range in the Irradiation Capsule No.7.

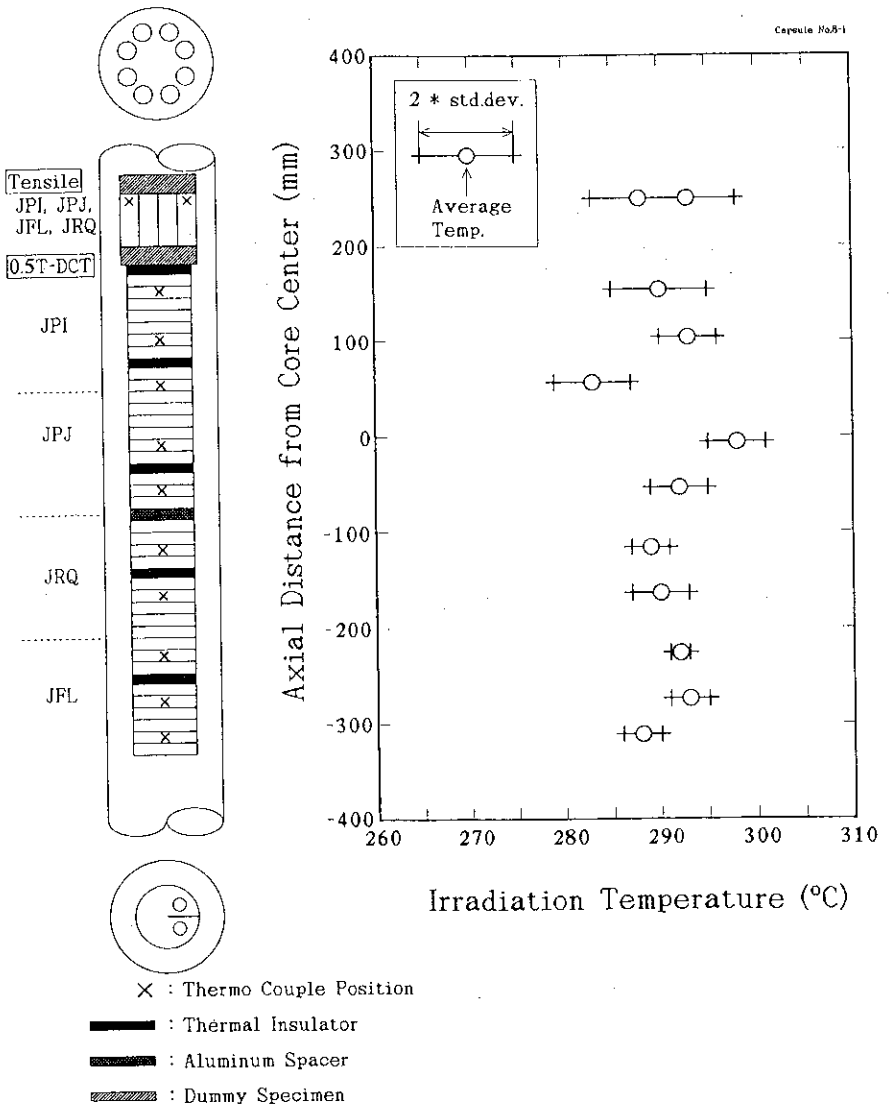

Figure B–8 Irradiation Temperature Range in the Irradiation Capsule No.8 (First Cycle)

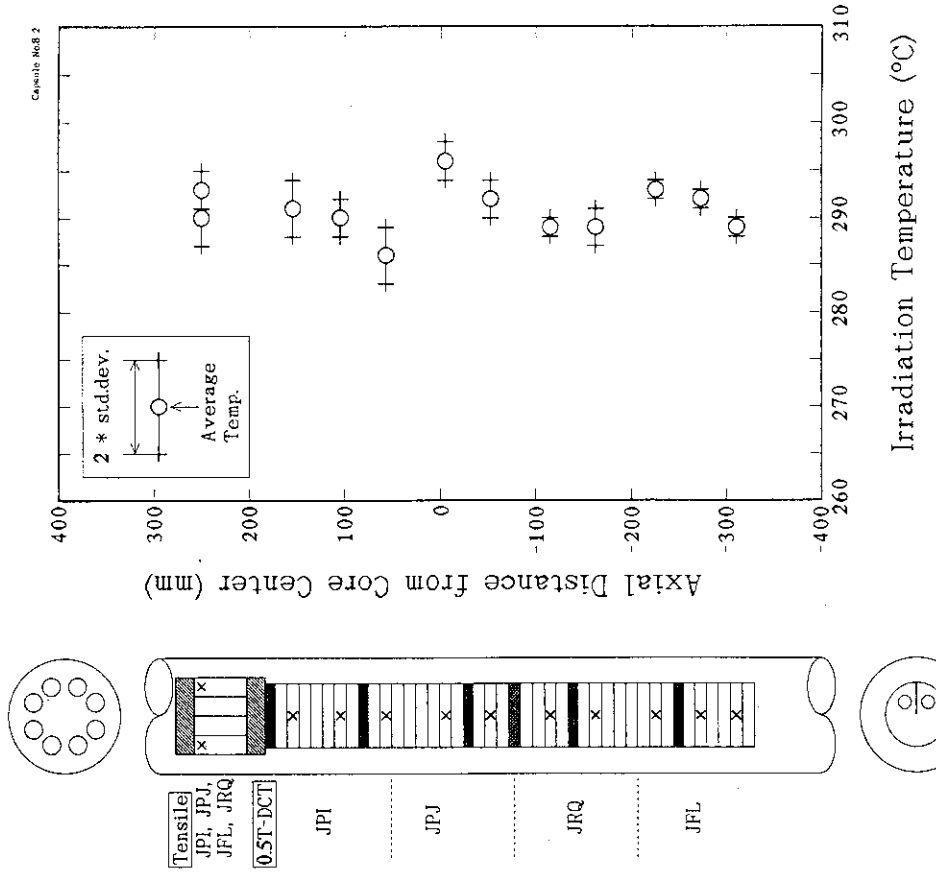

Figure B－9 Irradiation Temperature Range in the Irradiation Capsule No.8 (Second Cycle)

APPENDIX C

Tensile Test Results of All Materials

Table C-1 Summary of tensile properties for laboratory melts.

Material	Item \ Stress (MPa)		Test Temperature (°C)					Irrad. Temp. (°C)
			-50	R T	100	200	290	
JPD Cu:0.16 P:0.006 Ni:0.10	Yield	Unirrad.	476	444	428	398	359	285±2
		Increase	72	67	48	55	83	
	Ultimate	Unirrad.	634	572	543	556	594	
		Increase	54	62	56	58	40	
	Elong. (%)	Unirrad.	28.3	25.8	22.7	22.6	23.0	
		Irrad.	27.0	24.6	20.2	21.5	24.0	
	Fluence* (E>1MeV)		1.89	2.16	1.89	1.66	1.66	
JPF Cu:0.16 P:0.020 Ni:0.62	Yield	Unirrad.	538	497	465	453	457	300±1
		Increase	96	101	105	121	78	
	Ultimate	Unirrad.	683	620	582	605	646	
		Increase	86	96	103	79	55	
	Elong. (%)	Unirrad.	22.9	20.8	18.6	18.3	22.0	
		Irrad.	22.6	20.2	18.7	18.7	21.0	
	Fluence* (E>1MeV)		1.48	1.69	1.48	1.30	1.30	
JPH Cu:0.17 P:0.006 Ni:1.18	Yield	Unirrad.	554	511	490	461	461	293±2
		Increase	124	114	108	95	99	
	Ultimate	Unirrad.	695	634	608	610	651	
		Increase	101	99	97	83	63	
	Elong. (%)	Unirrad.	23.7	22.0	19.1	17.9	22.0	
		Irrad.	20.3	18.6	18.4	17.5	20.7	
	Fluence* (E>1MeV)		1.30	1.39	1.68	1.68	1.48	

Fluence*:Fast Neutron Fluence ($\times 10^{19}$ n/cm^2, E>1MeV)

Table C-2 Summary of tensile properties for heavy section steels.

Material	Item \ Stress (MPa)		Test Temperature (°C) -50	R T	100	200	290	Irrad. Temp. (°C)
JPI Cu:0.01 P:0.004 Ni:0.69	Yield	Unirrad.	523	481	458	443	422	295±4
		Increase	49	51	42	37	50	
	Ultimate	Unirrad.	670	604	569	580	593	
		Increase	33	40	36	31	50	
	Elong. (%)	Unirrad.	21.6	21.6	18.0	19.3	20.2	
		Irrad.	21.2	21.2	19.0	17.8	19.7	
	Fluence* (E>1MeV)		1.61	1.84	1.61	1.42	1.42	
JPJ Cu:0.05 P:0.005 Ni:0.64	Yield	Unirrad.	445	405	384	355	365	280±2
		Increase	60	59	50	49	32	
	Ultimate	Unirrad.	609	545	507	500	541	
		Increase	36	41	41	44	25	
	Elong. (%)	Unirrad.	26.8	24.8	22.5	21.0	21.6	
		Irrad.	25.8	23.5	20.0	18.8	19.2	
	Fluence* (E>1MeV)		1.76	2.00	1.76	1.54	1.54	
JFL Cu:0.01 P:0.004 Ni:0.75	Yield	Unirrad.	503	470	442	426	429	298±2
		Increase	45	43	45	24	27	
	Ultimate	Unirrad.	664	608	573	575	599	
		Increase	28	28	28	25	19	
	Elong. (%)	Unirrad.	21.2	22.6	19.8	18.4	18.9	
		Irrad.	24.7	20.9	17.2	17.9	18.5	
	Fluence* (E>1MeV)		1.60	1.83	1.60	1.41	1.41	
JRQ Cu:0.14 P:0.017 Ni:0.84	Yield	Unirrad.	570	477	449	431	441	288±4
		Increase	—	117	118	96	93	
	Ultimate	Unirrad.	724	615	578	574	613	
		Increase	—	107	110	97	81	
	Elong. (%)	Unirrad.	25.0	22.2	17.8	18.1	18.6	
		Irrad.	—	19.5	17.2	16.3	16.1	
	Fluence* (E>1MeV)		—	1.62	1.97	1.97	1.73	

Fluence*:Fast Neutron Fluence ($\times 10^{19}$ n/cm^2, E>1MeV)

Table C–3 Tensile properties for heavy section steels at room temperature and 290°C.

Material	Item	Stress (MPa)	Test Temperature (°C)				Irrad. Temp. (°C)
			R T		290		
			LF**	HF**	LF**	HF**	
JPI Cu:0.01 P:0.004 Ni:0.69	Yield	Unirrad.	481		422		LF: 295±4 HF: 290±8
		Increase	51	42	50	42	
	Ultimate	Unirrad.	604		593		
		Increase	40	65	50	31	
	Elong. (%)	Unirrad.	21.6		20.2		
		Irrad.	21.2	20.6	19.7	20.1	
	Fluence*(E>1MeV)		1.84	1.93	1.42	1.93	
JPJ Cu:0.05 P:0.005 Ni:0.64	Yield	Unirrad.	405		365		LF: 280±2 HF: 290±8
		Increase	59	66	32	41	
	Ultimate	Unirrad.	545		541		
		Increase	41	48	25	37	
	Elong. (%)	Unirrad.	24.8		21.6		
		Irrad.	23.5	21.6	19.2	18.3	
	Fluence*(E>1MeV)		2.00	2.67	1.54	2.67	
JFL Cu:0.01 P:0.004 Ni:0.75	Yield	Unirrad.	470		429		LF: 298±2 HF: 290±8
		Increase	43	48	27	35	
	Ultimate	Unirrad.	608		599		
		Increase	28	35	19	25	
	Elong. (%)	Unirrad.	22.6		18.9		
		Irrad.	20.9	19.9	18.5	18.7	
	Fluence*(E>1MeV)		1.83	2.21	1.41	2.21	
JRQ Cu:0.14 P:0.017 Ni:0.84	Yield	Unirrad.	477		441		LF: 288±4 HF: 290±8
		Increase	117	152	93	113	
	Ultimate	Unirrad.	615		613		
		Increase	107	132	81	97	
	Elong. (%)	Unirrad.	22.2		18.6		
		Irrad.	19.5	18.2	16.1	16.1	
	Fluence*(E>1MeV)		1.62	3.06	1.73	3.06	

Fluence*:Fast Neutron Fluence ($\times 10^{19}$ n/cm^2, E>1MeV)

LF**:Low Fluence

HF**:High Fluence

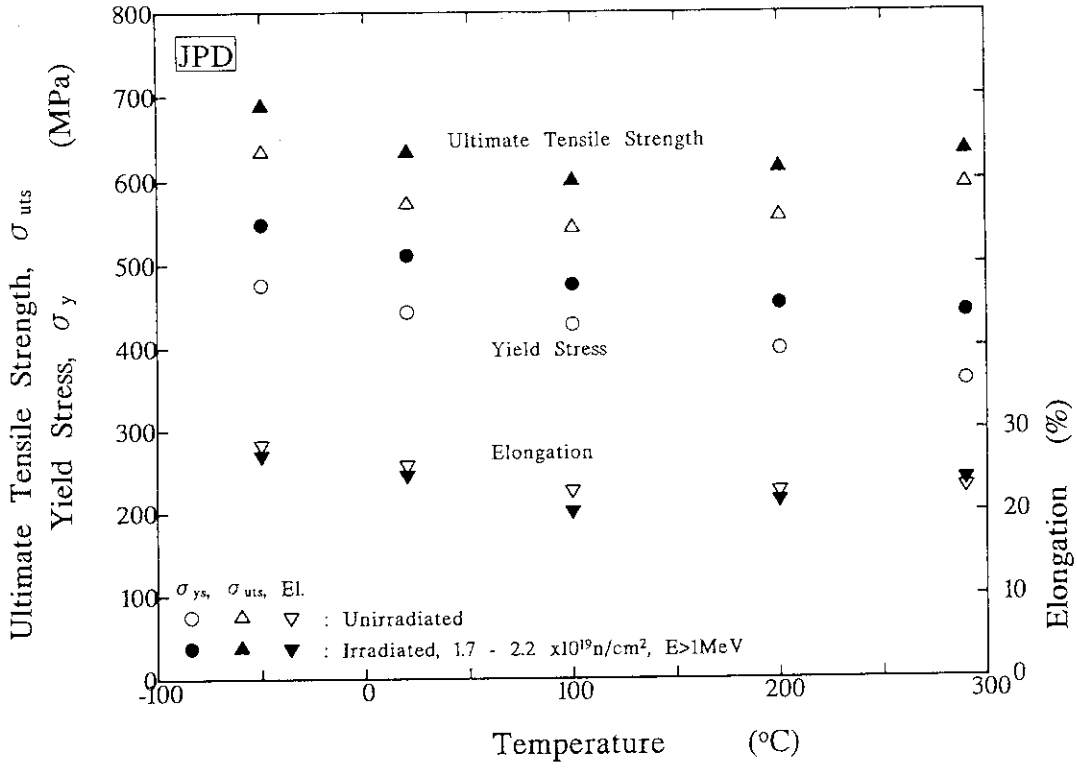

Figure C－1 Tensile Properties versus Temperature of JPD before and after Irradiation.

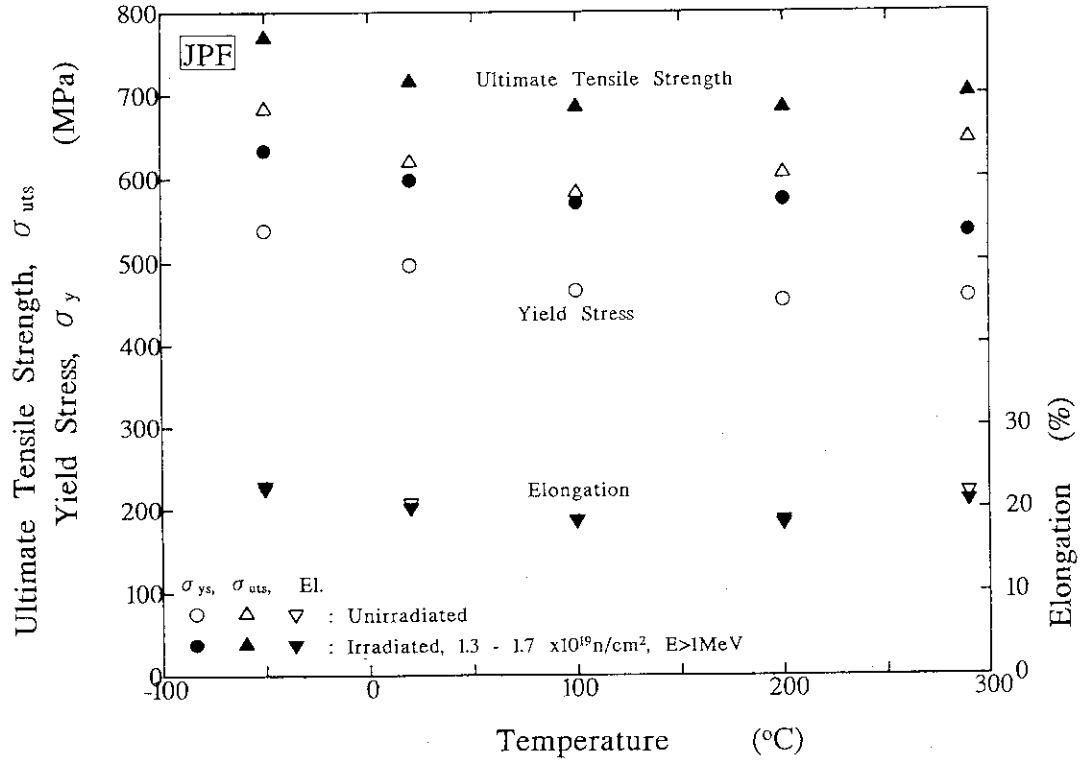

Figure C－2 Tensile Properties versus Temperature of JPF before and after Irradiation.

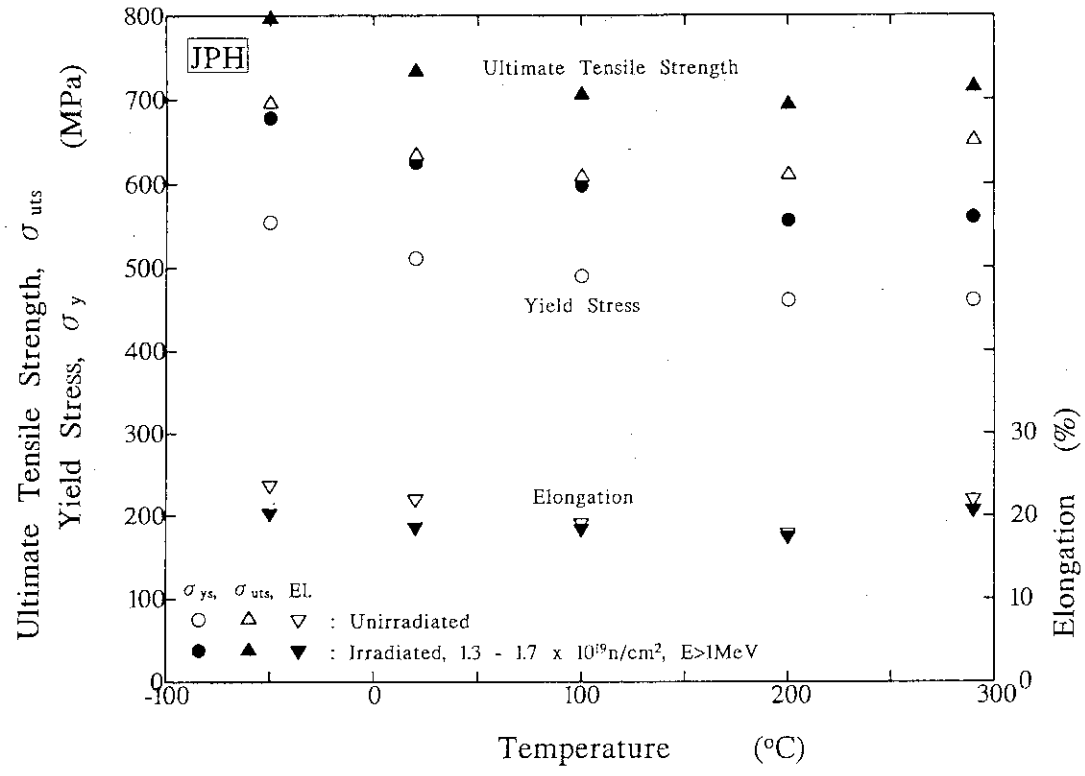

Figure C－3 Tensile Properties versus Temperature of JPH before and after Irradiation.

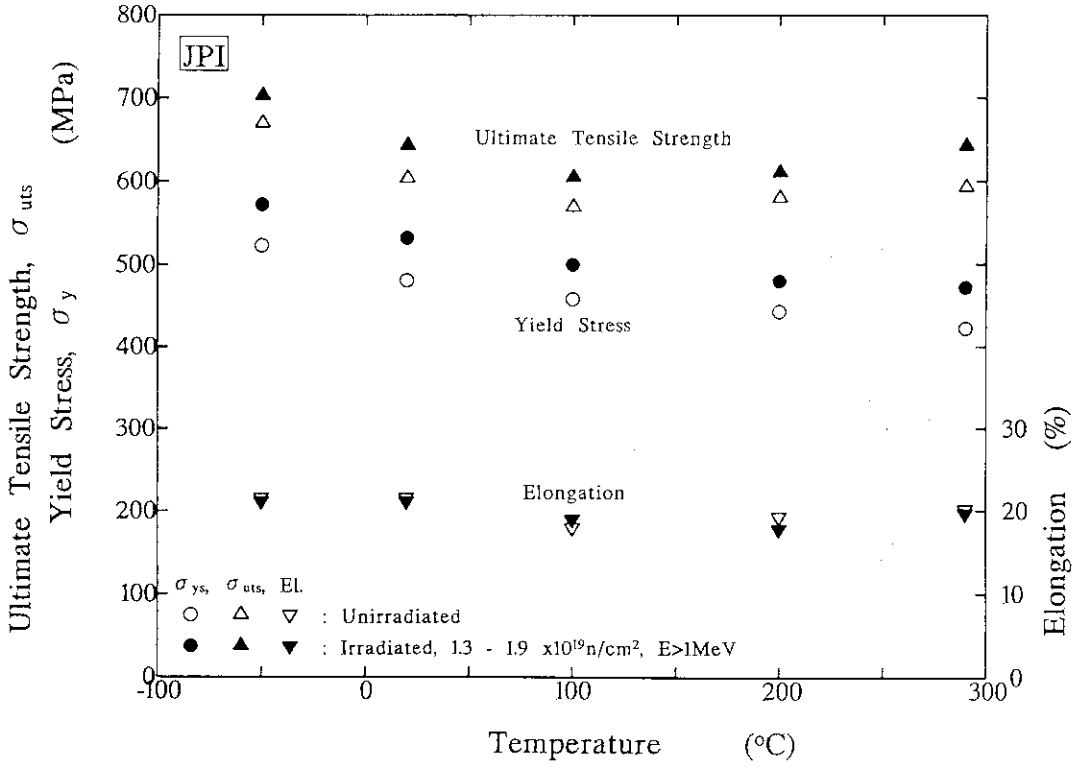

Figure C－4 Tensile Properties versus Temperature of JPI before and after Irradiation.

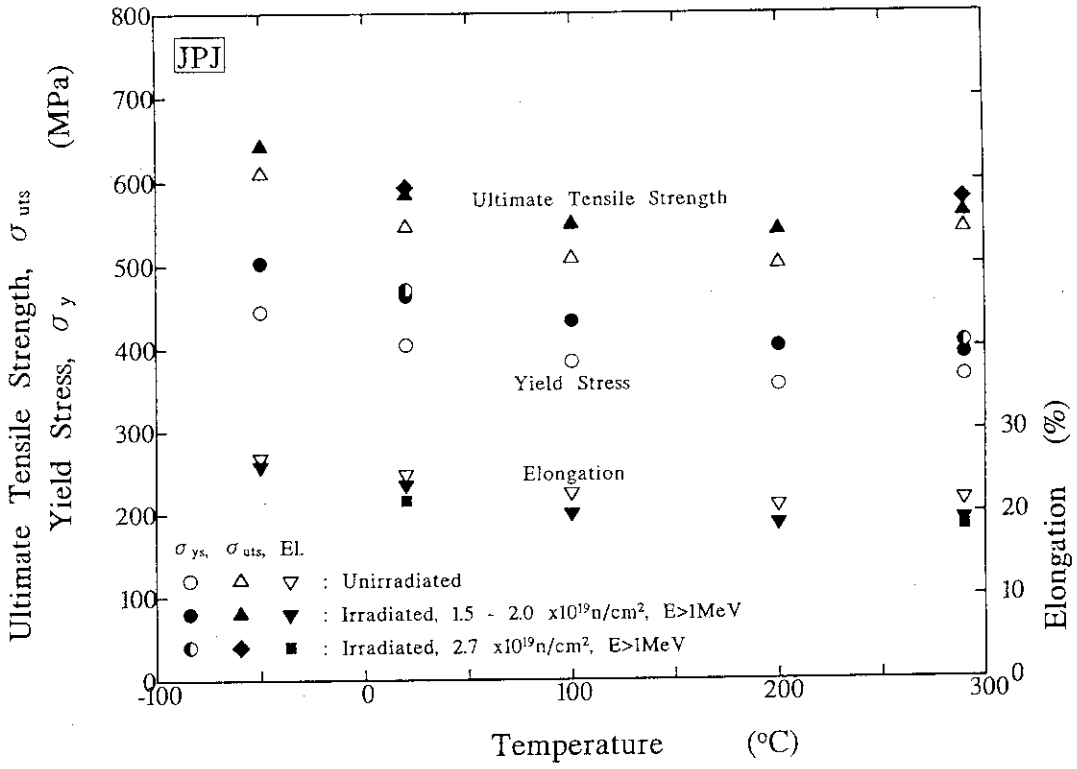

Figure C－5 Tensile Properties versus Temperature of JPJ before and after Irradiation.

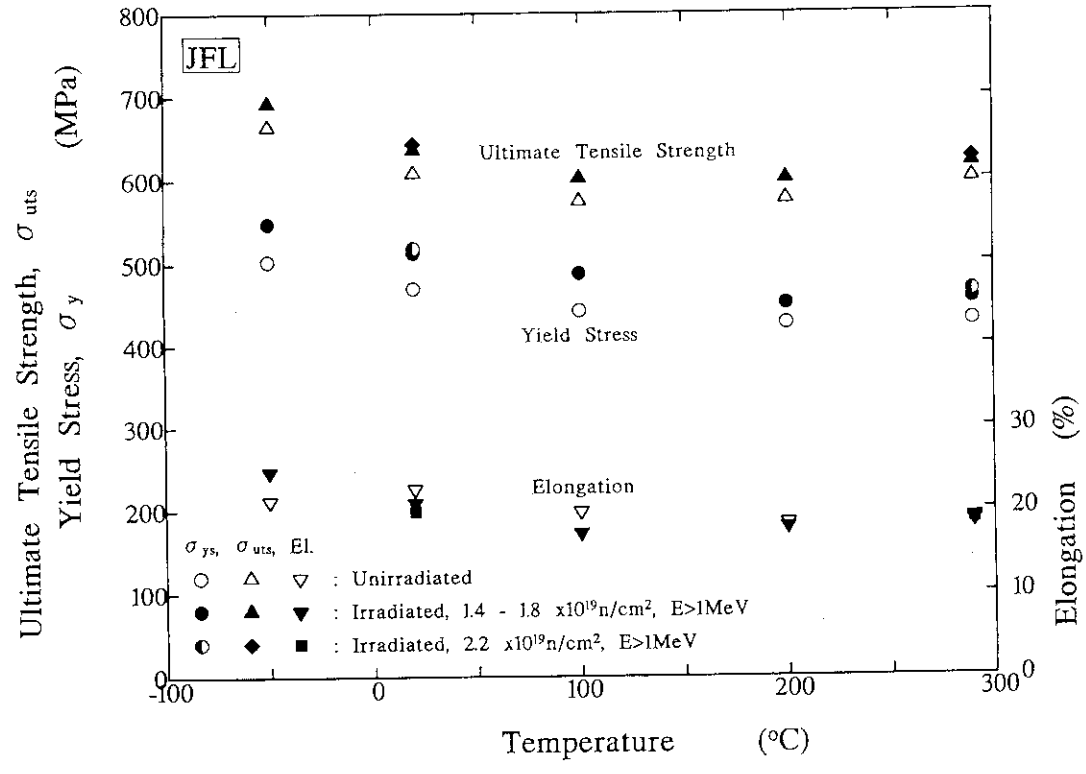

Figure C－6 Tensile Properties versus Temperature of JFL before and after Irradiation.

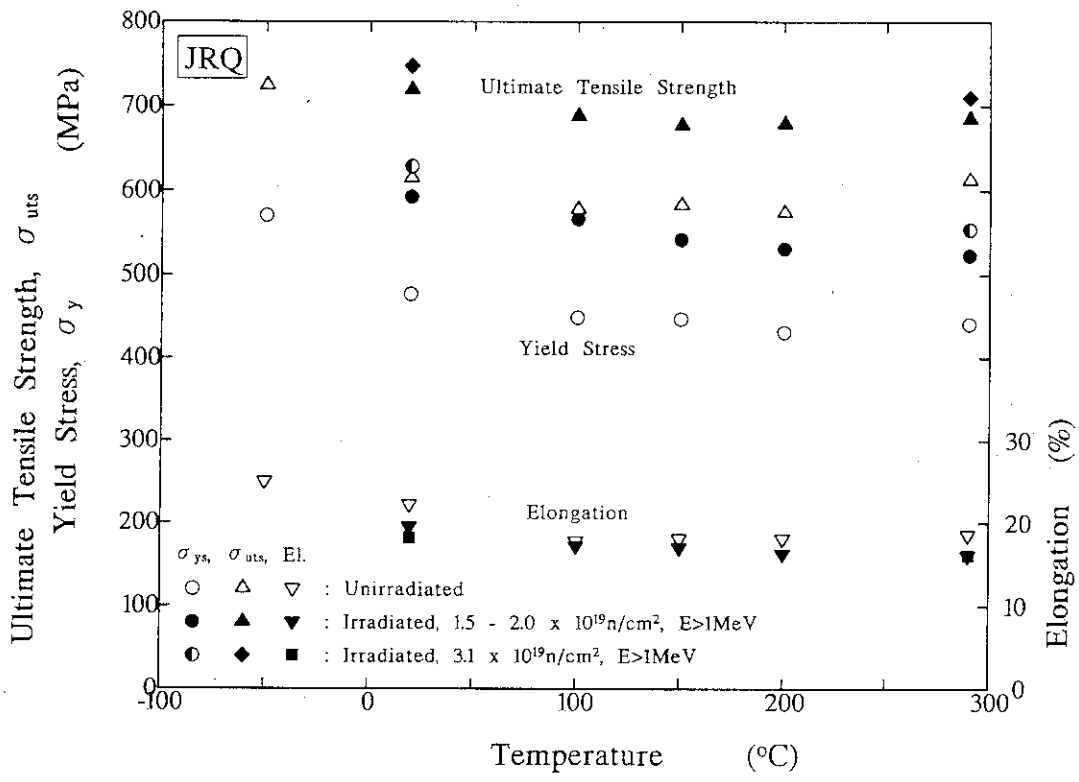

Figure C－7 Tensile Properties versus Temperature of JRQ before and after Irradiation.

APPENDIX D

Charpy Impact Properties of All Materials

Table D－1 Summary of the Charpy impact test results for seven materials.

Material	Fast Neutron Fluence (n/cm^2, E>1MeV)	Transition Temperature Index	Trans. Temp. (°C) Unirr.	Trans. Temp. (°C) Irr.	Shift (°C)	Predicted Shifts & Decrease*	Irrad. Temp. (°C)
JPD Cu:0.16 P:0.006 Ni:0.10	1.99-2.59 mean 2.33 x10^{19} (36.2 mdpa)	50% FA	-20.0	11.8	31.8	R1:101.8°C R2: 50.9°C JEAC: 44.7°C	287±4 | 295±3
		0.9mm LE	-66.4	-29.7	36.7		
		41J	-71.8	-41.0	30.8		
		68J	-62.9	-25.0	37.9		
		Upper Shelf	Energy (J)		Decrease(%)	R2: 30.1%	
			234.4	206.5	11.9		
JPF Cu:0.16 P:0.020 Ni:0.62	1.35-2.23 mean 1.82 x10^{19} (28.2 mdpa)	50% FA	-35.3	25.6	60.9	R1:133.0°C R2: 76.6°C JEAC: 79.0°C	283±5 | 297±3
		0.9mm LE	-73.9	-10.9	63.0		
		41J	-84.0	-42.6	41.4		
		68J	-71.7	-16.4	55.3		
		Upper Shelf	Energy (J)		Decrease(%)	R2: 29.6%	
			231.4	168.0	27.4		
JPH Cu:0.17 P:0.006 Ni:1.18	1.21-2.15 mean 1.72 x10^{19} (26.7 mdpa)	50% FA	-32.7	29.8	62.5	R1: 94.7°C R2: 86.2°C JEAC: 72.6°C	286±4 | 300±4
		0.9mm LE	-75.5	-24.9	50.6		
		41J	-86.6	-53.2	33.4		
		68J	-71.4	-20.3	51.1		
		Upper Shelf	Energy (J)		Decrease(%)	R2: 27.7%	
			252.3	182.4	27.7		
JPI Cu:0.01 P:0.004 Ni:0.69	1.31-2.37 mean: 1.88 x10^{19} (29.2 mdpa)	50% FA	-38.0	-23.8	13.7	R1: 30.5°C R2: 13.0°C JEAC: 19.5°C	288±3 | 295±3
		0.9mm LE	-80.5	-51.2	29.3		
		41J	-90.1	-63.9	26.2		
		68J	-78.5	-46.5	32.0		
		Upper Shelf	Energy (J)		Decrease(%)	R2: 22.5%	
			207.0		(5)		
JPJ Cu:0.05 P:0.005 Ni:0.64	1.86-2.42 mean 2.18 x10^{19} (33.8 mdpa)	50% FA	-0.5	49.0	49.5	R1: 32.7°C R2: 20.9°C JEAC: 18.1°C	285±5 | 297±5
		0.9mm LE	-21.5	29.9	51.4		
		41J	-31.5	23.0	54.5		
		68J	-20.3	38.3	58.6		
		Upper Shelf	Energy (J)		Decrease(%)	R2: 22.8%	
			233.2	157.8	32.3		
JFL Cu:0.01 P:0.004 Ni:0.75	1.34-2.37 mean 1.90 x10^{19} (29.5 mdpa)	50% FA	-21.2	-3.4	17.8	R1: 30.6°C R2: 13.1°C JEAC: 17.4°C	286±3 | 294±2
		0.9mm LE	-73.1	-40.6	32.5		
		41J	-83.3	-49.6	33.7		
		68J	-66.8	-32.8	34.0		
		Upper Shelf	Energy (J)		Decrease(%)	R2: 22.6%	
			225.3	188.9	16.2		
JRQ Cu:0.14 P:0.017 Ni:0.84	1.99-2.59 mean 2.33 x10^{19} (36.2 mdpa)	50% FA	16.5	96.0	79.5	R1:123.0°C R2: 71.8°C JEAC: 77.1°C	286±7 | 296±7
		0.9mm LE	-20.2	65.8	86.0		
		41J	-29.8	54.9	84.7		
		68J	-13.0	76.3	89.3		
		Upper Shelf	Energy (J)		Decrease(%)	R2: 28.2%	
			204.5	145.4	28.9		

*:R1;USNRC Regulatory Guide 1.99 Rev.1
R2;USNRC Regulatory Guide 1.99 Rev.2
JEAC;JEAC-4201-1991

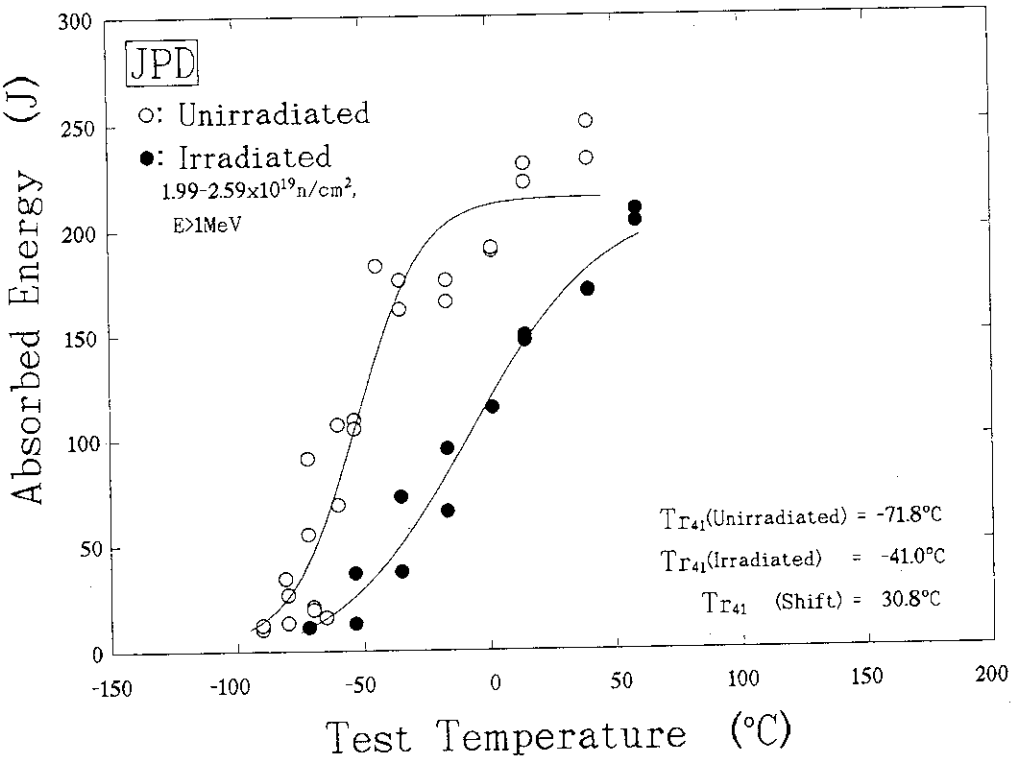

a) Absorbed energy

Figure D－1 Charpy transition curves of JPD.

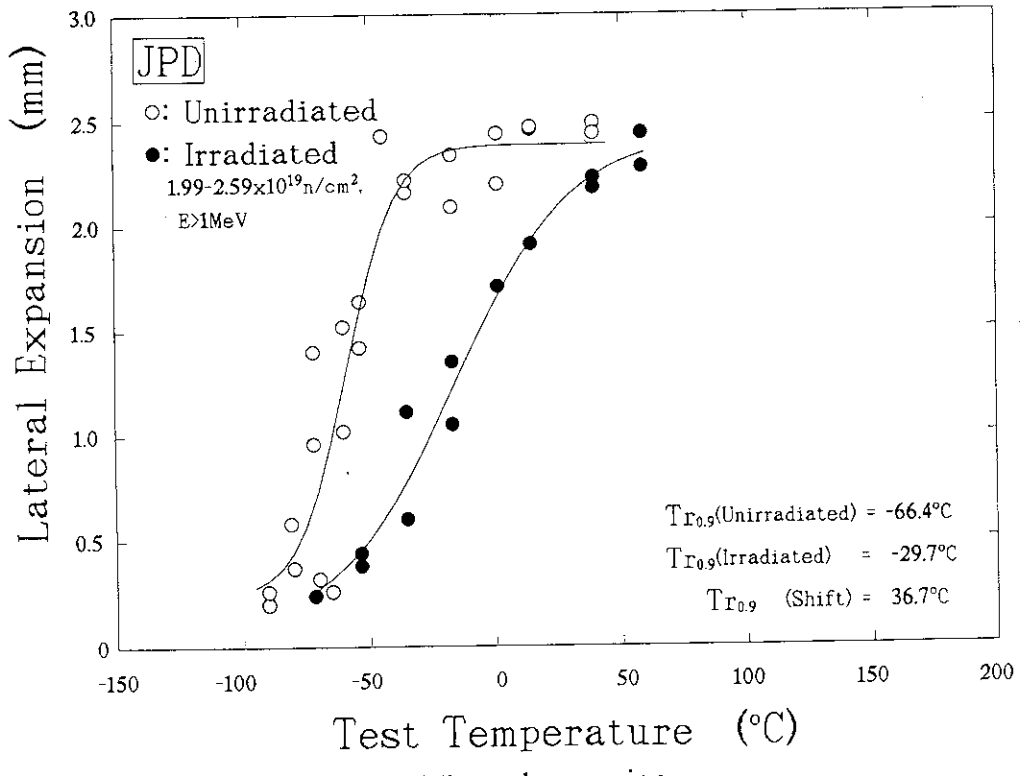

b) Lateral expansion

Figure D－1 Charpy transition curves of JPD.

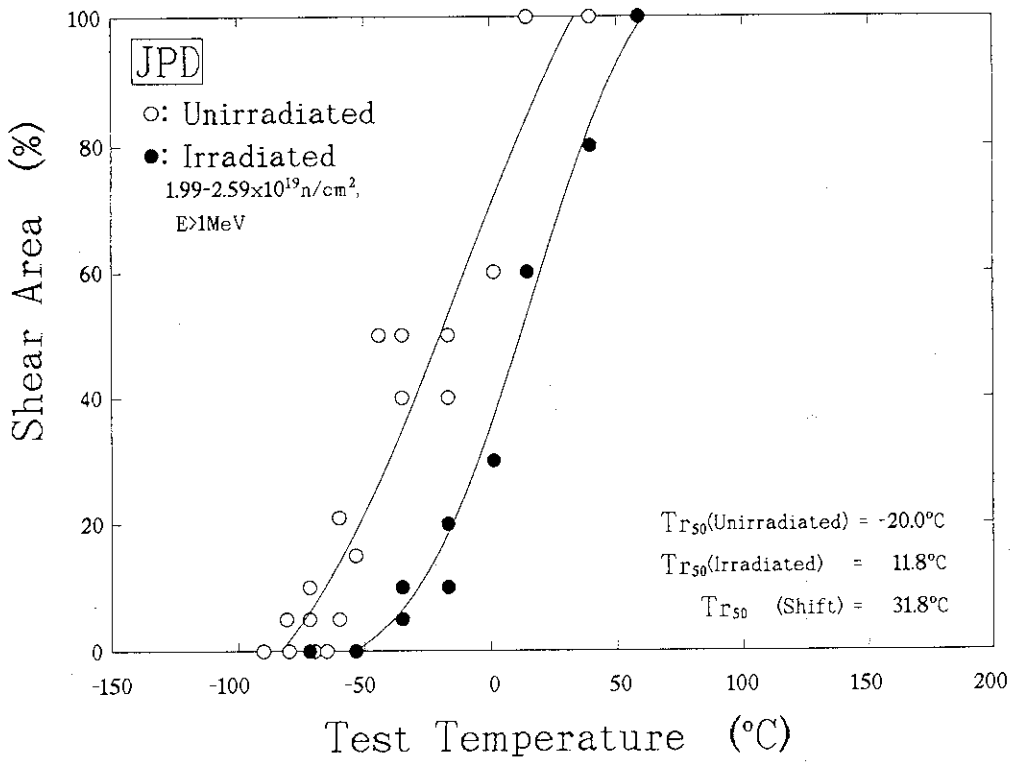

c) Shear fracture appearance

Figure D－1 Charpy transition curves of JPD.

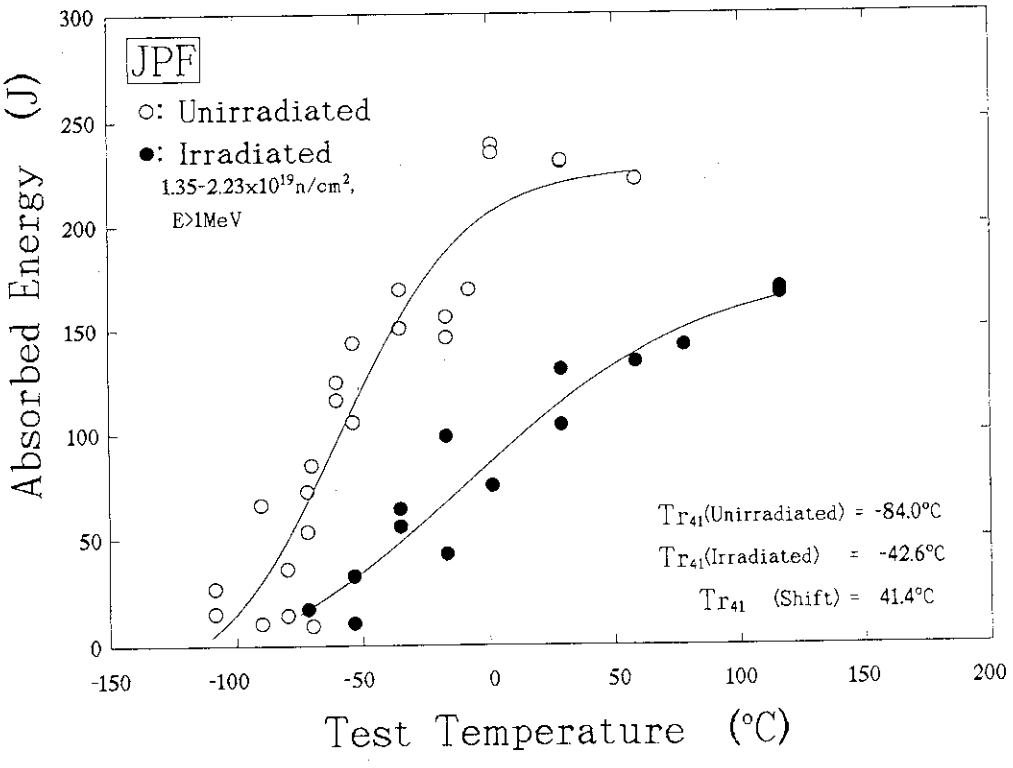

a) Absorbed energy

Figure D－2 Charpy transition curves of JPF.

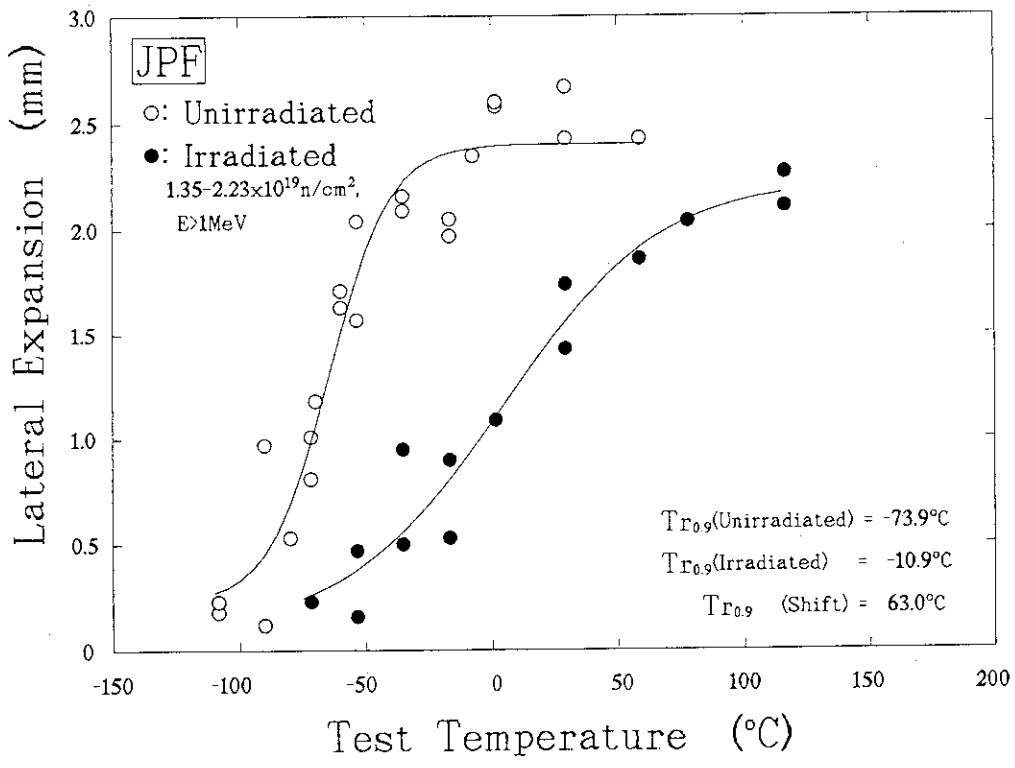

b) Lateral expansion

Figure D－2 Charpy transition curves of JPF.

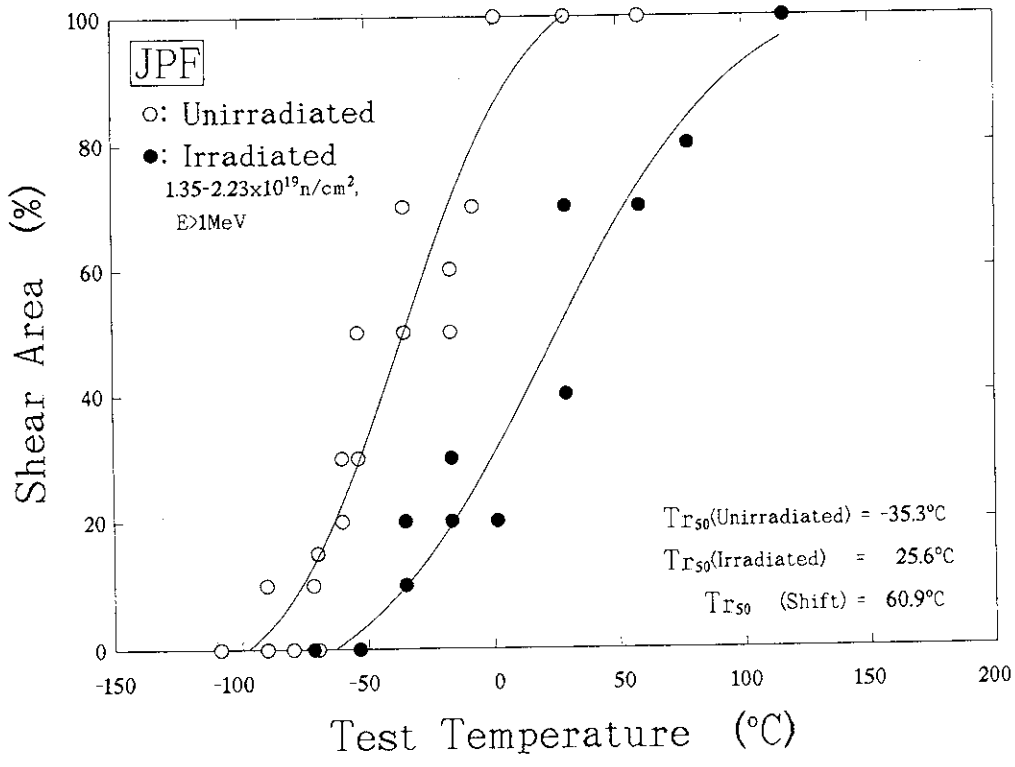

c) Shear fracture appearance

Figure D－2 Charpy transition curves of JPF.

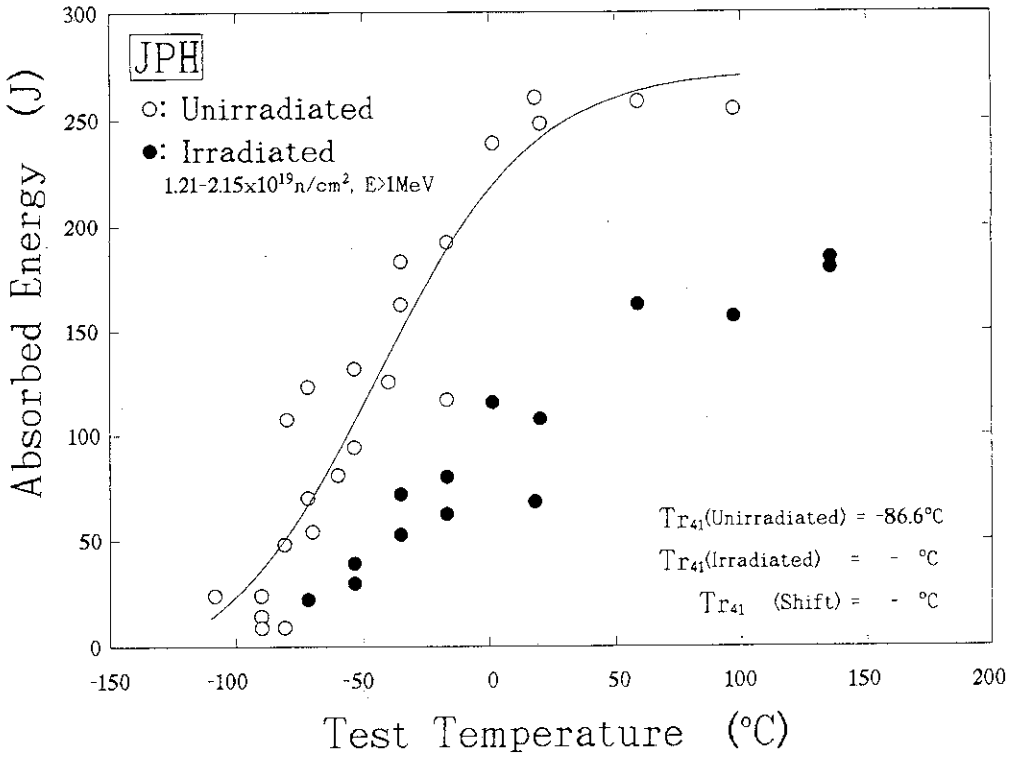

a) Absorbed energy

Figure D-3 Charpy transition curves of JPH.

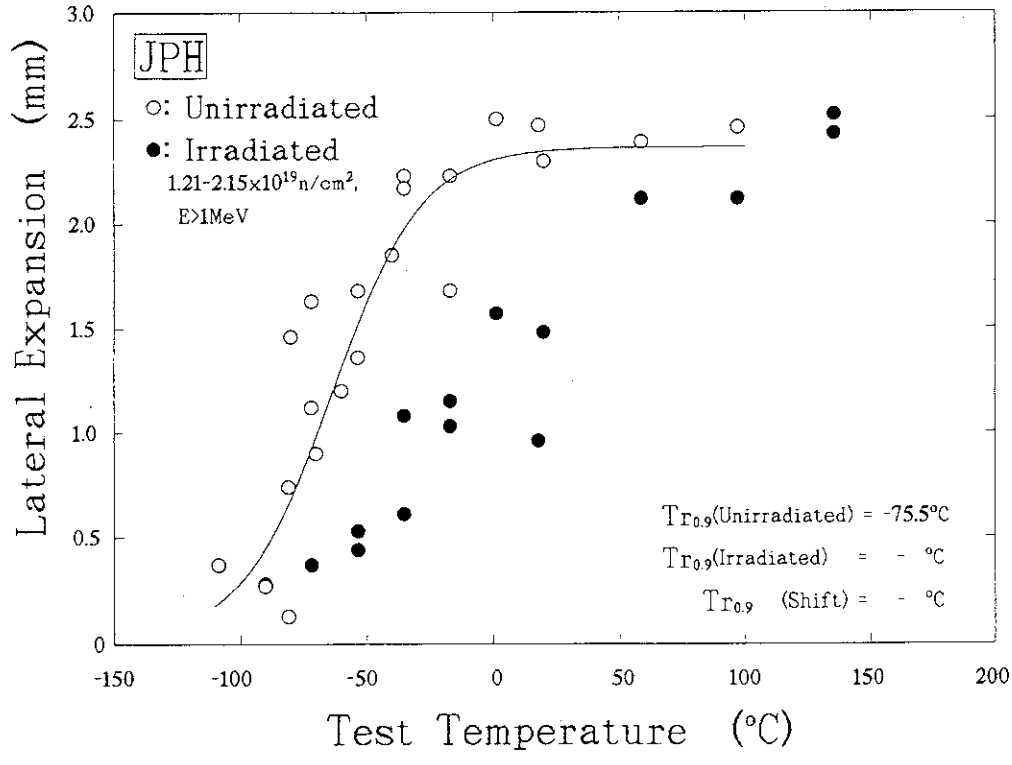

b) Lateral expansion

Figure D-3 Charpy transition curves of JPH.

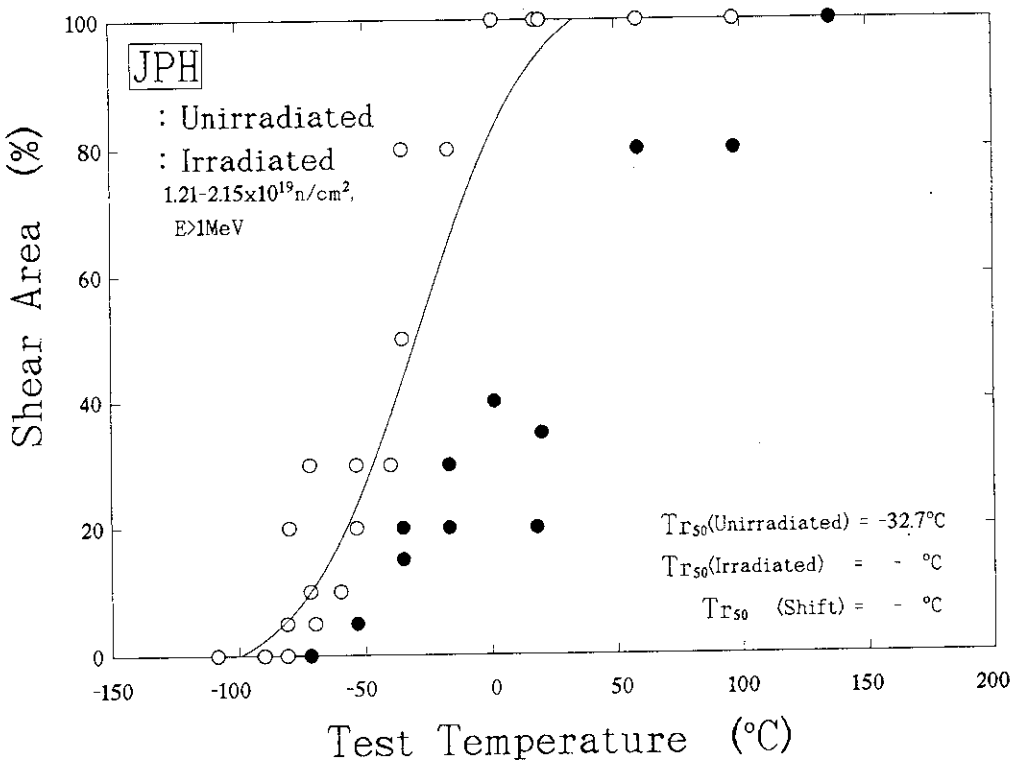

c) Shear fracture appearance

Figure D-3 Charpy transition curves of JPH.

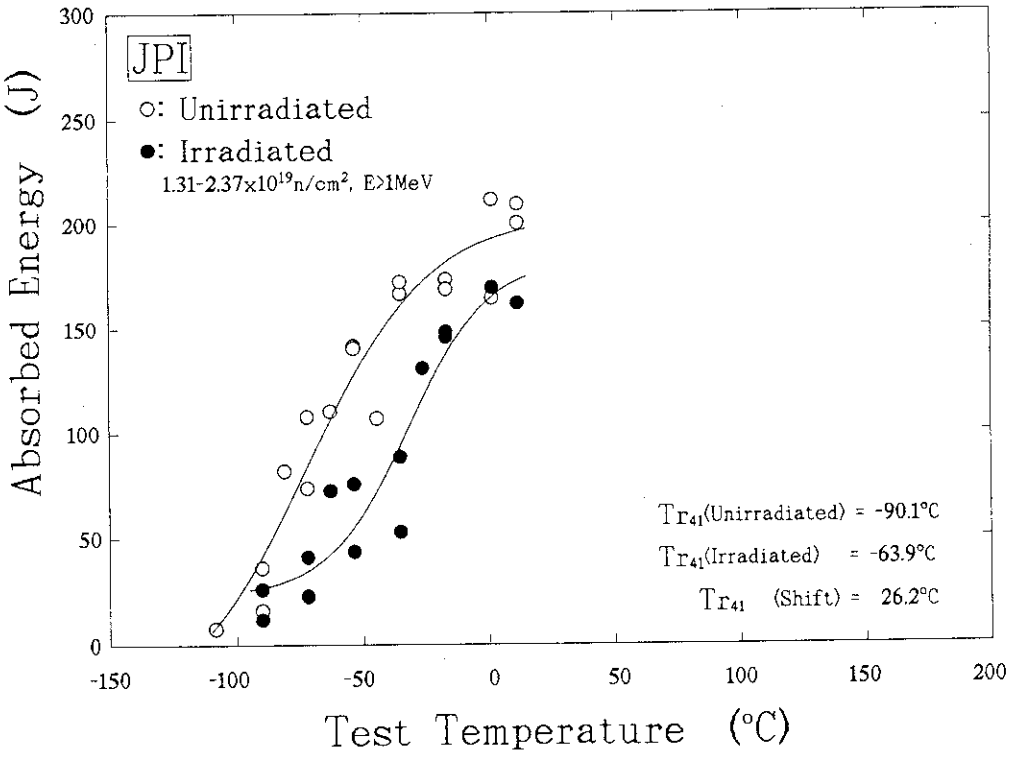

a) Absorbed energy

Figure D-4 Charpy transition curves of JPI.

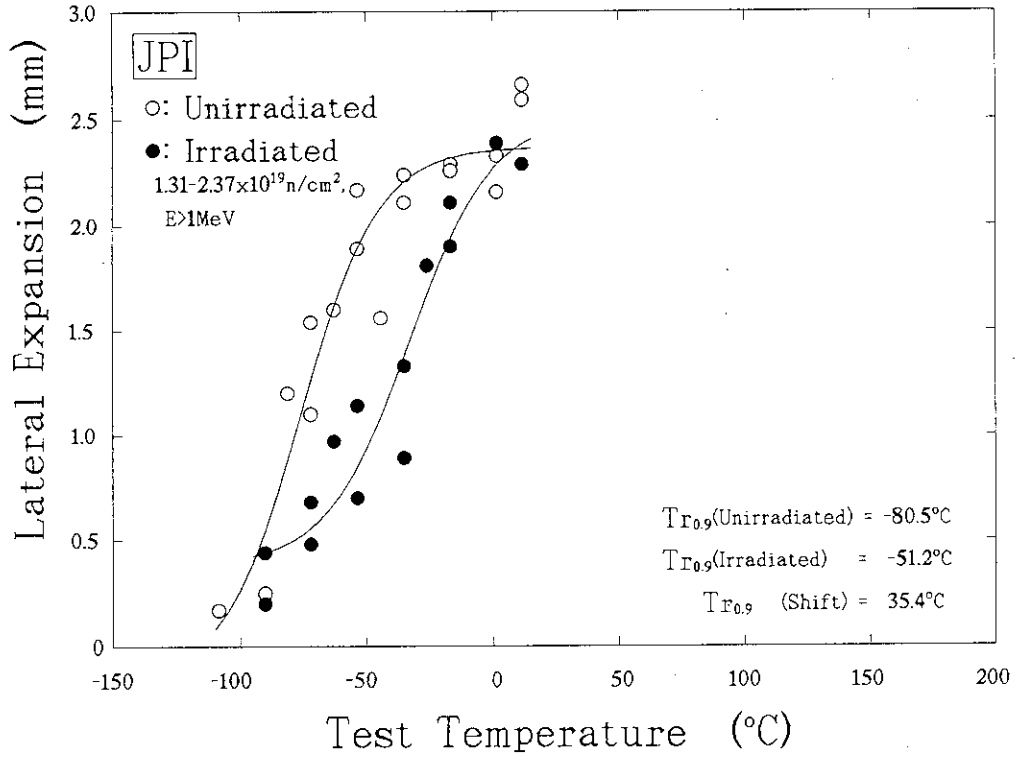

b) Lateral expansion

Figure D－4 Charpy transition curves of JPI.

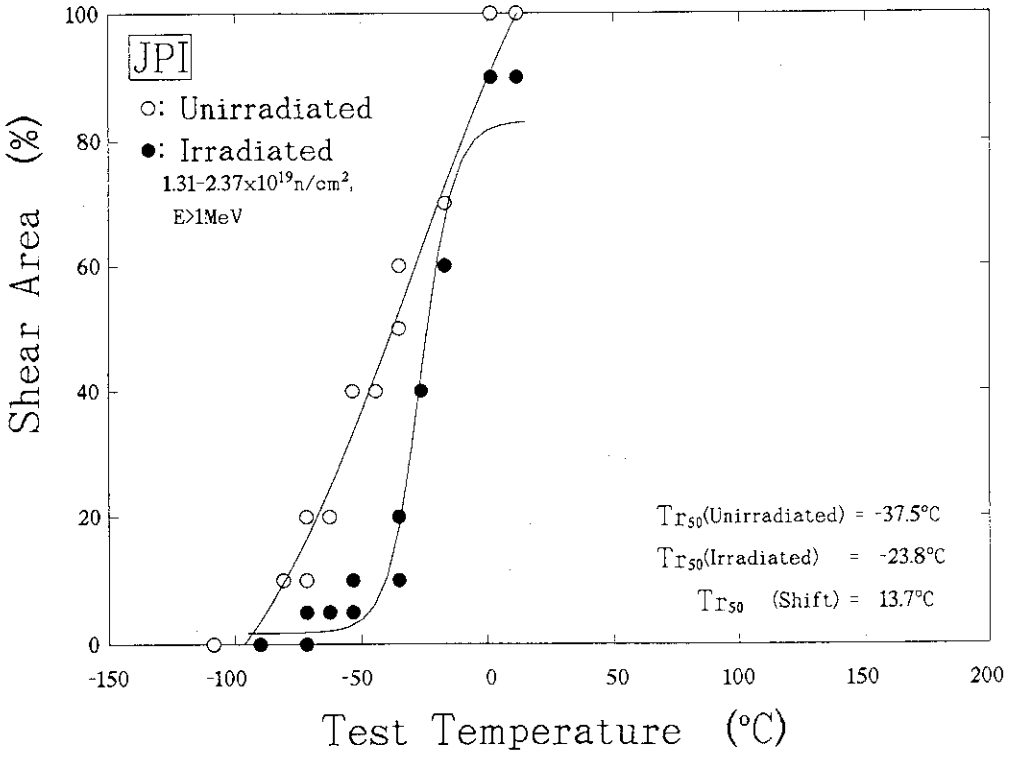

c) Shear fracture appearance

Figure D－4 Charpy transition curves of JPI.

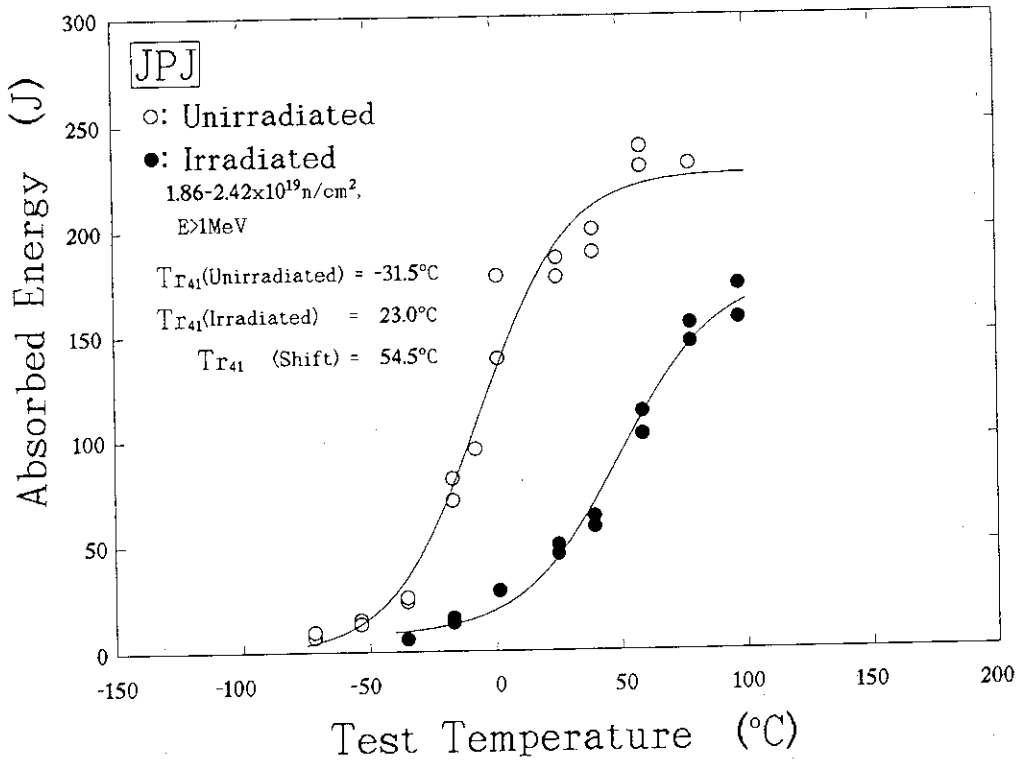

a) Absorbed energy

Figure D－5 Charpy transition curves of JPJ.

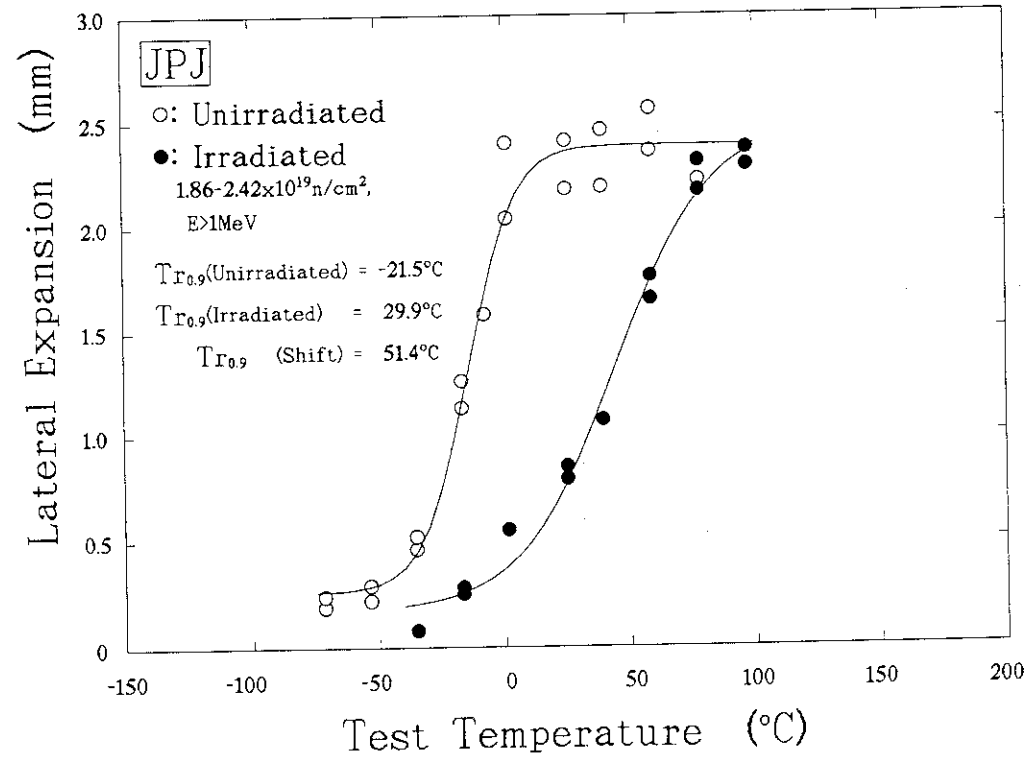

b) Lateral expansion

Figure D－5 Charpy transition curves of JPJ.

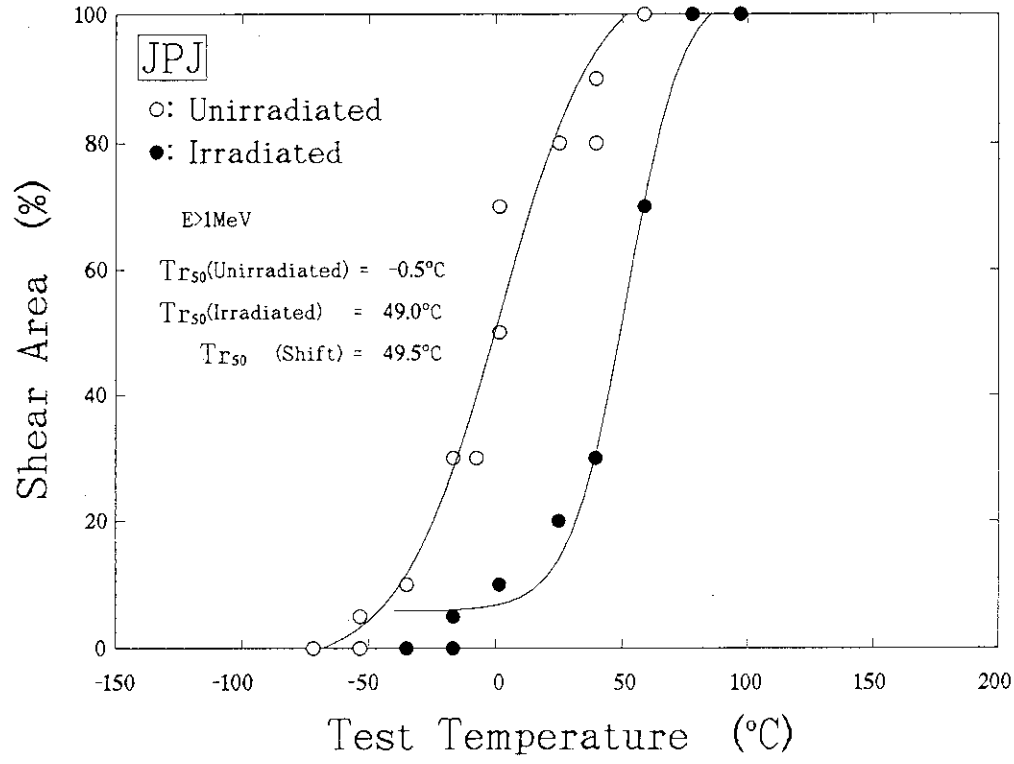

c) Shear fracture appearance

Figure D-5 Charpy transition curves of JPJ.

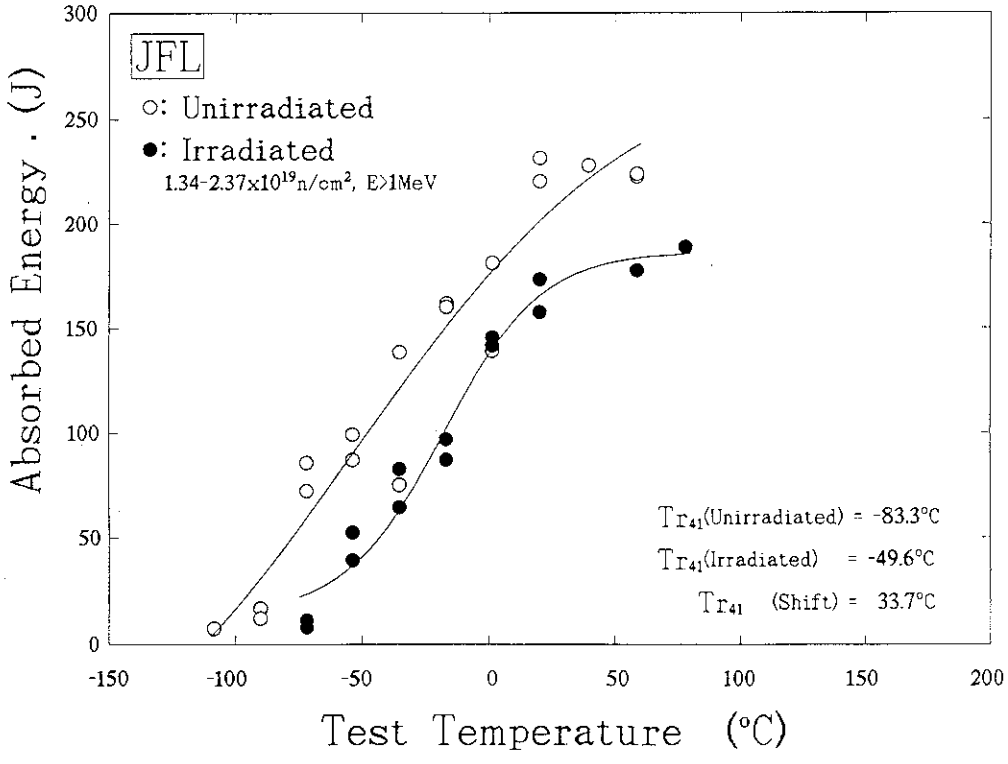

a) Absorbed energy

Figure D-6 Charpy transition curves of JFL.

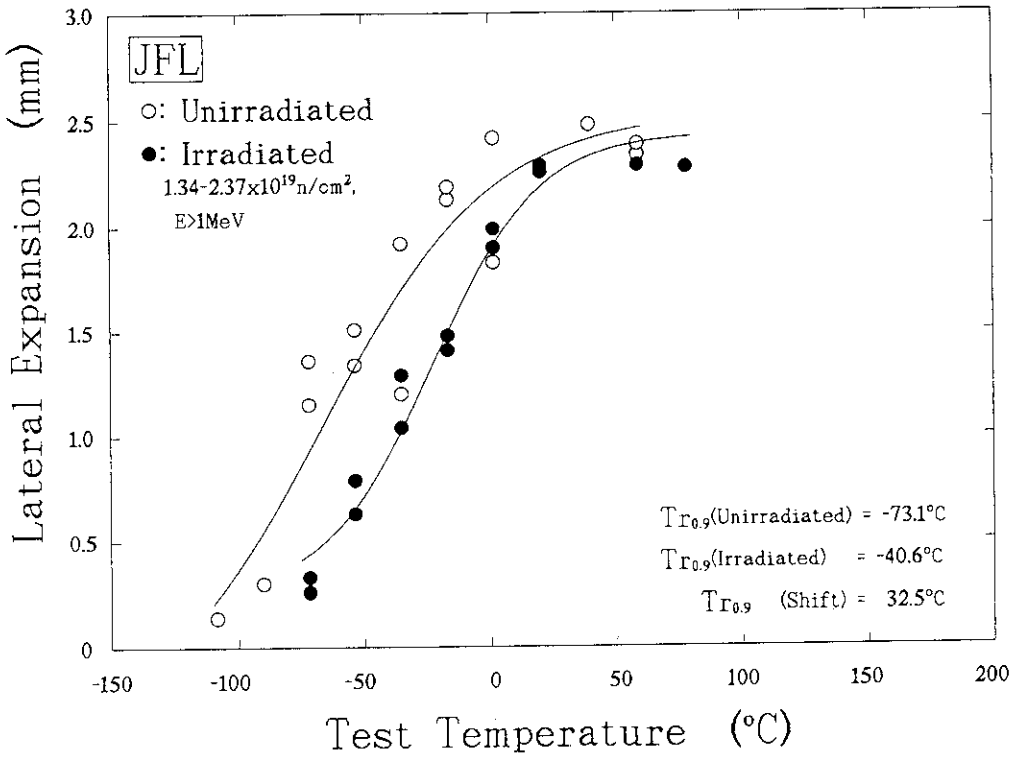

b) Lateral expansion

Figure D－6 Charpy transition curves of JFL.

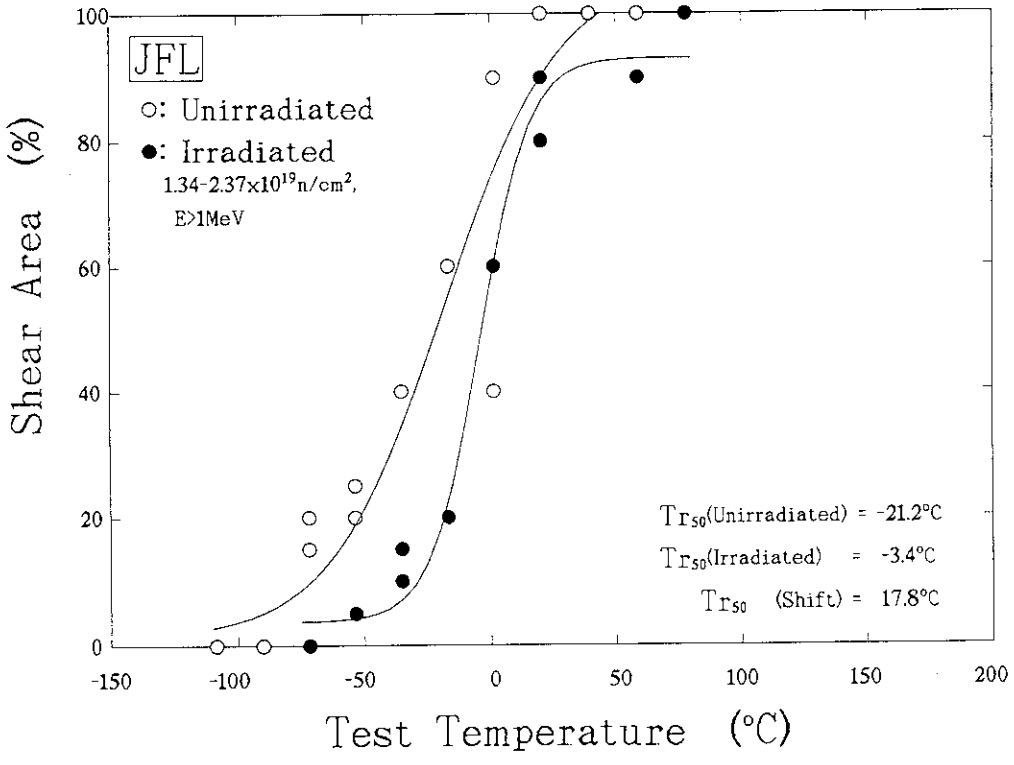

c) Shear fracture appearance

Figure D－6 Charpy transition curves of JFL.

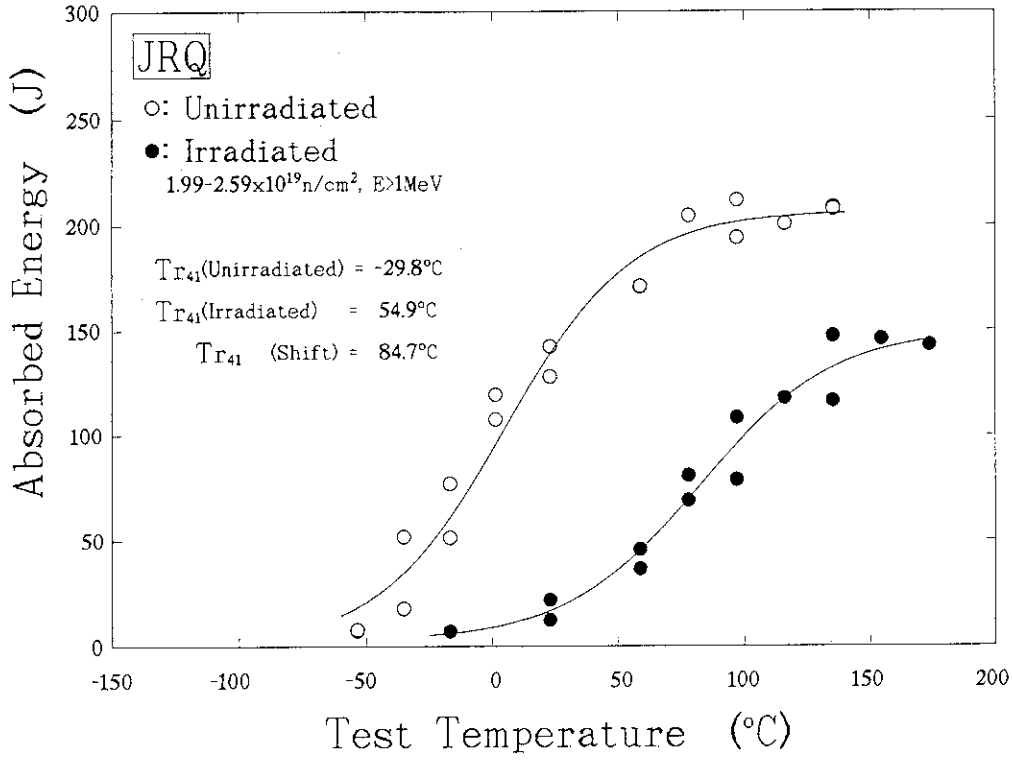

a) Absorbed energy

Figure D－7 Charpy transition curves of JRQ.

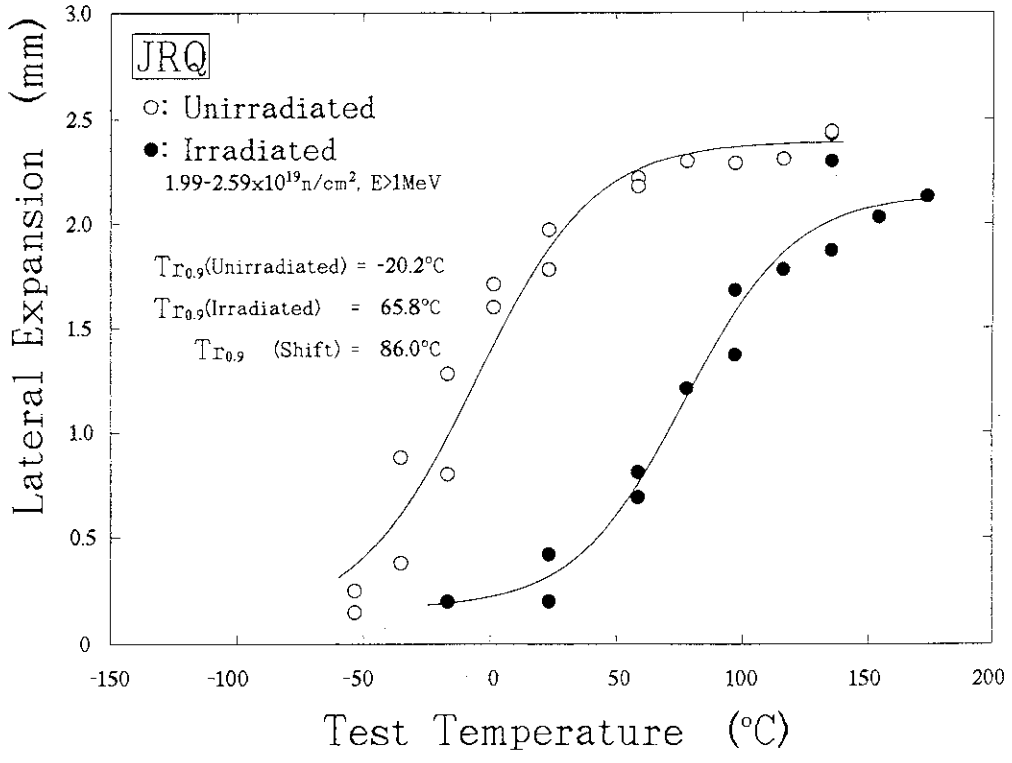

b) Lateral expansion

Figure D－7 Charpy transition curves of JRQ.

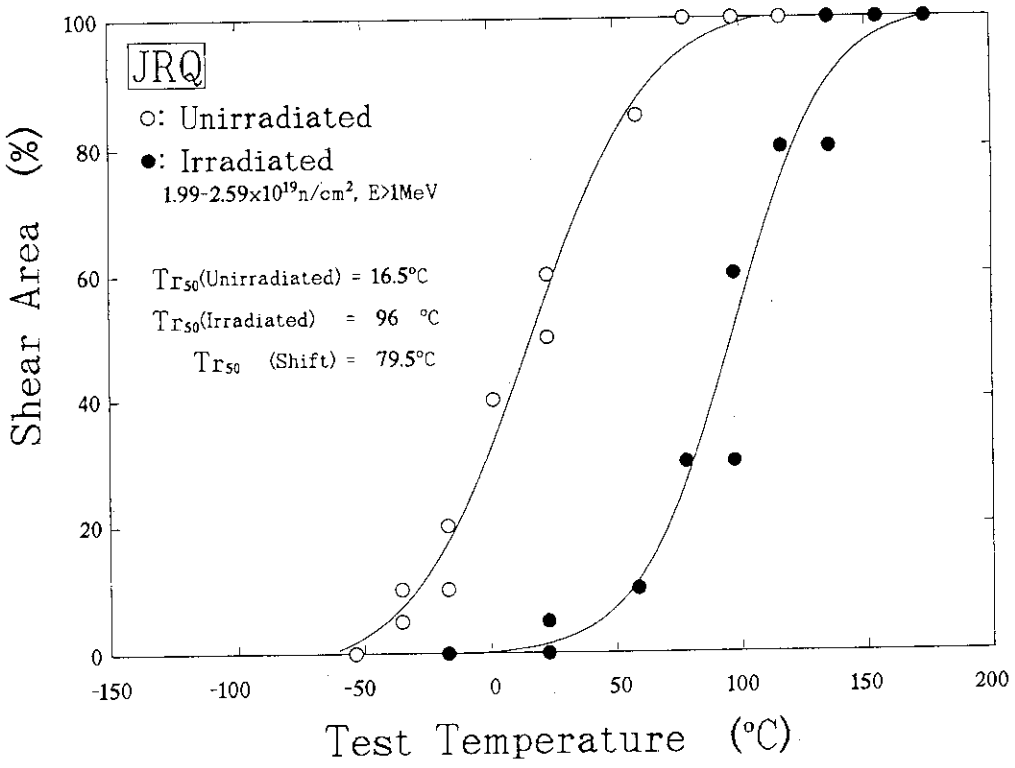

c) Shear fracture appearance

Figure D-7 Charpy transition curves of JRQ.

APPENDIX E

Fracture toughness Test Results of Heavy Section Steels

Table E－1 Fracture toughness test results using precracked Charpy type specimen of JPI steel.

Type	No.	Fluence*	Test Temp. ^{o}C	J_C or J_Q kJ/m^2	K_{JC} $MPam^{0.5}$	Δa_m** mm	Note
PCV	I31	0	-150	32	88	-	Clvg
PCV	I30	0	-125	219	228	2.0	Popin
PCV	I25	0	-100	256	246	3.2	Clvg
PCV	I26	0	-75	697	405	2.5	Pmax
PCV	I29	0	-65	(519)	-	0.75	dc-pd
PCV	I27	0	-50	(385)	-	0.76	dc-pd
PCV	I28	0	-25	(437)	-	0.85	dc-pd
PCV	I17	1.5	-125	116	167	3.8	Clvg
PCV	I16	1.3	-100	95	150	3.1	Clvg
PCV	I13	2.0	-85	111	162	2.7	Clvg
PCV	I10	2.0	-75	477	335	3.0	Pmax
PCV	I14	1.3	-50	414	-	0.80	Pmax
PCV	I15	1.5	-50	(392)	-	0.84	dc-pd
PCV	I11	1.7	0	(329)	-	0.88	dc-pd

Fluence*: $x10^{19} n/cm^2$ (E›1MeV)

K_{JC}: Cleavage Fracture Toughness,

Δa_m**: Measured Crack Extension,

Clvg: Cleavage Fracture,

Popin: J-integral Value to Pop-in Point,

Pmax: J-integral Value up to Maximum Load,

dc-pd: Direct Current Potential Drop Method.

Table E－2 Fracture toughness test results using precracked Charpy type specimen of JPJ steel.

Type	No.	Fluence*	Test Temp. ^{o}C	J_C or J_Q kJ/m^2	K_{JC} $MPam^{0.5}$	Δa_m** mm	Note
PCV	J36	0	-75	49	107	2.3	Clvg
PCV	J30	0	-50	69	128	1.4	Clvg
PCV	J34	0	-35	189	210	1.7	Clvg
PCV	J31	0	-25	246	239	1.7	Pmax
PCV	J32	0	0	354	-	0.69	Pmax
PCV	J35	0	0	(317)	-	0.82	dc-pd
PCV	J33	0	25	(297)	-	0.77	dc-pd
PCV	J21	2.4	-50	34	90	1.9	Clvg
PCV	J12	2.5	-25	36	91	1.7	Clvg
PCV	J13	2.1	0	112	161	1.1	Clvg
PCV	J20	2.1	15	184	206	0.93	Clvg
PCV	J16	2.5	25	158	-	0.92	Pmax
PCV	J19	2.4	25	(178)	-	0.79	dc-pd
PCV	J18	2.1	50	(264)	-	0.90	dc-pd

Fluence*: $x10^{19} n/cm^2$ (E>1MeV),

K_{JC}: Cleavage Fracture Toughness,

Δa_m**: Measured Crack Extension,

Clvg: Cleavage Fracture,

Popin: J-integral Value to Pop-in Point,

Pmax: J-integral Value up to Maximum Load,

dc-pd: Direct Current Potential Drop Method.

Table E-3 Fracture toughness test results using precracked Charpy type specimen of JRQ steel.

Type	No.	Fluence*	Test Temp. ^{o}C	J_C or J_i kJ/m^2	K_{JC} $MPam^{0.5}$	Δa_m** mm	Note
PCV	Q27	0	-75	20	68	-	Clvg
PCV	Q22	0	-50	298	264	2.0	Clvgn
PCV	Q28	0	-40	115	163	3.2	Clvg
PCV	Q25	0	-25	190	211	2.5	Clvg
PCV	Q24	0	0	312	-	0.75	Pmax
PCV	Q26	0	0	(348)	-	0.76	dc-pd
PCV	Q23	0	25	(314)	-	0.85	dc-pd
PCV	Q8	1.5	0	47	104	2.6	Clvg
PCV	Q9	1.3	25	119	165	2.2	Clvg
PCV	Q10	2.0	50	137	176	1.1	Clvg
PCV	Q14	2.0	60	70	126	1.3	Clvg
PCV	Q11	1.3	75	304	262	1.7	Clvg
PCV	Q12	1.5	100	(310)	-	0.71	dc-pd
PCV	Q13	1.7	125	(226)	-	1.24	dc-pd

Fluence*: $x10^{19}$ n/cm^2 (E>1MeV),

K_{JC}: Cleavage Fracture Toughness,

Δa_m**: Measured Crack Extension,

Clvg: Cleavage Fracture,

Popin: J-integral Value to Pop-in Point,

Pmax: J-integral Value up to Maximum Load,

dc-pd: Direct Current Potential Drop Method.

Table E-4 Fracture toughness test results using compact type specimen of JPI steel.

Type	No.	Fluence*	Test Temp. °C	C**	n**	J_Q kJ/m^2	dJdal MPa	σy MPa	Δa_m mm	Δa_c mm	Note
CT	I1	0	20	672	0.552	554	371	549	3.75	3.80	
CT	I2	0	20	634	0.615	480	390		3.56	3.53	
DCT	I6	0	20	653	0.482	550	315		1.96	2.09	
DCT	I7	0	20	633	0.596	487	377		1.75	1.96	
DCT	I8	0	20	568	0.522	433	296		2.72	2.96	
CT	I3	0	100	589	0.653	428	385	518	3.60	3.53	
DCT	I9	0	100	491	0.535	353	263		3.14	3.38	
DCT	I10	0	100	549	0.497	432	273		3.03	3.30	
DCT	I11	0	100	570	0.343	500	196		2.93	3.01	
CT	I4	0	200	526	0.595	377	313	507	3.67	3.38	
DCT	I12	0	200	458	0.398	363	182		2.81	2.77	
DCT	I13	0	200	463	0.442	356	205		3.10	3.20	
CT	I5	0	290	497	0.665	319	331	509	4.53	4.25	
CT	I6	0	290	548	0.709	360	389		4.01	3.75	
DCT	I14	0	290	485	0.384	396	186		2.94	3.27	
DCT	I15	0	290	466	0.277	404	129		3.18	3.33	
DCT	Im1	0	290	485	0.544	347	264		--	--	
DCT	Im2	1.23	20	724	0.499	622	361	578	--	--	
DCT	Im3	1.45	100	624	0.350	554	219	542	--	--	
DCT	Im4	1.82	290	517	0.402	416	208	544	--	--	
DCT	I22	3.24	20	824	0.576	739	475	587	2.09	1.78	
DCT	I23	3.36	20	653	0.703	444	459		1.68	1.89	
DCT	I24	3.47	100	568	0.653	381	371	556	2.77	2.60	
DCT	I25	3.58	100	577	0.550	430	317		2.70	2.69	
DCT	I27	3.79	200	460	0.573	299	264	550	2.52	2.55	
DCT	I29	4.04	290	420	0.469	292	197	560	3.06	2.78	

Fluence*: x10^{19}n/cm^2, E>1MeV
C**,n**: Fitting Parameters, $J=C(\Delta a)^n$,
dJdal: dJ/da at Δa=1mm,
Im1-Im4: Multi-Specimen Method,
Δa_m & Δa_c: Measured & Calculated Δa
LE: Linear Elastic Fracture,
Clvg: Cleavage Fracture,
J_{IC}: Valid J_{IC} for ASTM E813

Table E-5 Fracture toughness test results using compact type specimen of JPJ steel.

Type	No.	Fluence*	Test Temp. °C	C**	n**	J_Q kJ/m^2	dJdal MPa	σy MPa	Δa_m mm	Δa_c mm	Note
CT	J1	0	20	704	0.580	645	408	487	3.82	3.81	
CT	J2	0	20	653	0.626	553	408		3.54	3.35	
DCT	J6	0	20	638	0.353	591	225		2.20	2.19	
DCT	J7	0	20	647	0.458	584	296		2.50	2.68	
DCT	J8	0	20	591	0.533	490	315		2.72	2.81	
CT	J3	0	100	558	0.748	395	417	458	3.28	3.17	
DCT	J9	0	100	597	0.298	561	178		2.95	3.16	
DCT	J10	0	100	601	0.379	553	228		2.92	3.16	
DCT	J11	0	100	619	0.299	588	185		3.12	3.26	
CT	J4	0	200	498	0.633	368	315	439	3.73	3.57	
DCT	J12	0	200	444	0.519	335	230		3.17	3.17	
DCT	J13	0	200	487	0.407	414	198		3.23	3.43	
DCT	J14	0	200	493	0.287	447	141		3.07	3.08	
CT	J5	0	290	508	0.571	388	290	457	3.98	3.52	
CT	J6	0	290	494	0.605	361	299		3.88	3.65	
DCT	J15	0	290	503	0.349	440	176		2.97	3.20	
DCT	Jm1	0	290	493	0.375	422	185		--	--	
DCT	J2	1.94	20	-	-	142	-	524	-	-	Clvg
DCT	J4	2.01	20	-	-	118	-		-	-	
DCT	J22	1.92	20	-	-	137	-		-	-	
DCT	Jm2	2.13	200	584	0.475	500	277	480	--	--	
DCT	Jm3	2.17	290	475	0.501	358	238	486	--	--	
DCT	J24	4.12	20	-	- K_Q	(76.7)	-	543	-	-	LE
DCT	J25	4.20	20	-	- K_Q	(82.2)	-		-		
DCT	J32	4.55	60	187	0.593	89	111	526	-	2.28	J_{IC}
DCT	J26	4.27	100	420	0.598	264	251	510	2.48	2.65	
DCT	J27	4.33	100	454	0.541	315	246		2.35	2.32	
DCT	J29	4.43	200	456	0.501	333	229	498	2.85	2.80	
DCT	J31	4.53	290	344	0.493	225	169	503	2.67	2.68	J_{IC}

Fluence*: $\times 10^{19}$ n/cm^2, E>1MeV

C**,n**: Fitting Parameters, $J=C(\Delta a)^n$,

dJdal: dJ/da at Δa=1mm,

Jm1-Jm3: Multi-Specimen Method,

Δa_m & Δa_c: Measured & Calculated Δa

LE: Linear Elastic Fracture,

Clvg: Cleavage Fracture,

J_{IC}: Valid J_{IC} for ASTM E813

Table E－6 Fracture toughness test results using compact type specimen of JFL steel.

Type	No.	Fluence*	Test Temp °C	C**	n**	J_Q kJ/m^2	dJda1 MPa	σy MPa	Δa_m mm	Δa_c mm	Note
CT	L1	0	24	681	0.577	564	393	540	4.06	3.98	
CT	L2	0	24	706	0.512	619	362		4.49	4.34	
DCT	L32	0	24	642	0.569	513	365		1.96	1.97	
DCT	L33	0	24	659	0.601	525	396		1.88	1.93	
CT	L3	0	100	710	0.528	646	375	507	3.99	3.91	
DCT	L34	0	100	670	0.317	629	213		2.75	2.64	
DCT	L35	0	100	637	0.519	543	331		2.69	2.72	
DCT	L36	0	100	668	0.440	604	294		2.80	2.70	
CT	L4	0	200	564	0.646	414	364	494	4.06	3.83	
DCT	L37	0	200	512	0.400	426	205		2.56	2.58	
DCT	L38	0	200	508	0.484	397	246		2.86	2.91	
DCT	L39	0	200	526	0.402	442	211		2.78	2.79	
CT	L5	0	290	551	0.636	394	350	505	4.14	4.19	
CT	L6	0	290	554	0.670	385	371		4.39	3.97	
DCT	L40	0	290	501	0.398	411	199		2.49	2.55	
DCT	L41	0	290	504	0.378	419	190		2.55	2.62	
DCT	L42	0	290	494	0.408	400	202		2.69	2.66	
DCT	L20	1.42	20	735	0.739	559	543	570	1.68	1.75	
DCT	Lm1	1.42	20	813	0.562	742	457		--	--	
DCT	L18	1.65	100	638	0.765	-	-	545	1.73	1.71	***
DCT	Lm2	1.65	100	755	0.519	-	-		--	--	
DCT	L16	1.87	200	508	0.605	344	308	530	2.17	2.12	
DCT	Lm3	1.90	200	566	0.549	430	311		--	--	
DCT	L14	2.14	290	405	0.634	231	257	544	2.54	2.25	
DCT	Lm4	2.11	290	517	0.626	340	323		--	--	
DCT	L21	3.95	20	-	-	193	-	593	-	-	Clvg
DCT	L23	3.69	20	-	-	456	-		-	-	
DCT	L24	3.53	100	579	0.666	385	385	562	2.55	2.55	
DCT	L25	3.23	100	564	0.687	361	387	560	2.72	2.55	
DCT	L27	2.87	200	457	0.717	251	328	538	2.58	2.53	
DCT	L29	2.47	290	418	0.601	252	251	546	2.80	2.63	

Fluence*: $\times 10^{19}$ n/cm^2, E>1MeV　　Δa_m & Δa_c: Measured & Calculated Δa

C**,n**: Fitting Parameters, $J=C(\Delta a)^n$,　　LE: Linear Elastic Fracture,

dJda1: dJ/da at Δa=1mm,　　Clvg: Cleavage Fracture,

Lm1-Lm4: Multi-Specimen Method,　　J_{IC}: Valid J_{IC} for ASTM E813

***: High Temperature Irradiation (T>300°C)

Table E－7 Fracture toughness test results using compact type specimen of JRQ steel.

Type	No.	Fluence*	Test Temp °C	C**	n**	J_Q kJ/m^2	dJdal MPa	σy MPa	Δa_m mm	Δa_c mm	Note
CT	Q1	0	24	－	－	294	－	546	－	－	Clvg
CT	Q2	0	24	－	－	277	－		－	－	
DCT	Q31	0	20	－	－	328	－		－	－	
DCT	Q32	0	20	－	－	120	－		－	－	
DCT	Q33	0	20	－	－	299	－		－	－	
CT	Q3	0	100	516	0.586	366	303	512	4.27	4.3	
CT	Q4	0	100	552	0.571	414	315		4.09	3.98	
DCT	Q36	0	100	435	0.199	391	87		2.51	2.59	
CT	Q5	0	200	512	0.576	370	292	499	4.27	4.02	
CT	Q6	0	200	485	0.413	390	161		4.32	3.95	J_{IC}
DCT	Qm1	0	200	426	0.558	285	238		--	--	
DCT	Q41	0	200	407	0.350	324	142		2.13	2.17	
CT	Q7	0	290	391	0.593	235	232	529	4.24	4.09	J_{IC}
CT	Q8	0	290	443	0.469	321	208		4.21	4.01	J_{IC}
DCT	Q35	0	290	331	0.432	226	143		2.63	2.85	
DCT	Q46	0	290	358	0.269	293	96		2.65	2.79	
DCT	Q47	0	290	359	0.442	249	159		2.84	2.92	
DCT	Q48	0	290	366	0.319	289	117		2.59	2.75	
DCT	Q1	2.29	20	－	－	(87.4)	－	671	4.22	－	LE
DCT	Q18	2.36	20	－	－ K_Q	(50.4)	－		3.28	－	
DCT	Q19	2.30	20	－	－	(92.1)	－		－	－	
DCT	Q3	2.38	100	－	－	375	－	637	2.11	－	Clvg
DCT	Q6	2.50	100	－	－	234	－		2.53	－	
DCT	Q17	2.47	100	－	－	129	－		2.32	－	
DCT	Q16	2.52	200	323	0.476	199	154	621	2.13	2.31	J_{IC}
DCT	Q14	2.60	290	281	0.452	－	－	628	2.34	2.40	****
DCT	Q21	4.56	20	－	－ K_Q	(63.7)	－	718	－	－	LE
DCT	Q22	4.55	20	－	－	(55.2)	－		－	－	
DCT	Q23	4.53	100	－	－ K_Q	(98.9)	－	683	－	－	LE
DCT	Q24	4.49	100	－	－	(85.4)	－		－	－	
DCT	Q29	4.07	150	353	0.559	196	197	654	2.26	1.95	J_{IC}
DCT	Q26	4.34	200	296	0.456	181	135	658	2.11	2.29	J_{IC}
DCT	Q28	4.17	290	309	0.443	194	137	649	2.48	2.35	J_{IC}

Fluence*: $x10^{19}$ n/cm^2, E>1MeV

C**,n**: Fitting Parameters, $J=C(\Delta a)^n$,

dJdal: dJ/da at Δa=1mm,

Qm1: Multi-Specimen Method,

****: Low Temperature Irradiation (T<270°C)

Δa_m & Δa_c: Measured & Calculated Δa

LE: Linear Elastic Fracture,

Clvg: Cleavage Fracture,

J_{IC}: Valid J_{IC} for ASTM E813

APPENDIX F

Table F-1 Summary of Vickers hardness test results

Table F-1 Summary of Vickers hardness test results.

Material	Unirradiated				Irradiated				Increase delta Hv	Sigma *1
	Specimen Number	Hv[98N] (VHN)	Average	Sigma *1	Specimen Number	Neutron Fluence *2	Hv[98N] (VHN)	Sigma *1		
JPD	D17	182.1	181.9	1.5	D14	2.56	200.0	3.2	18.1	3.6
	D26	181.7								
JPF	F27	201.1	201.1	1.2	F6	2.23	230.8	4.3	29.8	4.5
	F29	201.1								
JPH	H26	208.2	207.5	6.1	H9	1.61	234.0	6.7	26.6	7.2
	H31	206.7								
JPI	I30	190.3	189.3	2.4	I1	1.99	210.6	6.0	21.3	6.5
	I31	188.2								
JPJ	J19	171.9	173.1	1.3	J14	2.39	186.6	0.9	13.5	1.6
	J21	174.3								
JFL	L17	189.3	188.0	1.7	L4	2.37	202.3	2.4	14.4	5.3
	L32	186.6								
JRQ	Q15	195.0	195.0	2.9	Q11	2.18	236.4	5.8	41.4	6.4
	Q30	195.0								

*1: Standard Deviation

*2: $x10^{19} n/cm^2, E>1MeV$